Centro de Investigación Científica y de Educación Superior de Ensenada, Baja California

Doctorado en Ciencias
en Electrónica y Telecomunicaciones
con orientación en Telecomunicaciones

Performance analysis of multi-hop broadcast protocols for distributed UAV formation control applications

Tesis
para cubrir parcialmente los requisitos necesarios para obtener el grado de
Doctor en Ciencias

Presenta:

Eduardo Giovanni Cabral Pacheco

Ensenada, Baja California, México
2019

Tesis defendida por

Eduardo Giovanni Cabral Pacheco

y aprobada por el siguiente Comité

Dr. Salvador Villarreal Reyes
Codirector de tesis

Dr. Gabriel Alejandro Galaviz Mosqueda
Codirector de tesis

Miembros del comité

Dr. Miguel Ángel Alonso Arévalo

Dr. José Antonio García Macías

Dr. David Muñoz Rodríguez

Dr. Mario Ángel Siller González Pico

Dr. Daniel Sauceda Carvajal
Coordinador del Posgrado en Electrónica y Telecomunicaciones

Dra. Rufina Hernández Martínez
Directora de Estudios de Posgrado

Resumen de la tesis que presenta **Eduardo Giovanni Cabral Pacheco** como requisito parcial para la obtención del grado de Doctor en Ciencias en Electrónica y Telecomunicaciones con orientación en Telecomunicaciones.

Análisis de desempeño de protocolos broadcast multi-salto para aplicaciones de control distribuido de formaciones UAV

Resumen aprobado por:

Dr. Salvador Villarreal Reyes	**Dr. Gabriel Alejandro Galaviz Mosqueda**
Codirector de tesis	Codirector de tesis

Los sistemas de múltiples vehiculos aéreos no tripulados (multi-UAV, por sus siglas en inglés) se han vuelto populares en aplicaciones como agricultura de precisión, sensado remoto, y monitoreo de contaminación. Comunmente, los sistemas multi-UAV requieren alcanzar y mantener un vuelo en formación específico durante la ejecución de una misión. Esto puede ser logrado mediante el uso de una estrategia de control de formación UAV distribuida en la cual cada UAV tiene un controlador de vuelo cuya función es calcular las consignas de control para los actuadores, y así mantener el vuelo en formación. Para llevar a cabo esta tarea, la estrategia de control requiere el intercambio confiable y oportuno de información dentro de la formación. La información requerida por el controlador es comúnmente refererida como información de estado (SI, por sus siglas en inglés). Se ha asumido que la SI puede ser diseminada correctamente por medio de comunicaciones multi-salto, i.e., mediante el desplege de una red ad hoc aérea (FANET, por sus siglas en inglés). En este sentido, los protocolos broadcast multi-salto (MBPs, por sus siglas en inglés) que fueron previamente propuestos para redes ad hoc móviles y vehiculares parecen ser factibles de usarse para esta tarea. Sin embargo, trabajos previos en control de formación UAV distribuido han hecho suposiciones en aspectos de comunicaciones y de redes que son difíciles de cumplir en escenarios de FANETs reales. Además, la eficiencia de los MBPs para diseminar la SI dentro de una FANET es un aspecto aún inexplorado. El objetivo de este trabajo de tesis es analizar como el desempeño de red ofrecido por diferentes MBPs impacta la efectividad de un sistema de control de formación UAV distribuido. Un marco de evaluación para llevar a cabo esta tarea se ha propuesto en este trabajo de tesis. Los resultados de simulación demuestran la relevancia del desempeño de los MBPs en la diseminación de mensajes SI, y por ende en la capacidad del controlador para mantener la formación.

Palabras clave: broadcast, control, disseminación, multi-salto, FANET, formation UAV.

Abstract of the thesis presented **by** Eduardo Giovanni Cabral Pacheco as a partial requirement to obtain the Doctor of Science degree in Electronic and Telecommunications with orientation in Telecommunications.

Performance analysis of multi-hop broadcast protocols for distributed UAV formation control applications

Abstract approved by:

Dr. Salvador Villarreal Reyes	**Dr.Gabriel Alejandro Galaviz Mosqueda**
Codirector de tesis	Codirector de tesis

Multi-unmanned aerial vehicle (multi-UAV) systems have become popular in applications such as precision agriculture, remote sensing, and pollution monitoring. Commonly, multi-UAV systems require to reach and maintain a specific flight formation during mission execution. This can be achieved by using a distributed UAV formation control strategy in which each UAV has a flight controller whose function is to calculate the control actions for the UAV actuators such that the UAV formation is maintained. To perform this task, the control strategy requires the reliable and timely exchange of information within the UAV formation. The information that is needed by the controller is commonly referred to as state information (SI). It has been assumed that SI can be properly disseminated by means of multi-hop communications, i.e., by deploying a flying ad-hoc network (FANET). In this sense, multi-hop broadcast protocols (MBPs) that were previously proposed for mobile and vehicular ad-hoc networks seem to be suited for this task. However, previous work dealing with distributed UAV formation control has made communication and networking assumptions that would be hard to fulfill in actual FANET deployments. Moreover, the efficiency of the MBPs to disseminate SI within an FANET remains unexplored. The goal of this thesis work is to analyze how the network performance offered by different MBPs impacts the effectiveness of distributed UAV formation control to maintain UAV formation. An evaluation framework to perform this task is proposed in this thesis work. The simulation results demonstrate the relevance of MBP performance in SI message dissemination and thus in the ability of the controller to maintain a formation.

Keywords: broadcast, control, dissemination, multi-hop, FANET, UAV formation.

Dedicatory

A mis Padres

Ma.Félix y Griseldo

A mi querida esposa

Mayra

Acknowledgments

Firstly, I would like to express my sincere gratitude to Dr. Salvador Villarreal and Dr. Alejandro Galaviz Mosqueda, for being two great mentors during this long journey; both have a great work ethic and are exceptional persons as well. Both deeply contribute to this thesis with hard work in all of the stages of this work. This work is also yours.

I would like to thank my thesis committee: Dr. Miguel Ángel Alonso Arévalo, Dr. José Antonio García Macías, and Dr. David Muñoz Rodriguez for their wise advice, and insightful comments throughout the course of the thesis.

Special thanks to Sergio Villarreal Reyes for his aid in the development of the evaluation framework used in this thesis work. Also, I would like to thank the ARTS team for their support when I needed some help with my work.

I acknowledge my gratitude to my beloved wife Mayra for supporting me during this journey. She always had my back even on the most though moments. This success is also yours. Additionally, I would like to thank my friends Gabriel Echeagaray, and Anela Sánchez for encouraging me all the time during the course of the thesis.

It is important for me to give my special thanks to all those people I met at CICESE. Each of those people gave me invaluable fellowship and friendship.

Finally, I would like to thank the Mexican Council for Science and Technology (CONACyT) for supporting my thesis work through the scholarship No. 404546 and the Basic Science Project No. 2016-01-285276. Furthermore, I would like to thank the Research and Higher Education Center of Ensenada (CICESE), the Department of Electronics and Telecommunications, for all the support that they provided me during the development of this thesis work.

Table of contents

Pages

List of figures

List of tables

Chapter 1. Introduction

Currently, the use of unmanned aerial vehicles (UAVs) has become very popular in both government (e.g., military) and civilian applications (George et al., 2011; Hassanalian and Abdelkefi, 2017; Hayat et al., 2016; Sharma et al., 2017). This popularity has gained momentum as a result of remarkable technological advances in several areas, including embedded systems, battery technology, materials, sensors, and telecommunication systems, among others (Cai et al., 2014). These advances have led to the development of small UAVs at affordable prices, which in turn have broadened the scope of the missions where UAV systems can be used (Sahingoz, 2014). These missions range from traffic monitoring, remote sensing, border surveillance, disaster monitoring, and managing wildfire, as shown in Figure 1. Regarding the use of UAVs in commercial applications, according to the PwC report (pwc, 2017): the addressable market value of UAVs for commercial applications is over $127 billion as shown in Figure 2. Note that civil infrastructure is expected to dominate the addressable market value of UAV uses, with a market value of $45 billion.

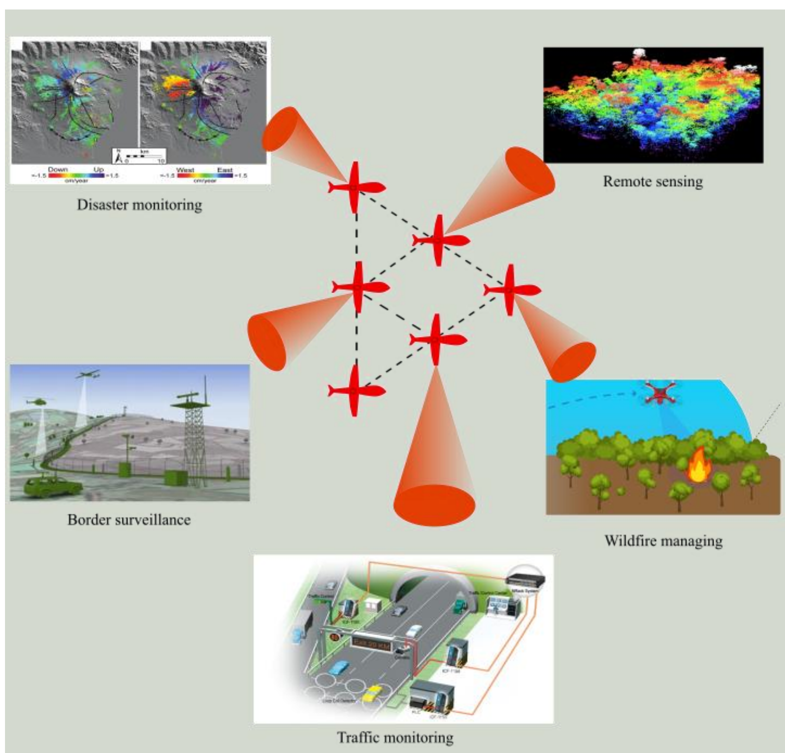

Figure 1. UAV mission applications.

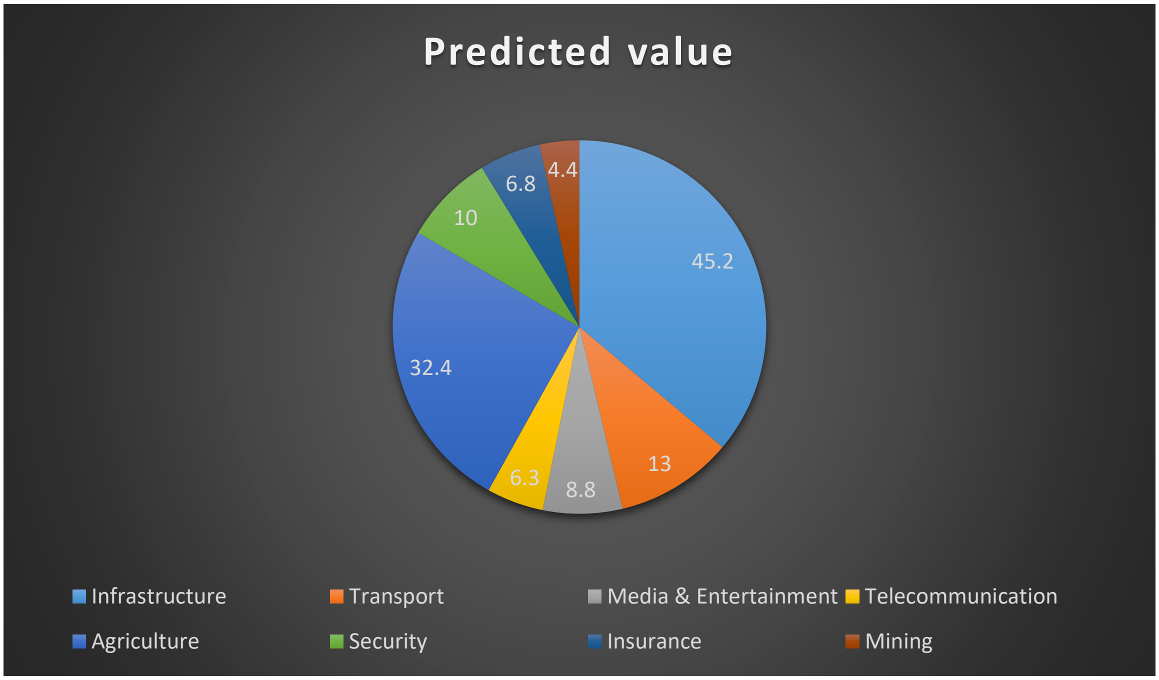

Figure 2. The predicted value of UAV solutions in key industries (billion). Image adapted from (Shakhatreh et al., 2019).

Along with the expected UAV usage growth in the upcoming years, a new approach: using a group of small UAVs (e.g., a multi-UAV system) is becoming relevant. This approach has many advantages regarding the cost, speed, scalability, and survivability of missions (Bekmezci et al., 2013). However, multi-UAV systems present different challenges that must be addressed for the successful deployment and execution of missions. For example, remote sensing multi-UAV missions can sweep large areas at once, but its execution requires that each UAV controls its position such that a spatial formation is achieved and maintained (see Figure 3). Multi-UAV missions strongly depend on wireless communications to exchange information (Andre et al., 2014). The exchanged information can be of different types such as control commands, mission execution reports, and collected information that is downloaded from the UAVs to the ground station. Note that if direct UAV-to-ground (U2G) and ground-to-UAV (G2U) radio links are used to send control commands to the UAVs, then the mission range would be restricted to the radio coverage range (Vidal et al., 2014). Although private repeaters could be used to extend the radio coverage area, doing so may prove to be costly, impractical or both. Alternatively, satellite communication links could be used to extend the mission range, (Simunek et al., 2013), but this would increase the mission cost and energy consumption.

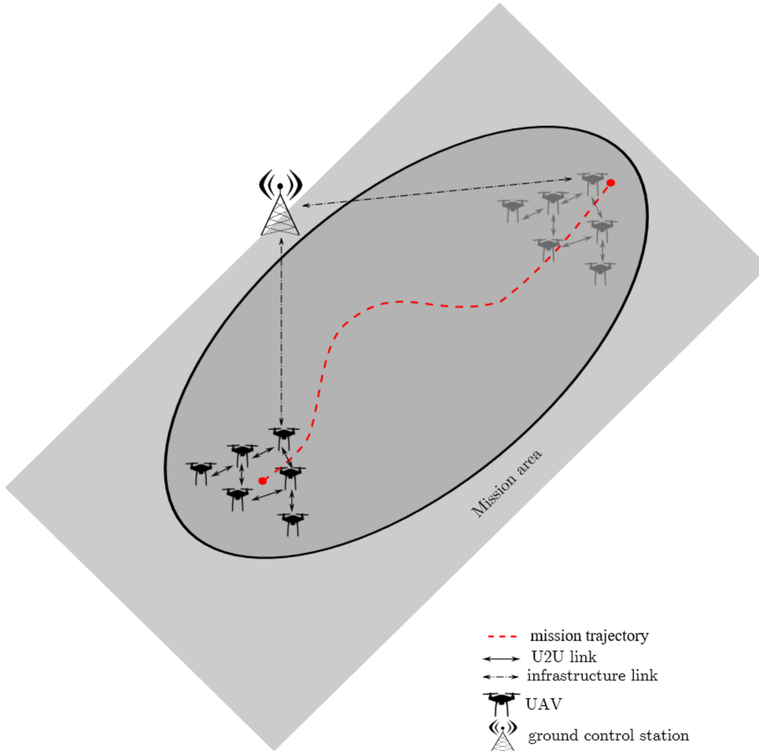

Figure 3. Multi-UAV system example using flight formation while performing a mission.

Multi-UAV systems are often required to reach and maintain a specific flight formation (referred to as the UAV formation throughout this document) during the mission execution (Zou et al., 2009). In a UAV formation, a group of UAVs flies as a rigid entity, keeping the distances between individual pairs of UAVs fixed (Anderson et al., 2008). This procedure can be performed for different purposes. For example, by using a UAV formation in a remote sensing mission, more accurate or redundant sensed data could be acquired in a shorter period. Another advantage of flying in formation is that UAVs can keep a safe distance between each other so that potential collisions are avoided. Furthermore, by flying in formation, the mission coverage area can be increased in a coordinated way. Figure 4 shows UAV formations that are commonly used in applications such as environment monitoring (Kristiansen et al., 2012), precision agriculture (Ju and Son, 2018), and aerial imaging (Kruggl et al., 2010). These formations are commonly referred to as closed formations and can be used to sweep large monitoring areas or to reduce aerodynamic drag when UAVs move to the next mission area.

Achieving and keeping a UAV formation is a challenging task, which requires each UAV to adjust its flight parameters (e.g., speed, orientation, and pitch) such that its relative position within the formation is maintained during the mission execution. Thus, each UAV must implement a formation controller (simply referred to as the controller in this work) whose task is to make the necessary control actions (e.g., speed, orientation, and pitch adjustments) to maintain its position within the formation. To be able to perform its task, the controller needs to have reliable and timely information about different kinematic variables during the mission execution, such as the relative position, speed, and attitude. The information that is needed by the controller to maintain the formation is commonly referred to as state information (SI), (Gu et al., 2006), and its content depends on the particular formation control strategy implemented.

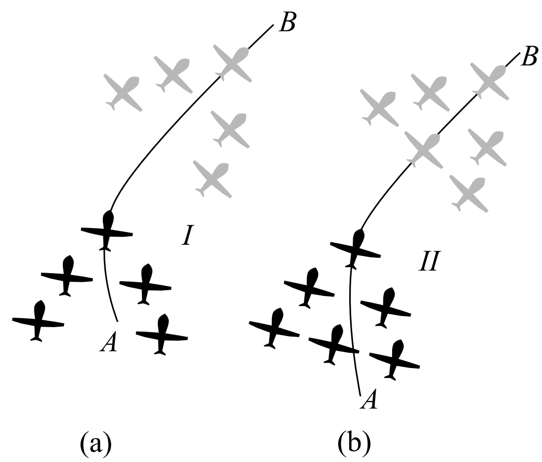

Figure 4. Typical UAV formations: (a) open-delta flight formation, and (b) delta flight formation. Open-delta formations are composed of external UAVs only, while delta formations are composed of external and internal UAVs.

In general, two different approaches are used for UAV formation control: centralized control and distributed control (Wang et al., 2016). In centralized control, all computations and controls are performed in a ground station. Therefore, the use of U2G and G2U radio links is required to send each UAV the control actions to be performed, and then the mission coverage area will be limited by the transceivers radio ranges. In contrast, in distributed control schemes, all the calculations needed for the control actions are performed in each UAV (Cao et al., 2013). Although U2G and G2U radio links could be used to send the required SI to each UAV, this would limit the mission coverage area. However, in addition to U2G and G2U links, UAV-to-UAV (U2U) radio links can be established within a UAV formation. These links can then be used to exchange information, thus defining a flying ad-hoc network (FANET), (Bekmezci et al., 2013, 2015). FANETs are a subset of mobile ad-hoc networks (MANETs) in which the mobile nodes are UAVs.

Therefore, UAVs can exchange information within a FANET without infrastructure support. Thus, when using a distributed approach for flight formation control, a natural approach would be to use a FANET for SI dissemination. This way, the mission coverage area is not necessarily limited by the U2G and G2U radio ranges. If the multi-UAV mission uses low-cost small UAVs with limited energy storage and radio resources, it might not be convenient to use a single hop approach for SI dissemination because of the power that is required by each transmission (Gupta et al., 2016; Sahingoz, 2014; Zeng et al., 2016). Instead, the use of multi-hop communications is attractive because of the possibility of using low-cost transceivers with reduced radio ranges and low power consumption. In this sense, the use of a multicast/broadcast protocol is a more efficient dissemination strategy compared to unicast routing protocols for the support of group communication applications (Panichpapiboon and Pattara-atikom, 2012). Thus, the first natural approach to disseminate SI within a FANET would be to use multi-hop broadcast protocols (MBPs) that were previously proposed for MANETs or vehicular ad-hoc networks (VANETs). In this context, the use of MBPs in FANETs for SI dissemination in distributed UAV formation control schemes is a topic of major interest for future applications of multi-UAV systems.

1.1 Common dissemination assumptions for UAV formation control applications

Disseminating information within FANETs is not a trivial task since FANETs present unique challenges regarding radio propagation, environmental conditions, mobility, and energy consumption (Bujari et al., 2017; Gupta et al., 2016; Oubbati et al., 2017). For example, although in many cases there is line-of-sight between UAVs, fading may still occur because of ground reflections. Furthermore, factors such as variable packet delay, packet loss, and overhead are inherently present in ad-hoc networks. Thus, when using an MBP for SI dissemination, its network performance may adversely affect the performance of the distributed UAV formation control strategy. For example, a decrease in the packet delivery ratio might affect the control strategy ability to keep UAV formation. Moreover, the MBPs that are commonly used for ad-hoc networks could perform differently under the network conditions that are found in FANETs. Therefore, there is a need to investigate if the use of different MBPs for SI dissemination within a FANET affects the performance of the distributed UAV formation control approach.

Several works addressing the design of distributed UAV formation control strategies consider that SI reaches the UAVs timely or within some fixed time window, (Ben-Asher et al., 2008; Chevet et al., 2019;

Ille and Namerikawa, 2017; Ke et al., 2018; Kuriki and Namerikawa, 2015; Lei et al., 2012; Park et al., 2015; Turpin et al., 2012). For instance, (Turpin et al., 2012) and (Park et al., 2015) assume that this can be achieved by using enough transmission power to reach all UAVs within the formation with a single hop. In contrast, (Ben-Asher et al., 2008; Ille and Namerikawa, 2017; Kuriki and Namerikawa, 2015; Lei et al., 2012) consider using multi-hop communications to disseminate SI, whereas (Chevet et al., 2019) assumes perfect communication between UAVs. However, all these works do not include the implementation or analysis of any particular multi-hop dissemination protocol. Furthermore, these contributions assume that the packet delay is constant while disseminating SI, which is not a realistic assumption when considering how multi-hop dissemination protocols work over ad-hoc networks (of which FANETs are a subset) (Panichpapiboon and Pattara-atikom, 2012). Other works have considered the possible occurrence of impairments in the communications process, such as packet delays or packet drops, e.g., (Abdessameud et al., 2015; Z. Chao et al., 2012). For example, the authors in (Abdessameud et al., 2015) consider that the communication process can experience time-varying delays and information losses. However, it is assumed that the blackout intervals do not exceed a known bound (1.3 s in the performed evaluations) and network connectivity can always be recovered. This means that if a UAV experiences a blackout period, it will be able to receive packets from its neighbors again once the blackout period has finished. However, actual transceivers have power constraints that limit their radio range. Therefore, if a UAV deviates enough from its intended position because of packet losses or a blackout, it may lose connectivity and get lost, regardless of the control strategy. Similarly, in (Z. Chao et al., 2012), it is assumed that wireless connectivity is always available, and random packets delays are the only communication impairment. Furthermore, the results presented in (Abdessameud et al., 2015) and (Z. Chao et al., 2012) do not consider the implementation, performance, or analysis of actual multi-hop communication protocols. Thus, the assumptions that are made in these works would be hard to fulfill in actual FANET scenarios.

1.2 Previous work related to the use of multi-hop broadcast protocols (MBPs) in FANETs

As commented in the previous section, disseminating information within a FANET is not a trivial task. Furthermore, there can be many dissemination strategies previously proposed for MANETs and VANETs that might be used in FANETs. For example, there exist dissemination strategies that are unicast-based or broadcast-based (Jayakumar and Gopinath, 2007; Panichpapiboon and Pattara-atikom, 2012). Note that a unicast-based approach might not be the best option for applications in which the information to be disseminated is required by more than one node. Thus, rather than using conventional unicast routing approaches (Jayakumar and Gopinath, 2007), it is more appropriate to use a broadcast-based approach for disseminating group-oriented information. The main advantage of a broadcast approach is that a node does not need to know a destination address and a route to a specific destination (Panichpapiboon and Pattara-atikom, 2012). This eliminates the complexity of route discovery, address resolution, and topology management.

In this thesis work, dissemination broadcast approaches that distribute information in one-to-all scenarios are the only analyzed. Other dissemination approaches such as geocasting (Ko and Vaidya, 2002), and multicasting (Li and Mohapatra, 2003) will not be addressed in this work. Within the broadcast-based approaches there are two types: multi-hop broadcasting and single-hop broadcasting. The major difference between these two types of schemes is in the way the information packets are spread in the network (Panichpapiboon and Pattara-atikom, 2012). In multi-hop broadcasting, a packet propagates through the network by a flooding-like scheme. For example, when a source node broadcasts an information packet, some of the nodes within its vicinity will become “next relay” nodes and will perform a relaying task by rebroadcasting the packet further ahead. In contrast, in single-hop broadcasting, nodes do not flood the information packets received. Instead, when a vehicle receives a packet, it keeps the information on its onboard database. Afterward, each node periodically selects some packets in its database to broadcast. Thus, with single-hop broadcasting, each node carries the information with itself as it travels, and this information is transferred to other nodes in its one-hop neighborhood in the next broadcast period. However, distributed UAV formation control schemes require that state information is disseminated periodically regardless of the node mobility. Therefore, using single-hop broadcasting in distributed UAV formation control applications is not a straightforward option for this application, since single-hop broadcasting relies heavily on node mobility to disseminate information. For this reason, this thesis work studies the use of multi-hop broadcast approaches in distributed UAV formation control applications since, as stated before, the use of multi-hop communications seems to be better suited for the SI dissemination task (compared to single-hop broadcasting) and is attractive because of the possibility of using low-cost transceivers with reduced radio ranges and low power consumption.

Multi-hop broadcast protocols (MBPs) design for UAV formation control applications is still an open issue which can be promising. To the best of our knowledge, a work that addresses this issue has not been published yet. For instance, in MANETs (Badarneh and Kadoch, 2009; Rehmani et al., 2012; Tseng et al., 2002), VANETs (Rosário et al., 2014; Schwartz et al., 2011; Wisitpongphan et al., 2007), and FANETs (Pires et al., 2016; Sharma et al., 2015) there are MBPs schemes that can be used for UAV formation control applications. For example, in (Pires et al., 2016) MBPs commonly used in MANETs and VANETs were tested in a FANET scenario. Nevertheless the use of these MBPs to address UAV formation control applications was not explored in these works. This is an important issue because, as mentioned in Section 1.1, from a control point of view, it has been commonly assumed that state information needed by the UAV formation control strategies can be seamlessly disseminated without losses and delays, (Chevet et al., 2019; Park et al., 2015; Turpin et al., 2012). Based on this, the problem statement about this issue: disseminating state information by an MBP in UAV formation control scenarios is discussed.

1.3 Problem statement

As previously mentioned, when designing distributed UAV formation control strategies, it is commonly assumed that the SI dissemination problem is somehow solved. That is, from the controller perspective, MBPs are seen as a black box that causes random packet losses and delays for the disseminated SI message (Abdessameud et al., 2015; Z. Chao et al., 2012; Ke et al., 2018; Kuriki and Namerikawa, 2015). However, different MBPs use different strategies to address the SI dissemination task. Thus, the network performance that is provided by different MBPs may differently affect the ability of the control strategy to maintain the UAV formation.

When an MBP is used for SI dissemination, packet loss and packet delivery delay variability will likely be present during the dissemination process since both are inherently present in ad-hoc networks and hence in FANETs (Panichpapiboon and Pattara-atikom, 2012). These factors could affect the controller ability to maintain the UAV formation in different ways. Furthermore, it can be inferred that if both, the packet loss and packet delivery delay variability, are large enough, a UAV might deviate from its expected course and even break away from the formation. Nevertheless, it is not clear beforehand how the network performance offered by a particular MBP will affect the controller ability to maintain the formation. Evaluating this is not a trivial task since a packet can experience delays that are caused by issues such as the number of hops, MAC contention, and retransmissions. Similarly, a packet can get lost because of PHY impairments, MAC drops, inhibited retransmissions by the MBP, etc. Hence, it is necessary to analyze this problem that, to the best of our knowledge, has not been addressed before.

For example, consider the scenario shown in Figure 5 where the leader UAV (UAV1) broadcasts an SI message. The UAVs in the second level (UAV2 and UAV3) receive the message, and using the MBP, they decide that UAV2 will rebroadcast the SI packet (Figure 5(a)). The rebroadcasted SI message is overheard by UAV1 and the other node in the same level (UAV3); thus, the MBP hinders the retransmission from UAV1 or the rebroadcast from UAV3. In the next step, note that if UAV5 rebroadcasts the SI packet (Figure 5(b)), all the UAVs in the third and fourth levels should be able to receive it. Contrastingly, if UAV4 rebroadcasts the SI packet (Figure 5(c)), then UAV10 will not receive the SI message. Furthermore, if UAV7 rebroadcasts the SI packet, UAV10 will not receive the SI message in the current sampling period (Figure 5(d)). This example helps to highlight one of the issues that may arise while disseminating SI messages through a FANET by means of an MBP. Since a particular MBP could provide low SI dissemination delays while another MBP may offer a better packet delivery ratio or less overhead, it is necessary to provide a common evaluation framework to assess the suitability of different MBPs for SI dissemination in distributed UAV formation control applications.

Based on the previous discussion, it can be asserted that choosing or designing a particular MBP aimed at disseminating SI for distributed UAV formation control is not a trivial task, and it is a topic of major interest as well. This research deals with the proposal of an evaluation framework to analyze how the network performance offered by different MBPs impacts the effectiveness of distributed UAV formation control in maintaining the flight formation during the mission execution. Therefore, the use of simulation tools such as OMNeT++ (Varga and Hornig, 2008) is important for this thesis work.

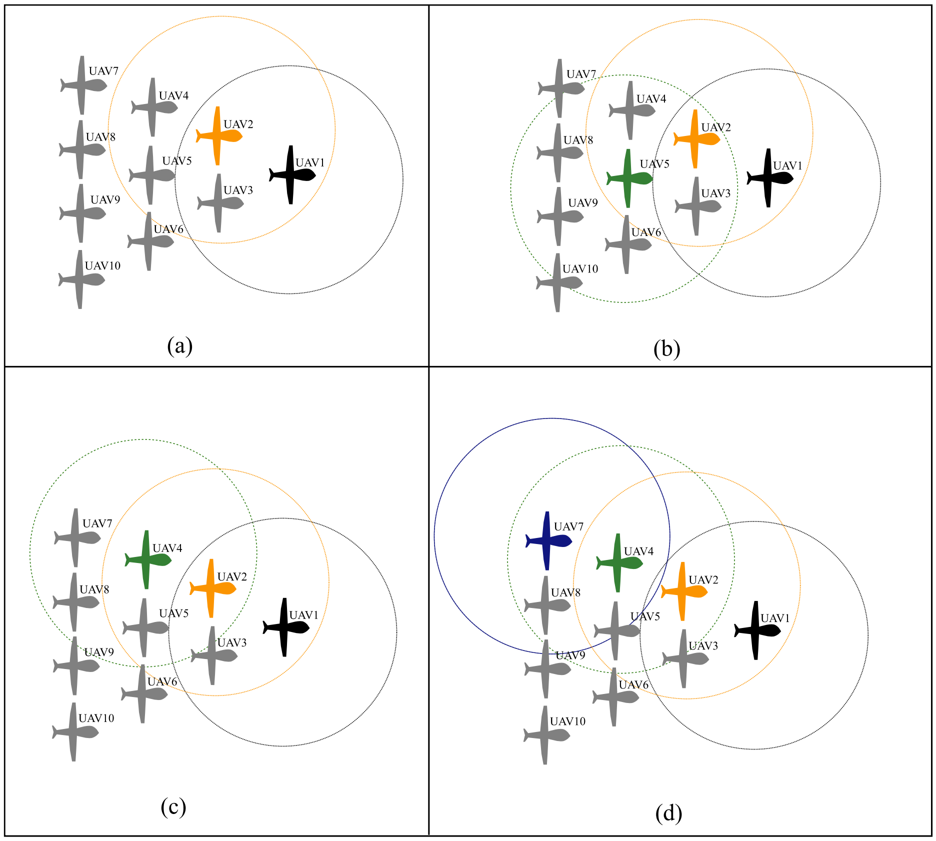

Figure 5. Multihop SI message dissemination with an arbitrary MBP.

1.4 Aim of the thesis

The research presented in this thesis work deals with the analysis, evaluation, and design of multi-hop broadcast protocols when used in distributed UAV formation control applications. In particular, this work evaluates the performance offered by multi-hop broadcast strategies when they are used for SI dissemination in FANETs.

The particular objectives of this thesis work can be listed as follows:

- Investigate the state of the art of MBPs in FANETs.
- Investigate the state of the art of UAV formation control strategies.

- Propose and implement a simulation testbed (evaluation framework) to evaluate the performance of MBPs when used for SI dissemination in distributed UAV formation control applications.

- Using the proposed framework, evaluate different MBPs strategies previously proposed in the literature that could be used for SI dissemination in FANETs for UAV formation control applications.

- Design a new MBP for FANETs which can be used for SI dissemination in UAV formation control applications.

- Using the proposed framework, evaluate the new MBP and compare its performance with that offered by the MBPs previously evaluated.

1.5 Thesis outline

Chapter 2 introduces concepts, terminology, and definitions that will be used throughout the entire thesis. In this chapter, two main areas can be identified. The first area introduces concepts related to distributed UAV formation control. Particularly, the UAV kinematic models and distributed formation control strategies used in UAV formation control applications are discussed in Section 2.2. The second area describes the MBP approaches used in this research. Several important MBPs used in MANETs and VANETs are reviewed in Section 2.3. Finally, a contextualization example which synthesizes the problem addressed in this work is provided. Some SI dissemination issues in UAV formation control applications are discussed.

In Chapter 3, the evaluation methodology framework proposed in this research work is provided. In this chapter, the design and implementation of the evaluation framework are described. Additionally, the evaluation metrics used to assess the performance of the MBPs are explained in this chapter.

Chapter 4 describes and reports the results obtained when testing traditional MBPs under the proposed evaluation framework. From the results obtained in this chapter, some important conclusions are also drawn.

A new MBP aimed at overcoming some of the challenges detected in the SI dissemination process for distributed UAV formation control is introduced in Chapter 5. A performance comparison between the proposed MBP and the MBP strategies analyzed in Chapter 4 is also introduced in this thesis work.

Finally, the contributions, general conclusions, and areas of future research derived from this thesis work are provided in Chapter 6.

A schematic diagram with the structure of this thesis is shown in Figure 6.

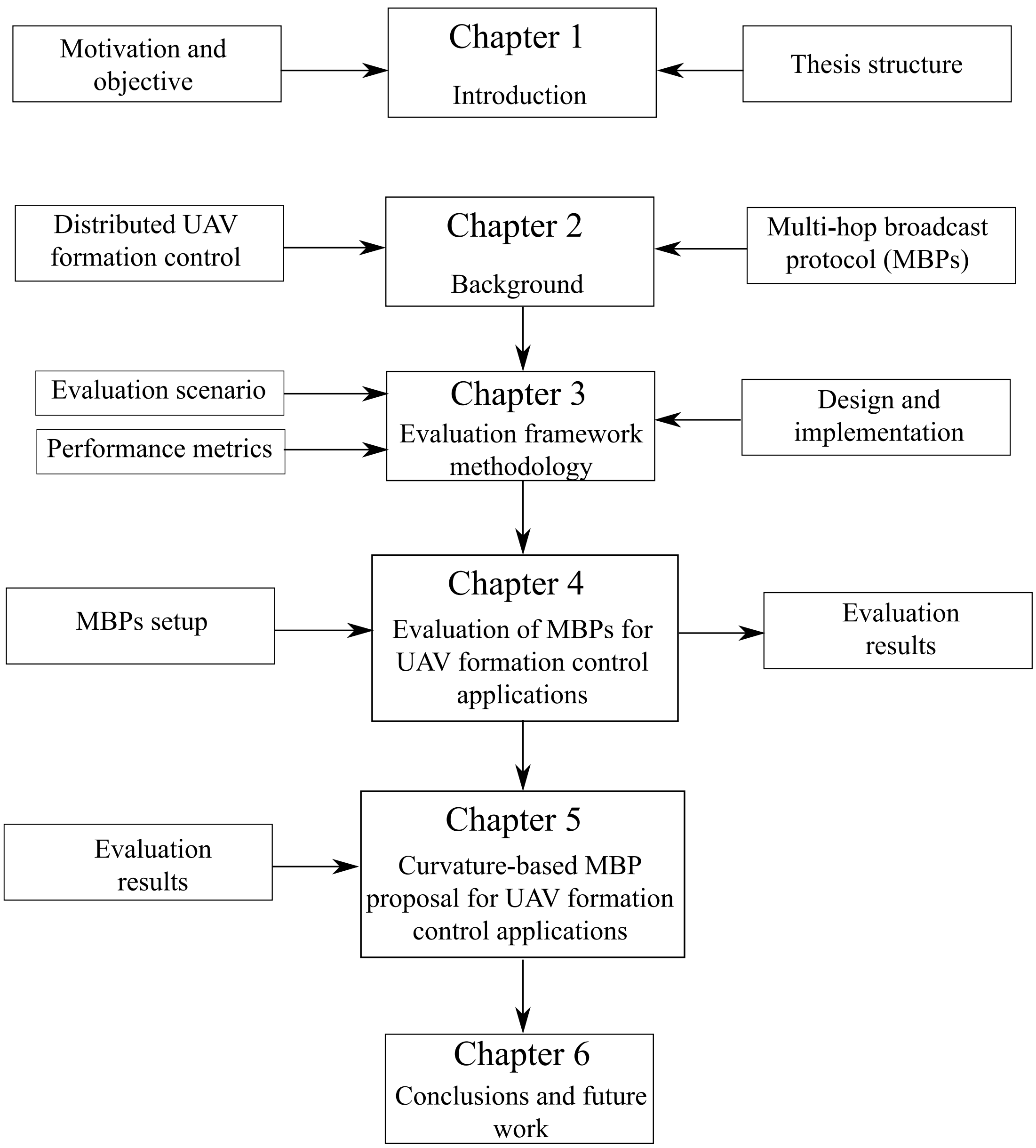

Figure 6. Thesis structure.

1.6 Main outcomes and contributions of the thesis

The main outcomes of this research work were published in the following paper, appearing in a journal indexed in the Journal Citation Report:

- Cabral-Pacheco, E. G., Villarreal-Reyes, S., Galaviz-Mosqueda, A., Villarreal-Reyes, S., Rivera-Rodriguez, R., Perez-Ramos, A. E. 2019. Performance Analysis of Multi-Hop Broadcast Protocols for Distributed UAV Formation Control Applications. IEEE Access, 7, 113548–113577. doi:10.1109/ACCESS.2019.2935307.

Chapter 2. Background

2.1 Introduction

Before presenting the analysis and evaluation performed in this thesis work, it is necessary to provide background regarding the MBPs that are evaluated and the distributed UAV formation control strategy used to perform the evaluation. First, some basic information about the MPC-based strategy implemented in the evaluation framework is presented. Afterward, a review of the different dissemination approaches used by the evaluated MPBs is provided. Then, a contextualization example of the problem addressed in this work is provided at the end of this chapter.

2.2 Distributed UAV formation control

There are different distributed UAV formation control approaches proposed in the literature, such as leader-follower (Chen et al., 2010; Do and Pan, 2007; Wang et al., 2016; Zhang and Mehrjerdi, 2013), virtual structure (Do and Pan, 2007), and behavioral (Lawton et al., 2003). All of these strategies require the exchange of SI among the UAVs. In a leader-follower strategy, the leader UAV is programmed to fly on some predefined reference trajectory while the follower UAVs are required to keep their preset distances (e.g., lateral and longitudinal) from the leader to maintain the formation. Thus, in a leader-follower approach, (Wang et al., 2016; Zhang and Mehrjerdi, 2013), SI originates from the leader, and it must reach every UAV within a specific timeframe to maintain the formation. Similarly, if the SI does not reach each UAV in the formation on time, the performance of the virtual structure control strategy might decrease.

As mentioned in the introduction, without loss of generality, the evaluation framework implements an MPC-based distributed UAV formation control similar to that reported in (Z. Chao et al., 2012). Nevertheless, the analysis and results presented in this work can be used as a reference for the evaluation of other control strategies, knowing that in general, any distributed UAV formation control strategy will require the SI to reach each UAV within a specific timeframe to maintain the formation. The MPC-based distributed UAV formation controller reported in (Z. Chao et al., 2012) is a feedback controller in which a trajectory optimization problem is solved in each time step. It can handle the constraints and nonlinearities of UAVs dynamics in a very intuitive way. Prior to this control strategy description, the kinematic model of the UAVs implemented in the evaluation framework will be provided next

2.2.1 UAV kinematic Model

Based on how they generate lift, UAVs can be classified as fixed-wing or rotatory-wing (Cai et al., 2014; Dobrokhodov, 2015; Hazel and Aoude, 2015; Shraim et al., 2018). Each of these approaches has different flight capabilities and limitations to consider when planning a mission. Regardless of this, distributed UAV formation control involves the design of distributed control laws under imperfect or partial measurements, which have to deal with the flight dynamics of the particular UAVs used for the mission. Thus, without loss of generality, fixed-wing UAVs are considered for the analysis presented in this thesis work. In particular, the analysis considers the two-dimensional motion of a fixed-wing UAV in a horizontal plane where each UAV is equipped with velocity hold and heading hold autopilots, as described in (Ren and Atkins, 2005). This assumption will enable to isolate UAV formation problems which can be directly related to the performance of the different MBPs under evaluation.

The first-order kinematic model of the fixed-wing UAV considered for the analysis is described by the following equations (Ren and Atkins, 2005):

$$
\begin{aligned}
\dot{x}_i &= v_i \sin \psi_i, \\
\dot{y}_i &= v_i \cos \psi_i, \\
\dot{\psi}_i &= \frac{g \tan \phi_i}{v_i}, \\
\dot{v}_i &= \frac{1}{\alpha_v}(v_i^c - v_i), \\
\dot{\phi}_i &= \frac{1}{\alpha_\phi}(\phi_i^c - \phi_i),
\end{aligned}
\tag{1}
$$

where (x_i, y_i), ψ_i, v_i, and ϕ_i are the i-th UAV inertial position, heading angle, speed, and roll angle, respectively; v_i^c and ϕ_i^c are the commanded speed and roll angle, respectively; and α_v and α_ϕ are positive constants.

Additionally, due to the thrust and roll angle limitations of fixed-wing UAVs, the following constraints are imposed on each UAV:

$$
\begin{aligned}
&0 < v_{min} \le v_i \le v_{max}, \\
&-\phi_{max} \le \phi_i \le \phi_{max}, \\
&-\dot{v}_{max} \le \dot{v}_i \le \dot{v}_{max}, \\
&-\dot{\phi}_{max} \le \dot{\phi}_i \le \dot{\phi}_{max},
\end{aligned} \tag{2}
$$

where $\phi_{max}, \dot{v}_{max}$, and $\dot{\phi}_{max} > 0$.

2.2.2 The MPC distributed UAV formation Control Strategy

The MPC-based controller described in (Z. Chao et al., 2012) adopts a virtual point tracking approach for UAV formation control. Virtual point tracking uses a virtual moving reference point, O_r, that follows a preloaded reference trajectory during the mission execution. Figure 7 shows O_r in a typical delta UAV formation. The reference trajectory at time step n is uniquely determined by the position, (x_r, y_r), of the reference point, O_r, and the velocity vector (v_r, ψ_r), where v_r is the reference speed and ψ_r is the reference heading angle. Thus, the SI vector, $\mathbf{x}_n^r$, is defined as

$$
\boldsymbol{x}_n^r = [x_r, y_r, v_r, \psi_r]^T. \tag{3}
$$

The UAV that knows the reference trajectory in advance (source/leader UAV in Figure 7) disseminates $\mathbf{x}_n^r$ by transmitting an SI message at fixed time intervals nt_d, where t_d is the SI dissemination period.

Ideally, SI messages must timely reach each UAV in the formation. However, an SI message might require several hops to reach the UAVs that are located farther away from the source (e.g., UAV7 to UAV10 in Figure 7). In this work, UAVs flying in formation are grouped into M levels according to their longitudinal distances from the source UAV. For example, in Figure 7, the first level includes the source UAV (UAV1); the second level includes UAV2 and UAV3; the third level consists of UAV4, UAV5, and UAV6; and so on.

Note in Figure 7 that the number of hops required for the SI to reach a particular UAV is directly related to its level group (at least for the transceiver radio range assumed in this figure).

The formation structure in Figure 7 can be defined in terms of the rotating coordinate system $X_r O_r Y_r$ such that in each sampling period the moving reference point is located at O_r. In this coordinate system, each of the UAVs (e.g., the i-th UAV) in the formation must try to maintain the desired reference position (x_i^{dr}, y_i^{dr}) during the mission execution. As the rotated coordinate system $X_r O_r Y_r$ changes in each sampling period (i.e., the reference point is moving), it is better to calculate the desired position (x_i^d, y_i^d) of each UAV referred to a fixed XOY coordinate system. Thus, each UAV position (x_i^{dr}, y_i^{dr}) in the $X_r O_r Y_r$ coordinate system is transformed to the (x_i^d, y_i^d) position in the fixed XOY system by using:

$$\begin{bmatrix} x_i^d \\ y_i^d \end{bmatrix} = \begin{bmatrix} x_r \\ y_r \end{bmatrix} + \begin{bmatrix} \cos\psi_r & \sin\psi_r \\ -\sin\psi_r & \cos\psi_r \end{bmatrix} \begin{bmatrix} x_i^{dr} \\ y_i^{dr} \end{bmatrix}, \tag{4}$$

where (x_r, y_r) and ψ_r (defined as positive clockwise) are given referred to the XOY system.

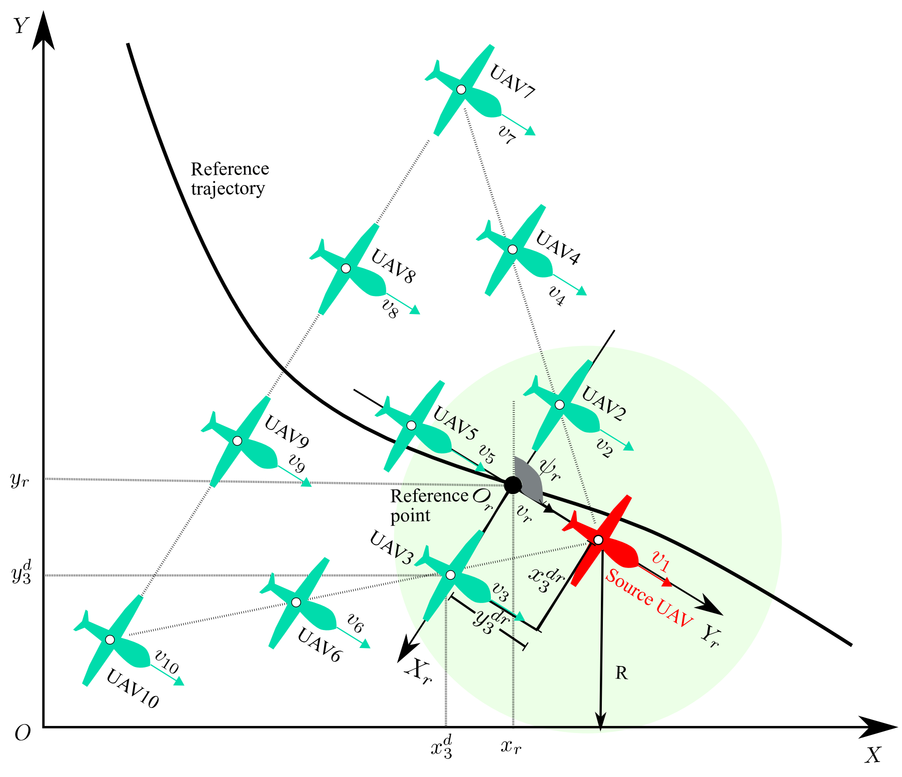

Figure 7. Delta UAV formation in the reference point coordinate system $\boldsymbol{X_r O_r Y_r}$. R is the radio range of the UAVs transceivers. $(\boldsymbol{x_3^{dr}}, \boldsymbol{y_3^{dr}})$ is UAV3 desired position referred to the rotated coordinate system $\boldsymbol{X_r O_r Y_r}$. $(\boldsymbol{x_3^d}, \boldsymbol{y_3^d})$ is UAV3 desired position referred to the fixed coordinate system $\boldsymbol{XOY}$.

The MPC control law requires that each follower UAV has a formation control scheme such as the one depicted in Figure 8. In this scheme, the *i*-th follower UAV that receives a message containing the SI vector, $\mathbf{x}_n^r$, stores the reference position, (x_r, y_r); reference speed, v_r; and reference heading angle, ψ_r, in an $\mathbf{x}_{i,\max(n)}^r$ vector. Thus, $\mathbf{x}_{i,\max(n)}^r$ contains the latest SI vector that is received. Then, after setting a timer to wait for the next MPC controller sampling period, kt_c, the *i*-th UAV calculates a desired state vector $\mathbf{x}_{i,k}^d = \left[x_{i,k}^d, y_{i,k}^d, v_{r,k}, \psi_{r,k}\right]^T$ by substituting the content of $\mathbf{x}_{i,\max(n)}^r$ in (4) to obtain $(x_{i,k}^d, y_{i,k}^d)$. Then, $\mathbf{x}_{i,k}^d$ is fed to the MPC block together with the estimated current state vector, $\mathbf{x}_{i,k} = \left[x_{i,k}, y_{i,k}, v_{i,k}, \psi_{i,k}\right]^T$. This vector contains the estimated current position, $(x_{i,k}, y_{i,k})$; speed, $v_{i,k}$; and heading angle, $\psi_{i,k}$ of the *i*-th UAV. For every MPC controller sampling period, kt_c, the MPC provides an actuator control vector, $\mathbf{u}_{i,k} = \left[v_{i,k}^c, \phi_{i,k}^c\right]^T$, which is obtained by minimizing a cost function over a discrete time period Nt_c, where *N* is called the predictive horizon. The cost function includes $\mathbf{x}_{i,k}^d$ and $\mathbf{x}_{i,k}$, along with predicted state and control vectors, $\mathbf{x}_{i,k+s+1|k}$ and $\mathbf{u}_{i,k+s|k}$, covering the predictive horizon (i.e., $s = 0,1,2, \dots, N$), which are calculated locally as part of the optimization process. Once $\mathbf{u}_{i,k}$ has been obtained, it is fed to the UAV actuators with the aim of maintaining the formation (i.e., $\mathbf{u}_{i,k}$ is sent to the UAV actuators which convert the speed, v_i^c, and roll angle, ϕ_i^c, commands into mechanical motion). Note that the SI dissemination period, t_d, is not restricted to be equal to the MPC controller sampling period, t_c; thus, it is possible to disseminate SI more frequently. It is important to mention that, different from (Z. Chao et al., 2012), no obstacle or inter-UAV collision avoidance was included in the evaluation framework implementation. This was done to focus the analysis on studying UAV formation deviations that are caused by the network performance of different MBPs while disseminating SI. For the sake of brevity, the reader is referred to (Z. Chao et al., 2012) for more details about the MPC strategy used in the evaluation framework.

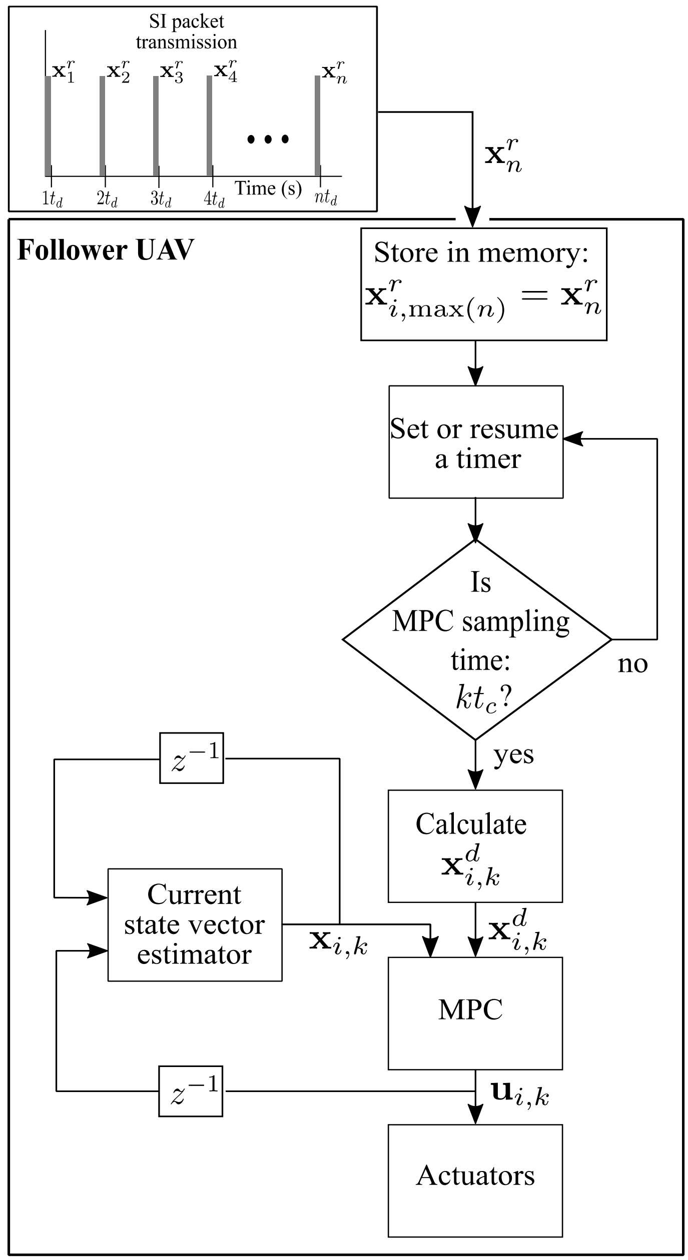

Figure 8. Formation control scheme of each follower UAV.

It is important to timely receive SI messages for the proper operation of the distributed control strategy. To explain this, consider that $t_d = t_c$. Under this assumption, if the SI vector corresponding to sampling time *k*, $\mathbf{x}_k^r$, is not received by the *i*-th UAV (e.g., the SI packet was lost) or if it is received after kt_c (e.g., the SI packet arrival was delayed), then will have to be calculated using the current value of $\mathbf{x}_{i,\max(n)}^r$, where $\max(n) < k$. Note that $\max(n)$ is the discrete time index of the latest SI vector that is successfully received (not necessarily $\max(n) = k - 1$). Therefore, depending on the trajectory followed, a UAV can experience slight deviations from its intended flight path that are caused by packet delays and losses. Furthermore, if the deviations are large enough, the UAV could get out of radio coverage and get completely lost. Thus, it is important to analyze the suitability of different MBPs to disseminate the SI within a FANET and the effects that common ad-hoc networking impairments (e.g., packet loss and delay) might have on losing UAV formation. The next section provides a brief introduction to the different MBP strategies evaluated in this work.

2.3 Multi-hop Broadcast Protocols (MBPs)

Often, it has been assumed that the SI for distributed UAV formation control can be disseminated by employing multi-hop communications. An MBP operates at the network layer, and its primary goal is to timely deliver information from a source node (e.g., leader UAV) to all nodes or a subgroup of nodes that are located in a zone of relevance. However, when using MBPs, the SI dissemination process will experience packet losses, variable delays, and other factors inherent to FANETs. Thus, a drop in the MBP network performance might negatively impact the effectiveness of the distributed UAV formation control strategy in maintaining the formation. In this sense, an MBP is commonly evaluated by considering its average network efficiency in terms of the overhead, delay, and packet delivery ratio. However, in order to assess its suitability for SI message dissemination, the MBP performance should be weighted according to its impact on the controller effectiveness at maintaining the flight formation during a mission execution.

A straightforward way to address SI dissemination in FANETs would be to implement a Simple Flooding dissemination mechanism. In this mechanism, each node that receives a message for the first time retransmits it with no further restrictions. Note that Simple Flooding is inefficient in terms of network performance. In ad-hoc networks with high node density, using Simple Flooding results in over-occupancy of the radio channel resources, higher communication overhead, increased contention and packet collisions, which is referred to as the broadcast storm problem (BSP) (Tseng et al., 2002).

There are different proposals in the literature focused on developing more efficient MBPs than Simple Flooding for multi-hop ad hoc networks, such as MANETs (Sharma et al., 2015) and VANETs (Lee et al., 2014; Wisitpongphan et al., 2007). In this sense, FANETs can be considered to be a subgroup of VANETs, which are a subgroup of MANETs. Thus, it is natural to use MBPs that were previously developed for MANETs and VANETs to address multi-hop broadcast dissemination within FANETs. However, it is necessary to study if the network performance offered by different MBP strategies enables the distributed UAV formation controller to maintain flight formation during a mission execution. To this end, representative protocols of different approaches used in multi-hop broadcasting for MANETs and VANETs were selected and implemented in the evaluation framework that is proposed in this work. Specifically, Simple Flooding (Lee et al., 2014), Distance-Based (Lee et al., 2014; Tseng et al., 2002), Probability-Based (Wisitpongphan et al., 2007), and Counter-Based (Tseng et al., 2002) MBPs were chosen to evaluate their suitability for SI dissemination. The dissemination strategies used by these protocols to address the packet dissemination task are presented in the next section.

2.3.1 MPBs description

MBPs use different parameters to select a subset of relay nodes instead of flooding the messages through all intermediate nodes. Regardless of the specific parameters used to make the relay decision, MBPs have the generic architecture shown in Figure 9. The SI broadcasted by the leader is handed to the MBP at delivery point 1 (DP1) in Figure 9. The protocol makes the relay/drop decision according to the dissemination strategy used. MBPs share similar problems related to the physical (PHY) and multiple access control (MAC) layers. However, there are some issues that have specific dissemination strategies tailored to address them. To better explain these issues, the dissemination strategies used by the MBPs that are evaluated in this work are discussed next.

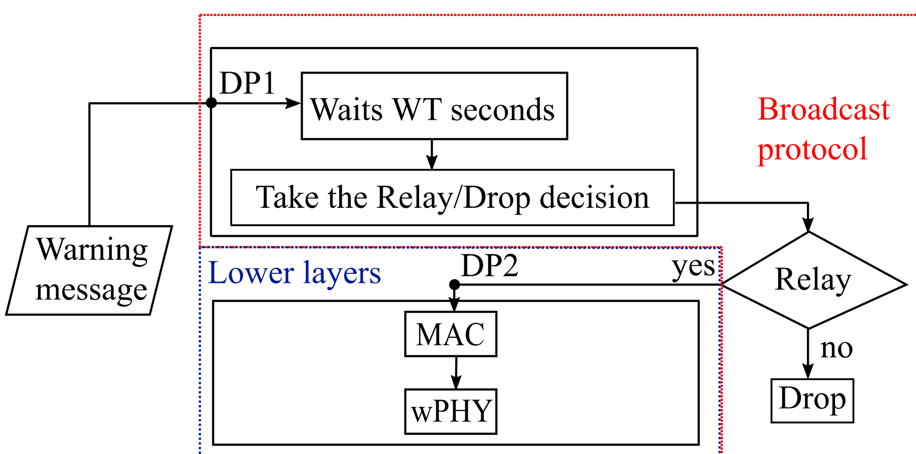

Figure 9. MBP generic architecture.

The Simple Flooding protocol (Lee et al., 2014) implements a procedure where each node will instantly rebroadcast a message after receiving it for the first time. If duplicated messages are received, they will not be rebroadcasted.

The Distance-Based MBP introduced in (Tseng et al., 2002) (hereafter referred to DTh-Distance-Based protocol) aims to maximize the additional coverage that each potential relay node provides. To achieve this, when a node j receives a particular broadcast message for the first time, it estimates the relative distance, d_{ij}, between the node sending the message and itself. Afterwards, node j compares d_{ij} to a predefined distance threshold, D. If $d_{ij} < D$, the transmission is canceled; otherwise, the node j waits for a random waiting time, *RT*, before attempting to rebroadcast the message. If during the waiting period, *RT*, node j receives a duplicated broadcast message, it estimates the relative distance, $\hat{d}_{ij}$, between the node that transmitted the duplicated message and itself. Then, if $\hat{d}_{ij} < d_{ij}$, node j updates $d_{ij} = \hat{d}_{ij}$; otherwise, the value of d_{ij} is kept. If $d_{ij} < D$ the transmission is canceled; otherwise, *RT* is resumed. If another duplicated message is received before *RT* expires, the procedure described before must be repeated. If the waiting time expires and the current $d_{ij} > D$, node j rebroadcasts the message. All duplicated messages that are received after *RT* expires are discarded.

In the Distance-Based MBP introduced in (Lee et al., 2014) (hereafter referred as a WT-Distance-Based protocol), a node *j* that receives a message for the first time listens for duplicate messages during a waiting period, *WT*. If during this period a duplicate message is received by node *j*, the message is discarded, and node *j* does not rebroadcast the information. If *WT* expires and no duplicate is received, the message is rebroadcasted by node j. The waiting time, *WT*, is calculated by using:

$$WT = -\frac{MaxWT}{R} d_{ij} + MaxWT, \tag{5}$$

where d_{ij} is the relative distance between the sender node (e.g., node i) and node j, $MaxWT$ is the maximum waiting time, and R is the radio range of the transceivers. Therefore, the node that is farther away from the sender will have the shortest WT and hence the higher priority to rebroadcast the message.

The Probabilistic-Based protocol introduced in (Wisitpongphan et al., 2007) assigns a higher relaying probability to nodes that are located farther away from the current sender. To do this, when a node j receives a particular broadcast message for the first time, it estimates (e.g., based on RSSI measurements or GPS coordinates) the relative distance, d_{ij}, between the node sending the message and itself. Then, a forwarding probability, p_{ij}, is calculated as follows:

$$p_{ij} = \frac{d_{ij}}{R} \tag{6}$$

where R is the transceiver radio range. Before node j attempts to rebroadcast the message, it listens for duplicate broadcasts during the waiting time, *WT*. If during *WT* node j receives a duplicate broadcast, it estimates its relative distance, $\hat{d}_{ij}$, from the node that sent the duplicate. Then, a probability, $\hat{p}_{ij}$, is calculated by substituting $\hat{d}_{ij}$ in (6). If $\hat{p}_{ij} < p_{ij}$, then node j updates its forwarding probability to $p_{ij} = \hat{p}_{ij}$; otherwise, the current value of p_{ij} is kept. Once *WT* expires, node j can rebroadcast the message with a probability of p_{ij}. If the message is not rebroadcasted, then the message is buffered by an additional period, δ. If a rebroadcast from the message is received before δ expires, the message is discarded from the buffer and node j does not perform a rebroadcast. Otherwise, node j rebroadcasts the packet with $p_{ij} = 1$. The additional waiting time δ (which is typically less than *WT*) accounts for one-hop transmissions and propagation delays.

The Counter-Based protocol introduced in (Tseng et al., 2002) (hereafter referred to as the C-Counter-Based protocol) prevents a node from rebroadcasting after receiving the same message C times. To achieve this, when a node j receives a particular broadcast message for the first time, a counter, c, is initialized. Afterward, node j waits a random waiting time, *RT*, before attempting to rebroadcast the message. If during *RT* node j receives a duplicate message, c is increased by one. If $c < C$, where C is a counter threshold, the waiting is resumed. Otherwise, the rebroadcast of the message is canceled. If $c < C$ after *WT* expires, the message is rebroadcasted by node j.

In order to provide the reader with a more precise idea about the constraints found when using MBPs to disseminate the SI required by distributed UAV formation control mechanisms, a contextualization example is presented next.

2.4 SI dissemination issues in UAV formation control applications

To further illustrate the problem addressed in this thesis work, consider the SI reception process in a follower UAV under ideal and non-ideal SI dissemination assumptions as shown in Figure 10 and Figure 11, respectively. In these figures, it was assumed that the SI dissemination period, t_d, and the MPC controller sampling period, t_c, are equal. As can be observed in Figure 10, under an ideal SI dissemination assumption all the SI messages originated by the source UAV will arrive to the follower UAVs timely and without packet losses. However, when a MBP is used for SI dissemination, a particular UAVs might not receive a particular SI message or might receive it after experiencing some delay. As an example, Figure 11 illustrates the reception of SI messages in a follower UAV when packet loss and delays are present in the dissemination process. Note in this figure the critical role that the dissemination strategy can play in distributed UAV formation control applications. For example, in the case where the SI packet was received slightly after $2t_c$, the controller had to use the "old" SI received at t_c, i.e., $\mathbf{x}^r_{\max(n)} = \mathbf{x}^r_1$, to calculate the desired state vector, $\mathbf{x}^d_2$, and the input control vector, $\mathbf{u}_2$, at the controller sampling time $2t_c$. This is the equivalent of losing the SI vector $\mathbf{x}^r_2$. Therefore, for this scenario, a MBP offering high packet delivery ratio but larger delay (i.e., the SI is not disseminated timely) might provide a performance similar to that obtained with a MBP offering inferior packet delivery ratio but lower delay. As another example consider the SI packet loss at $3t_c$ followed by the SI packet delay at $4t_c$ depicted in Figure 11. This situation is the equivalent of losing two consecutive SI packets which, depending on the UAV formation trajectory, might even cause the follower UAV to break formation.

From the previous discussion, it can be asserted that choosing or designing a particular MBP aimed at disseminating SI for distributed UAV formation control is not a trivial task. Thus, an evaluation framework to assess the MBPs suitability for SI dissemination in FANETs is proposed in the following chapter. Then, the evaluation framework is used to evaluate the performance of the representative MBPs introduced in the previous section.

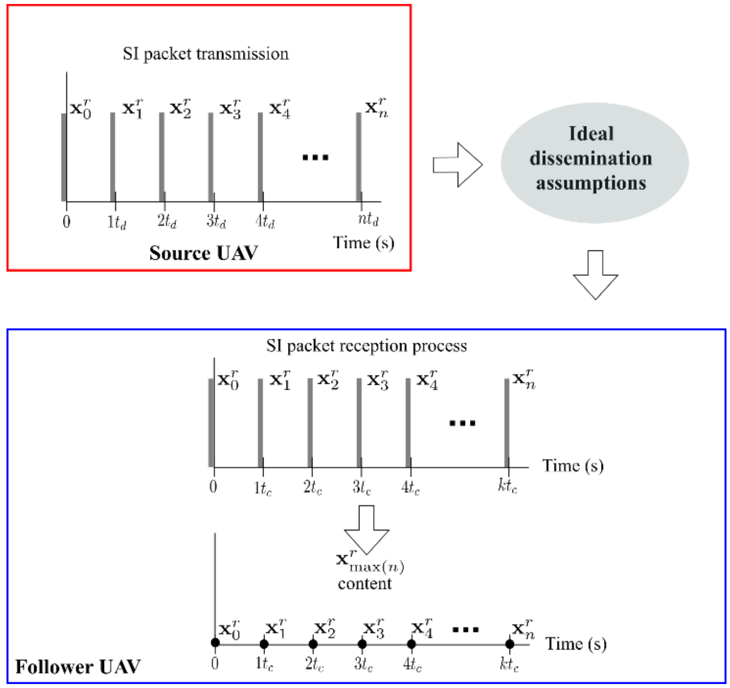

Figure 10. Reception of SI messages under an ideal SI dissemination assumption. $\boldsymbol{t_d}$ is the dissemination period while $\boldsymbol{t_c}$ is the MPC controller sampling period. $\mathbf{x}_\mathbf{n}^\mathbf{r}$ is the SI vector that receives a follower UAV. $\mathbf{x}^\mathbf{r}_{\mathbf{max(n)}}$ is the latest $\mathbf{x}_\mathbf{n}^\mathbf{r}$ vector stored. Note in this figure that $\boldsymbol{t_d = t_c}$ with $\boldsymbol{n = k}$.

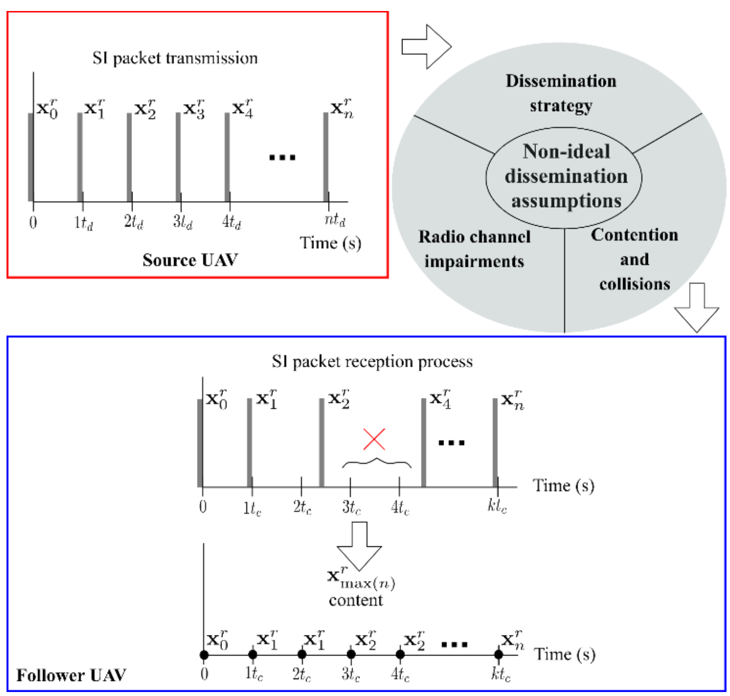

Figure 11. Representation of the SI packet losses and delays that can occur when using a MBP for SI dissemination. $\boldsymbol{t_d}$ is the dissemination period while $\boldsymbol{t_c}$ is the MPC controller sampling period. $\boldsymbol{x_n^r}$ is the SI vector that receives a follower UAV. $\mathbf{x}^\mathbf{r}_{\mathbf{max(n)}}$ is the latest $\boldsymbol{x_n^r}$ vector stored. Note in this figure that $\boldsymbol{t_d = t_c}$ with $\boldsymbol{n = k}$.

Chapter 3. Evaluation framework methodology

3.1 Introduction

This section introduces the evaluation framework methodology developed to study the effects of the SI dissemination process in distributed UAV formation control applications. Traditionally, metrics such as the packet delivery ratio (PDR) and dissemination delay are used to evaluate and compare the performance of multi-hop broadcast protocols. However, metrics aimed at measuring the impact of the MBP on the flight formation have to also be considered. For this purpose, in addition to network metrics, the use of trajectory metrics is proposed in this thesis work. Specifically, this work considers the root mean square (RMS) error between the ideal and actual trajectories of each UAV and the number of lost UAVs. Thus, the proposed methodology allows to compare the performance of different dissemination strategies in terms of: a) trajectory metrics such as the RMS error and the number of lost UAVs; and b) network metrics such as the PDR.

To evaluation framework proposed in this thesis work is based on the well-known OMNeT++ network modeler (OMNeT++, 2012), MATLAB® and the ACADO toolkit (Houska et al., 2013). Additionally, specific software routines were developed and programmed for the framework. These routines include C++ scripts and MATLAB® code, which can be provided to the interested reader upon request.

To implement the evaluation framework, a comparison of different network simulators/modelers was performed. The considered simulators are presented in Table 1. This table summarizes the main characteristics of different simulators able to fulfill the needs of the proposed evaluation framework. The final selection process involved verifying the inclusion of features such as propagation models, MAC standards, communications protocols, and documentation availability, with the additional requisite of being able of modifying or incorporating new features as needed to implement the evaluation framework proposed in this thesis work. After a careful analysis of the features offered by each of the networks modelers presented in Table 1, the well-known OMNeT++ network modeler (OMNeT++, 2012) was chosen to implement the evaluation framework.

Table 1. Comparative of network modelers (adapted from (Korkalainen et al., 2009)).

	OMNeT++	OPNET	NS-2	NS-3
Licence	Academic/ commercial	Commercial	GPL	GPL
Platform	Linux, Mac OSX, Windows	Linux, Windows	Unix (FreeBSD, Linux, SunOS, Solaris), Cygwin (windows)	Linux, Mac OSX, Cygwin (windows)
Language	C++/NED	C/C++	C++/OTcl	C++/Python
GUI-based	Good	Excellent	Bad	Bad
Complexity	Moderated	High	High	High
Documentation	Excellent	Excellent	Excellent	Good
Scalability	Good	Good	Good (limited in some cases)	Good
Propagation models	Free space, Two-ray ground reflection, Rayleigh, Rician, Showdown	Free space, CCIR, Hata, Longley-Rice, TIREM, Walfish-Ikegami	Free space, Two-ray, Shadowing	Free space, Two-ray, Nakagami, Okumura-Hata, Two-ray ground reflection, Shadowing
MAC standards	IEEE 802.11, IEEE 802.16, IEEE 802.15.4, IEEE 802.3	IEEE 802.11, IEEE 802.16, IEEE 802.15.4, IEEE 802.3	IEEE 802.11, IEEE 802.15.4	CSMA, IEEE 802.11, IEEE 802.16, IEEE 802.15.4
Routing protocols	AODV, BATMAN, DSDV, DSR, OLSR, DYMO	AODV, DSR, GRP, OLSR, OSPFv3, TORA	DSDV, DSR, TORA, AODV	AODV, Click, DSDV, DSR, OLSR, Nix-Vector
Mobility models	Gauss-Markov, Random Waypoint, Real-world Traces, Artificial Mobility Traces, Bidirectionally coupled	Pathway, Overlap mobility, Random Waypoint, Real-world Traces, Artificial Mobility Traces	Gauss-Markov, Random Waypoint, Real-world Traces, Artificial Mobility Traces, Bidirectionally coupled	Gauss-Markov, Random Waypoint, Random Walk, Random Direction, Real-world Traces, Artificial Mobility Traces

The ACADO control toolkit (Houska et al., 2013) was used within the evaluation framework to implement the distributed UAV formation control strategy. The ACADO toolkit is an open-source software environment and a collection of algorithms for automatic control and dynamic optimization. It provides a general framework for using a great variety of algorithms for direct optimal control, including MPC, state and parameter estimation, and robust optimization. The ACADO toolkit is implemented as self-contained C++ code, its object-oriented design allows its extension with user-written applications, and includes a Matlab® interface. Within the evaluation framework, the ACADO module is responsible for generating the MPC and state-estimation code that each UAV needs for flying in formation.

The following sections elaborate on the evaluation scenario, the performance metrics used, and the design and implementation details of the evaluation framework.

3.2 Evaluation scenario

Within the evaluation scenario, it is necessary to first define the U2U link and flight parameters that are used in each trial. Another variable to consider is the reference trajectory of the multi-UAV mission. In particular, it is important to define a trajectory (within the kinematic capabilities of the UAV) that enables differentiating the performance provided by the MBPs under evaluation. This is done in order to obtain relevant conclusions regarding the suitability of the MBPs for SI dissemination.

3.2.1 U2U link parameters

One of the most relevant considerations when evaluating communication protocols is to define the wireless propagation conditions. Thus, the radio channel propagation model introduced in (Goddemeier and Wietfeld, 2015), that was designed for U2U radio links, was implemented within the evaluation framework.

Another parameter to consider is the wireless technology used by the transceiver. Different technologies have been proposed to enable U2U communications such as IEEE 802.11a/b/g/n, IEEE 802.15.4, 3G/LTE, and infrared (Andre et al., 2014). However, several FANET proposals rely on the IEEE 802.11p standard (IEEE Standar for information technology—local and metropolitan area networks—specific requirements-part 11: wireless LAN Mediuam Access Control (MAC) and Physical Layer (PHY) specifications amendment 6: wireless accesss in vehicular environments, 2010), which is the most prominent option for VANETs. The IEEE 802.11p standard was specifically designed for VANET deployments where the nodes have high mobility, speed, and acceleration. Since these characteristics are also observed in FANET deployments, the evaluation scenario considers the use of IEEE 802.11p transceivers to enable U2U communications. Table 2 summarizes the values of each variable used by the 802.11p transceivers considered within the evaluation framework.

Table 2. Parameters of the U2U 802.11p transceivers considered in the evaluation scenario.

General parameters	
Wireless technology	IEEE 802.11p
Base frequency	5.880 GHz
Data rate[1]	3 Mbps
Nominal radio range R	200 m
Reachable radio[2] **RR**	300 m

3.2.2 Flight parameters

The UAVs mobility is ruled by three main factors within the evaluation scenario: 1) the kinematic model defined in subsection 2.2.1; 2) the distributed formation control strategy discussed in Section 2.2.2; and 3) the control constraints that are defined considering the typical specifications found in commercial UAVs (Hazel and Aoude, 2015; Shraim et al., 2018). Table 2 provides the values that are used by the kinematic model and the MPC controller in the evaluation scenario. These values were chosen such that realistic fixed-wing UAV movements are generated within the simulation testbed (e.g., smooth turns and speed changes).

Table 3. Values used in the kinematic model for the fixed-wing UAV and the MPC controller.

Symbol	Kinematic model parameters	
v_r	Reference speed	{15, 17.5, 20, 22.5, 25, 27.5} m/s
l_d	Lateral distance	100 m
L_d	Longitudinal distance	100 m
v_{min}	Minimum velocity	2 m/s
v_{max}	Maximum velocity	40 m/s
$\dot{v}_{max}$	Maximum acceleration	2 m/s^2
ϕ_{max}	Maximum roll angle	40 deg
$\dot{\phi}_{max}$	Maximum roll angle speed	40 deg/s
	MPC parameters (Z. Chao et al., 2012)	
t_N	Prediction horizon time	2.5 s
t_c	Sampling period	0.5 s

[1] The data rate is chosen to be the lowest supported by this standard, i.e., 3 Mbps. This is because the modulation used for this data rate fulfills the data rate requirements and offers better power efficiency.

[2] Beyond the reachable radio, RR, it is assumed that none of the UAVs can sense and receive packets since there is high communication degradation.

3.2.3 Flight trajectories

When performing a multi-UAV mission, a distributed UAV flight formation controller aims to keep all UAVs within the formation. Thus, the trajectory that is followed during the mission is of particular relevance to evaluate the control strategy effectiveness. Note that a sinuous trajectory will be a harder challenge for the controller than a simple straight line. Thus, to adequately measure the effectiveness of the SI dissemination process in the formation controller performance, special attention should be paid to the UAVs trajectory selection.

One of the most relevant applications of multi-UAV systems is in missions involving sweeping large geographic areas at once for data-gathering, e.g., multispectral and visual data. Commonly, for this kind of task, the area to be covered by the UAVs is divided into several straight paths or rows (Avellar et al., 2015; Maza and Ollero, 2007), which is known as a sweep trajectory (Mansouri et al., 2018). In this trajectory, at the end of each row, the UAVs make a U-turn outside the area of interest to follow the next row, as shown in Figure 12. This sweep trajectory was considered as the reference trajectory within the evaluation scenario. Thus, since the MPC controller implemented in this work uses virtual point tracking (see Section 2.2.2), during each trial, the UAVs will try to keep their relative distance from the virtual point while they follow the sweep trajectory (Figure 12) at a fixed speed.

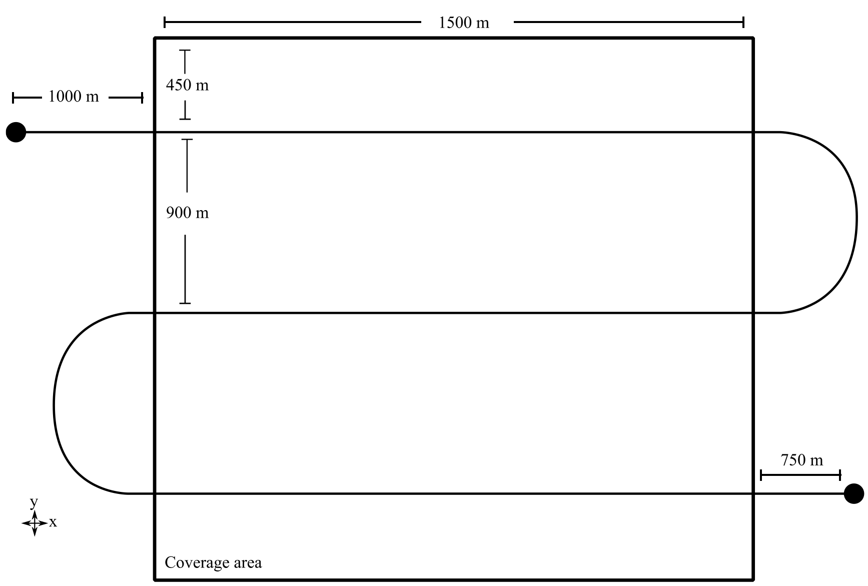

Figure 12. Sweep trajectory considered in the evaluation scenario. It is assumed that the trajectory starting point is coordinate $(\boldsymbol{x_{r0}}, \boldsymbol{y_{r0}}) = [\mathbf{750}, \mathbf{2000}]$ m with a heading angle of $\boldsymbol{\psi_{r0}} = \mathbf{90}$ deg. At the beginning of each trial, the UAV formation follows a straight line measuring 2500 m. A simulation warm-up period is considered where no metrics are collected for the first 1000 m of this straight line. The trajectory includes U-turns following a semicircle with a diameter equal to 900 m.

3.3 Performance metrics

To assess the suitability of a particular MBP for SI dissemination in UAV formation control scenarios, two kinds of metrics are considered:

1. Metrics that measure the deviation between the ideal and actual trajectories that are followed by each UAV when using a particular MBP.

2. Metrics related to the performance of each MBP from a networking point of view.

These metrics are explained next.

3.3.1 Trajectory metrics

The trajectory metrics provide information regarding how close each UAV follows its ideal path during a mission execution. It is important to highlight that, depending on its objective, significant deviations from the ideal paths could compromise a multi-UAV mission. Furthermore, a particular UAV could get lost if the deviation from its ideal path is large enough at certain points in the trajectory. Thus, within the evaluation framework, the actual path that is followed by each UAV in each trial is recorded in order to obtain the following metrics:

a) *Path Root Mean Square Error (P-RMSE).* The P-RMSE measures the root mean square error between the ideal and actual trajectories of each UAV. Thus, the P-RMSE helps to quantify the performance of the SI dissemination strategy in terms of the trajectory errors that should be addressed by the controller. Specifically, in each trial, the P-RMSE_i of the i-th UAV is calculated as

$$P\text{-}RMSE_i = \sqrt{\frac{\sum_{k=1}^{S}[(x_i^{ac}[k] - x_i^{de}[k])^2 + (y_i^{ac}[k] - y_i^{de}[k])^2]}{S}}, \tag{7}$$

where $(x_i^{ac}[k], y_i^{ac}[k])$ is the i-th UAV actual position at sample time k, $\left(x_i^{de}[k], y_i^{de}[k]\right)$ is the i-th UAV desired (ideal) position at sample time k, and S is the total number of samples considered in the simulation. The average P-RMSE is then defined as:

$$P\text{-}RMSE = \frac{1}{\lambda_3} \sum_{i \in S_{\lambda_3}} P\text{-}RMSE_i, \tag{8}$$

where S_{λ_3} is the subset of UAVs that are located in level three and above in the formation, and λ_3 is the total number of UAVs belonging to S_{λ_3}. Note that the P-RMSE does not consider the error generated once a particular UAV is considered definitively lost.

b) *Lost UAVs (LU).* This measures the number of UAVs whose deviation from the ideal path leaves them definitely outside the wireless range of any other UAV that is still within the formation. Thus, the LU metric is used to weigh the trajectory errors measured by the P-RMSE. The LU metric is calculated by counting the number of UAVs that, at some point during the simulation, are outside a reachable ratio, RR, which is defined as:

$$RR = d_{max} + 1.5R, \tag{9}$$

where R is the nominal radio range, and d_{max} is the distance between the source UAV and the follower UAVs that are located farther away but are still within the formation. It is important to mention that once a particular UAV is outside the *RR*, it is considered definitively lost, even though it might rejoin the formation by chance (e.g., the flight path followed by a UAV that is lost in the first curve eventually leads it to encounter the UAV formation after the second U-turn).

3.3.2 Network metrics

Network metrics are used to assess the performance of the SI dissemination process when using a particular MBP. Traditionally, when evaluating the performance of MBPs in ad-hoc networks, it is assumed that the network topology changes over time as nodes move and its one-hop neighborhood changes. Thus, the number of hops that a message needs to perform to reach a particular node varies over time. Note that for the problem under study in this work this is not necessarily the case, especially if the distributed UAV formation control strategy is working properly. This is particularly true for the nodes that are located in the second level of the formation (see Section 2.2.2) since the SI will reach all nodes in this level with a single hop from the source UAV. This means that the SI will reach these nodes on-time with a high probability. Thus, if metrics such as the packet delivery ratio are calculated considering these nodes, the results may become biased, thus making it challenging to assess the network performance that is experienced by nodes that are located farther away from the source. Therefore, in this work, the network metrics are calculated by considering the nodes needing two hops or more to receive the SI from the source (i.e., level two and higher in the formation). Under this consideration, the network metrics considered in the analysis performed in this thesis work are introduced next.

a) *Packet Delivery Ratio (PDR).* The PDR is the average number of SI packets (not counting duplicated packets) that are successfully received within the UAV formation. Thus, the PDR measures the overall efficiency of the SI dissemination strategy. For each trial, define $N_{SI_{rx}}^{i}$ as the number of SI packets that are successfully received by the *i*-th UAV. Then, the packet delivery ratio for the *i*-th UAV, PDR_i, is calculated as:

$$PDR_i = \frac{N_{SI_{rx}}^{i}}{N_{SI_{tx}}} \tag{10}$$

where $N_{SI_{tx}}$ is the total number of SI messages that are transmitted by the source UAV during a simulation trial. The average PDR is then defined as:

$$PDR = \frac{1}{\lambda_3} \sum_{i \in S_{\lambda_3}} PDR_i, \tag{11}$$

where S_{λ_3} is the subset of UAVs that are located in level three and above in the formation, and λ_3 is the total number of UAVs belonging to S_{λ_3}. Note that for the analysis performed in this thesis work, the UAVs that are located in level 2 are not included in the calculation of the metrics since they are located a single hop from the leader UAV (SI source – level 1).

b) *Average SI age (AvgSIage)*. The average SI age (AvgSIage) provides a measure about how “old” the SI, $\mathbf{x}_{i,\max(n)}^{r}$, used by the controller in each controller sampling time, kt_c, is. Thus, the AvgSIage metric measures the quality or “freshness” of the SI used by the controller in each sampling period. That is, if

$$\boldsymbol{x}_{i,max}^{r}(kt_c) = \boldsymbol{x}_{i,max(n)}^{r}, \tag{12}$$

then the SI age, $SIage_{\mathrm{i}}(\mathrm{k})$, for the *i*-th UAV at sampling time kt_c is defined as

$$SIage_i(k) = k - max(n)_i, \tag{13}$$

where $\max(n)_{\mathrm{i}}$ is the discrete time index of the latest SI packet that is successfully received by the i-th UAV. Then, the average SI age (AvgSIage) metric for the i-th UAV is defined as

$$AvgSIage_i = \frac{1}{N_{cst}} \sum_{k=1}^{N_{cst}} SIage_i(k), \tag{14}$$

where N_{cst} is the number of controller sampling times during a simulation run. For the analysis, it is convenient to define:

$$AvgSIage_{L_m} = \frac{1}{N_{L_m}} \sum_{i \in S_{L_m}} AvgSIage_i, \tag{15}$$

where S_{L_m} is is the subset of UAVs that are located in level m in the formation, and $\mathrm{J}_{\mathrm{L_j}}$ is the total number of UAVs belonging to $S_{\mathrm{L_m}}$.

c) *Burst average length (BAL)*. The BAL metric measures how many consecutive packets (i.e., length) are lost on average. In wireless communication systems, packet losses could be induced by issues such as propagation phenomena or topological changes (Rappaport, 2002). In this sense, ideally, MBPs should overcome such issues and disseminate data through alternative paths. Thus, measuring the lengths of the burst losses allow us to compare the efficiency of different MBPs to overcome the topological changes in the evaluated scenario. To calculate the BAL_i metric for the *i*-th UAV, a received packet register, $RPreg_{\mathrm{i}}$, is generated during each trial. The *k*-th position of $RPreg_{\mathrm{i}}$ is set to "1" if the SI packet containing $\mathbf{x}_k^r$ is successfully received by the *i*-th UAV, which is independent of when it was received. Otherwise, if the SI packet containing $\mathbf{x}_k^r$ is lost, the *k*-th position of $RPreg_{\mathrm{i}}$ is set to "0". Then, runs (bursts) of two or more consecutive "0"s are searched in the list, and the length of each run that is found is stored in a variable B_m. Once this is done, the BAL_i metric is calculated by using:

$$BAL_i = \frac{1}{N_B}\sum_{m=1}^{N_B} B_m \tag{16}$$

where B_m is the length of the *m*-th burst sequence and N_B is total number of bursts that are found in $RPreg_{\mathrm{i}}$. Note that even though two sequences can have the same packet loss, their *BAL* metric could differ. For example, consider the content of the following registers:

$$RPreg_1 = [0, 0, 1, 1, 0, 0, 1, 1, 0, 0, 1, 1, 0, 0, 1] \tag{17}$$

$$RPreg_2 = [1, 0, 0, 0, 0, 1, 1, 1, 0, 0, 0, 0, 1, 1, 1]. \tag{18}$$

Note that $\mathrm{BAL}_1 = 2$ and $\mathrm{BAL}_2 = 4$, even though the packet loss is the same for both UAVs.

The trajectory and network metrics previously introduced are used in Chapters 4 and 5 to study and evaluate the performance of MBPs when they are used for SI dissemination. Furthermore, in these chapters, the time moving averages of these metrics are calculated, which is done in order to analyze the evolution of the metrics as the UAV formation follows the reference trajectory. The time moving average metrics are calculated by considering an averaging sliding window of 10 consecutive controller samples. To obtain a plot, the averaging sliding window is displaced by a controller sampling period, t_c, each time. The sliding window of 10 samples is enough to capture the network interactions occurring within the reachable radio range of each UAV. Hereafter, these metrics are called metrics by segments.

3.4 Design and implementation of the evaluation framework

The evaluation methodology was implemented by developing an evaluation framework based on the well-known OMNeT++ network modeler (OMNeT++, 2012), MATLAB®, and the ACADO toolkit (Houska et al., 2013). The following sections elaborate on the design and implementation details of the evaluation framework, which can be made available to the interested reader upon request.

The designed evaluation framework considers three main building blocks (see Figure 13): 1) a reference trajectory generator, 2) a mobility controller API, and 3) a FANET simulator implemented in OMNeT++. The reference trajectory generator works offline, and the mobility controller API is used by the FANET simulator to determine the flight parameters of each follower UAV, as explained next.

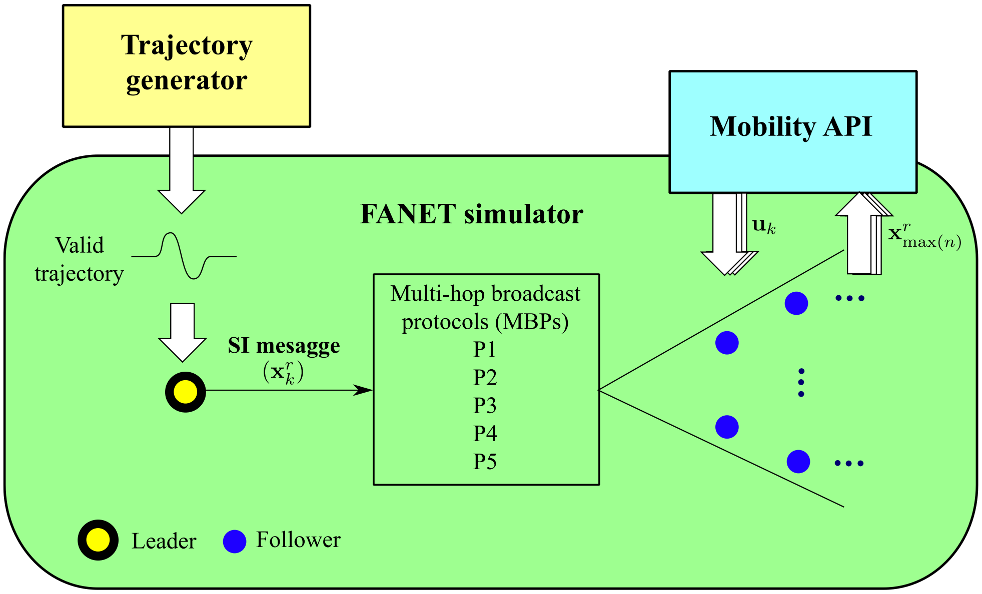

Figure 13. Proposed implementation framework.

3.4.1 Reference trajectory generator

To generate and use the trajectory defined in Section 3.2.3 within the evaluation framework, a reference trajectory generator was designed and implemented using MATLAB® and the ACADO toolkit. It is worth noting that defining the UAV trajectories for evaluation purposes is not a simple task since the trajectories must satisfy the restrictions imposed by the UAVs kinematic model.

The reference trajectory generator works offline from the FANET simulator (implemented in OMNeT++). Thus, a valid reference trajectory for virtual point tracking must be generated before starting a simulation trial. The process to generate the trajectory is as follows:

1. A reduced set of milestones are defined by considering the kinematic model of the UAV explained in Section 2.2.1 and the values provided in Table 2. These milestones are delivered to the ACADO toolkit through the MATLAB® interface.

2. The ACADO toolkit returns the reference trajectory, which includes the set of points corresponding to the intermediate points between each pair of milestones and the milestones themselves. The sampling period of the controller directly determines the number of intermediate points between milestones.

3. The valid trajectory that is returned by the ACADO toolkit is formatted in MATLAB® for compatibility with the FANET simulator, which is based on the OMNeT++ network modeler.

Once a valid trajectory is generated, it is feed to the FANET simulator where it will be used by the source/leader UAV to disseminate the SI that is needed for virtual point tracking.

Note that with the reference trajectory generator, any valid trajectory can be easily adjusted to different controller sampling periods and formatted for the OMNeT++ network modeler. In fact, with small variations in the template, the trajectory could be formatted to be used with other network modelers such as NS-2.

3.4.2 Mobility controller

A mobility controller API to solve the nonlinear MPC equations that are required to determine the flying parameters (e.g., speed and roll angle) of each follower UAV was programmed and included in the FANET simulator. At each sampling time step, the API is used to solve the MPC equations on the fly for each UAV within the formation (see Section 2.2.2). The generated API is based on the MPC controller of the ACADO toolkit.

3.4.3 FANET simulator

The FANET simulator is the core module of the implementation framework and is based on the OMNeT++ network modeler (OMNeT++, 2012). The simulator integrates the mobility controller API and the trajectory generator modules.

The FANET simulator allows modeling the delay and packet loss behavior that are observed when a particular MBP is used for SI dissemination within a FANET. Thus, the MBPs described in Section 2.3.1 were implemented in the simulator such that they can be used to disseminate the SI needed by the distributed MPC control strategy described in Section 2.2.2. It is important to recall that in this strategy, the SI messages originate from the source/leader UAV while the rest of the UAVs within the formation have no prior information regarding the mission trajectory. Being based in OMNeT++, the FANET simulator provides the tools that are necessary to obtain common network performance statistics, as explained in Section 3.3.2.

Chapter 4. Evaluation of MBPs for UAV formation control applications

4.1 Introduction

This chapter introduces the results obtained when the evaluation framework and methodology proposed in Chapter 3 is used to evaluate the performance of the MBPs introduced in Chapter 2. Thus, an assessment of these MBPs suitability for SI dissemination in distributed UAV formation control applications is provided in this chapter.

4.2 MBP evaluation setup

From Figure 13, one can note the interaction between the modules detailed in Sections 3.4.1, 3.4.2, and 3.4.3 during a simulation trial. As it can be seen in this figure, the virtual point trajectory (Figure 12) is uploaded to the source/leader UAV before the simulation starts. A warm-up period corresponding to a straight-line of 1000 m is considered at the beginning of every simulation trial. Then, in each SI dissemination period, t_d, the source/leader UAV generates the SI message containing the SI vector, $\mathbf{x}_n^r$, which will be disseminated to all UAVs within the formation by means of a particular MBP. In each controller sampling period, t_c, the mobility controller API is used to calculate the actuator control vector, $\mathbf{u}_k$, of each UAV based on its current estate vector, $\mathbf{x}_k$, and the latest SI, $\mathbf{x}_{\max(n)}^r$, successfully received.

As previously mentioned, this chapter studies the suitability of the different MBPs introduced in Section 2.3 when used for SI dissemination. The particular parameters used for each of the evaluated MBPs are provided in Table 3. These parameters were taken from (Lee et al., 2014) for Simple flooding, (Tseng et al., 2002) for DTh-Distance-Based, (Lee et al., 2014) for WT-Distance-Based, (Wisitpongphan et al., 2007) for Probabilistic-Based, and (Tseng et al., 2002) for C-Counter-Based. The values were chosen to avoid any bias in the evaluation.

Table 4. MBP parameters in the evaluation scenario.

MBP	Parameters
Simple Flooding	-
DTh-Distance-Based	$\{D = 135$ m, $RT \in \mathbb{N} \in [1,10]$ ms $\}$
WT-Distance-Based	$\{MaxWT = 10$ ms $\}$
Probabilistic-Based	$\{WT = 5$ ms, $\delta = 5$ ms $\}$
C-Counter-Based	$\{C = 3$, $RT \in \mathbb{N} \in [1,10]$ ms $\}$

To evaluate the performance of a particular MBP, the metrics described in Section 3.3 were calculated at the end of each simulation trial. Additionally, the results of a minimum of 2000 trials were averaged to achieve statistical significance. Furthermore, all metrics that are presented in the following section were obtained by considering that $t_d = t_c = 0.5$ s and a packet size of 512 bytes.

Note that because of the modular design of the FANET simulator, MBPs different from those described in Section 2.3 can be readily implemented for its evaluation.

4.2.1 Flight formation network topology

Flight formation determines the network topology. Thus, it is one of the most relevant factors to consider in the evaluation. To illustrate this, Figure 14 shows a single simulation run for an open-delta formation with $\lambda = 9$ and a delta formation with $\lambda = 15$. The sweep trajectory shown in Figure 14 was used with a reference speed of $v_r = 25\ m/s$. The SI messages were generated by the leader UAV every 500 ms and were disseminated using Simple Flooding.

As can be readily seen in Figure 14, the number of paths through which SI messages can reach UAVs in the last level of each formation can be very different for the open-delta and delta formations. This could lead to significant differences in the MBP performance evaluations. In addition, note in Figure 14 that two UAVs are lost when flying in open-delta formation, whereas none are lost when flying in delta formation. However, this result does not imply that for a delta formation with $v_r = 25\ m/s$ and $\lambda = 15$, Simple Flooding will enable the proper functioning of the UAV formation control strategy since Figure 14 only shows the results of a single simulation run. Thus, an extended analysis of how the performance of the MBPs affects the distributed UAV formation control strategy is provided next.

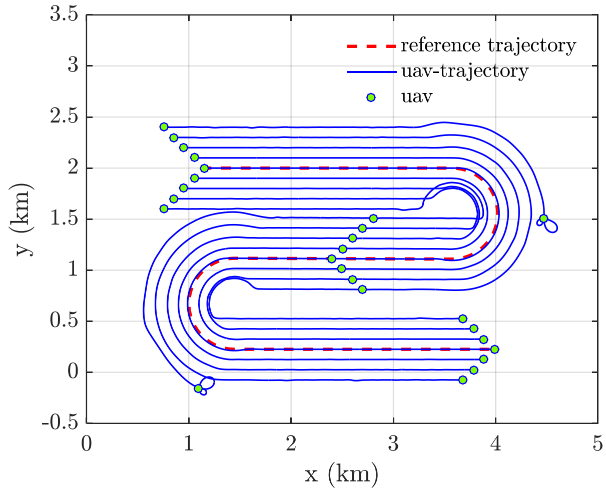

(a)

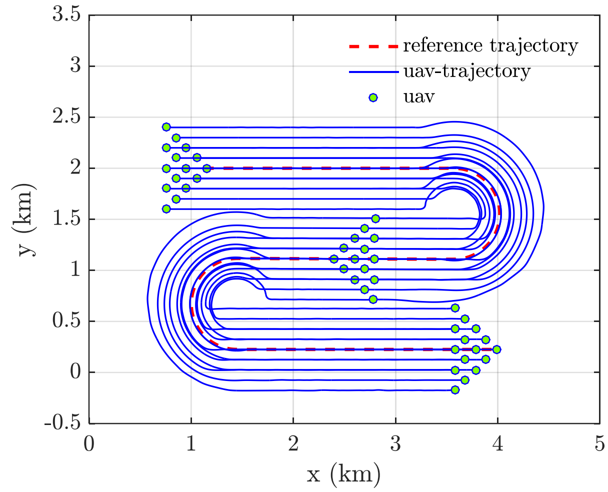

(b)

Figure 14. Examples of the UAV trajectories that are obtained when using Simple Flooding for SI dissemination in (a) open-delta and (b) delta formations. The sweep trajectory shown in Fig. 6 with a reference speed of $\boldsymbol{v_r} = \mathbf{25}$ m/s was assumed. The open-delta formation size was set to $\boldsymbol{\lambda} = \mathbf{9}$, and the delta formation size was set to $\boldsymbol{\lambda} = \mathbf{15}$.

4.3 MBP overall results

This section presents the performance evaluation of the MBPs under study considering open-delta and delta formations, two formation sizes, and different reference speeds for the mission. The metrics used for the evaluation are the P-RMSE, LU, PDR and $\mathrm{AvgSIage}_{\mathrm{L_m}}$ that were introduced in Section 3.3.

Figure 15 and Figure 16 show the P-RMSE and LU results obtained for the MBPs under evaluation for the open-delta formation and different reference speeds. In addition, Figure 16 shows the P-RMSE for the ideal protocol, i.e., all SI messages arrive on time to every UAV in the flight formation. In these figures, it can be seen that both the P-RMSE and the LU increase as the reference speed increases, especially from 22.5 m/s to 27.5 m/s. Some of this behavior can be attributed to factors related to the controller and the UAV flight dynamics since in the ideal case (red line) the P-RMSE increases with the speed as well. However, note how there are no lost UAVs in the ideal case, while when using MBPs, the LU metric increases significantly for 25 m/s and 27.5 m/s.

By closely examining Figure 15 and Figure 16, the following observations can be made:

- The P-RMSE and LU metrics are worse for the largest formation size. This is expected, because as the formation size increases, the number of hops needed to reach the UAVs that are located at the edge increases as well.

- In general, the worst performance is offered by the WT-Distance-Based protocol.

- Overall, for the high reference speeds (25 m/s and 27.5 m/s), the trajectory performances offered by the 135Th-Distance-Based and the 3-Counter-Based MBPs are better than the others.

- Simple Flooding seems to work well for low and medium speeds; however, as the speed increases, its trajectory performance worsens.

The average PDR and $\mathrm{AvgSIage}_{\mathrm{L_m}}$ for this setup are presented in Figure 17, Figure 18, and Figure 19. Only plots of $\mathrm{AvgSIage}_{\mathrm{L_m}}$ for the last two formation levels are provided in Figure 18 ($\lambda = 7$) and Figure 19 ($\lambda = 9$). The following observations can be made from these figures:

- The PDR and $\mathrm{AvgSIage}_{\mathrm{L_m}}$ are worse for $\lambda = 9$ (the largest formation size).

- For both $\lambda = 7$ and $\lambda = 9$, the WT-Distance-Based MBP provides the worst performance (the lowest PDR and highest $\mathrm{AvgSIage}_{\mathrm{L_m}}$).

- Simple Flooding provides a PDR and $\mathrm{AvgSIage}_{\mathrm{L_m}}$ that seem to be close to the best among the MBPs.

- The 135Th-Distance-Based and the 3-Counter-Based MBPs provide the best overall network performance.

- It seems that when the PDR is below 0.7 and the $\mathrm{AvgSIage}_{\mathrm{L_m}}$ is above 1, the LU metric increases significantly for all MBPs.

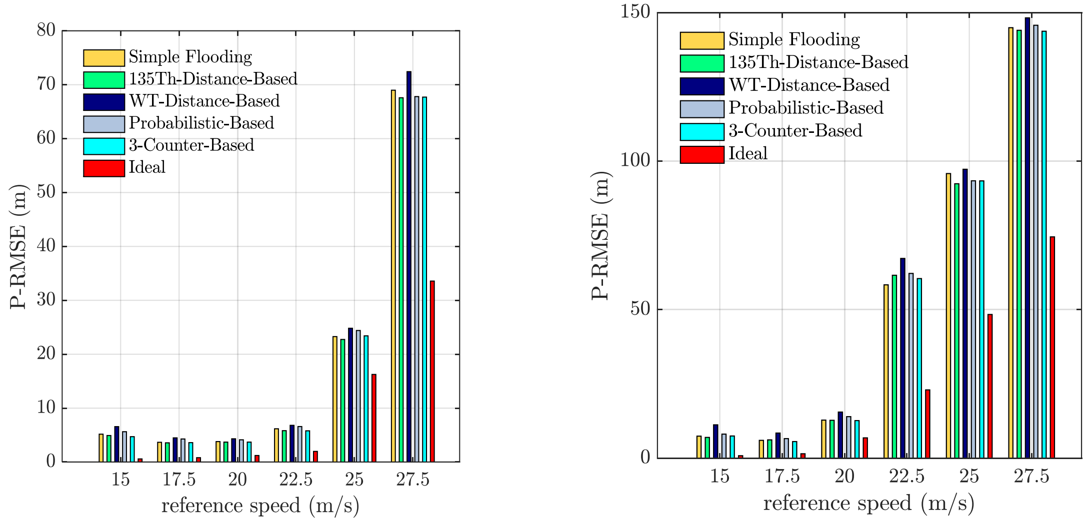

(a) (b)

Figure 15. P-RMSE obtained with different MBPs in a UAV mission using the open-delta formation with (a) $\boldsymbol{\lambda} = \mathbf{7}$ and (b) $\boldsymbol{\lambda} = \mathbf{9}$. The reference speed varies from $\boldsymbol{v_r} = \mathbf{15}$ to $\boldsymbol{v_r} = \mathbf{27.5}$ m/s. The results were obtained by averaging a minimum of 2000 runs to achieve statistical significance.

By analyzing the results presented in Figures. 15 to 19, it can be observed that, in general, there is a good correspondence between the trajectory performance metrics and the network performance metrics. That is, the MBPs that provide better network performance provide better trajectory performance for the open-delta formation. Particularly, the 135Th-Distance-Based and the 3-Counter-Based MBPs exhibited the best trajectory and network performances overall. Note that these protocols use a random waiting time before a rebroadcast attempt, and the probability of canceling a packet rebroadcast is low for the evaluation scenario that is considered. Also, observe that Simple Flooding does not provide the worst performance. Thus, the results allow to infer that the best option for open-delta formations is to use MBPs where: a) the probability of canceling packet rebroadcasts is low (but not necessarily equal to zero as in Simple Flooding); and b) the PDR is high and the $\mathrm{AvgSIage}_{\mathrm{L_m}}$ is low.

Continuing with the analysis of the results provided in Figures. 15 to 19, note that at high speeds the trajectory and network metrics do not show the same tendencies for the WT-Distance-Based, the Simple Flooding, and the Probabilistic-Based MBPs. For example, for $\lambda = 7$ and $v_r = 27.5$ m/s, the protocols with the worst trajectory metrics are WT-Distance-Based and Simple Flooding. However, for these values, the protocols providing the worst network metrics are the WT-Distance-Based followed by the Probabilistic-Based. In this sense, note that when the formation enters and leaves a turn, the network topology could change. Thus, in order to explain this behavior, an in-deep analysis of the evolution of the metrics through the trajectory is provided in the next section.

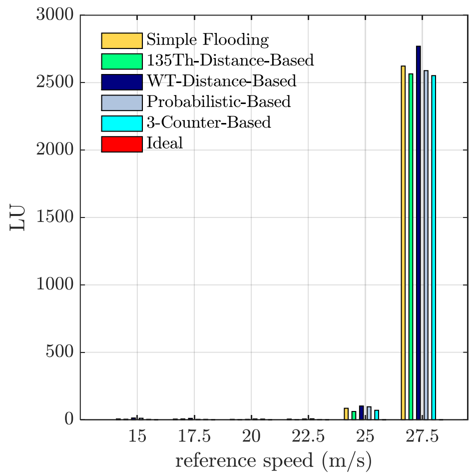

(a)

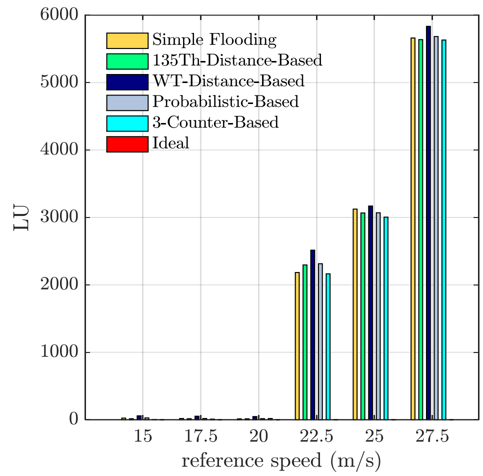

(b)

Figure 16. LU (lost UAVs) metric obtained with different MBPs in a UAV mission using the open-delta formation with (a) $\boldsymbol{\lambda = 7}$ and (b) $\boldsymbol{\lambda = 9}$. The reference speed varies from $\boldsymbol{v_r = 15}$ to $\boldsymbol{v_r = 27.5}$ m/s. The results were obtained by averaging a minimum of 2000 runs to achieve statistical significance.

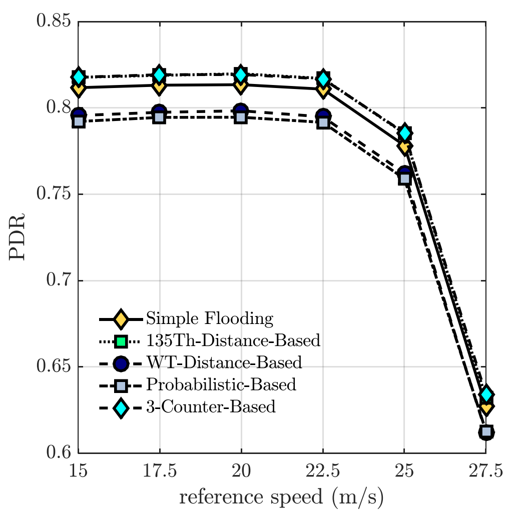

(a)

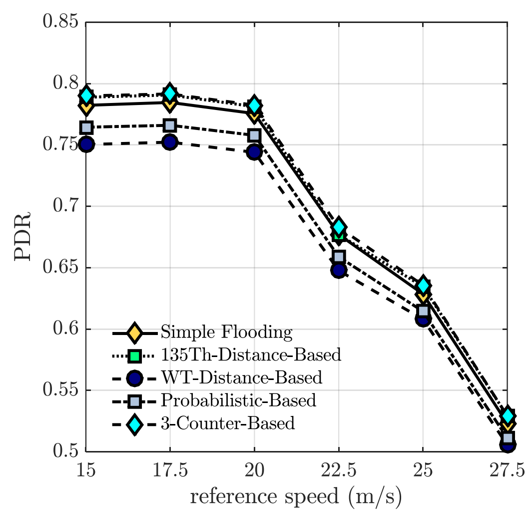

(b)

Figure 17. PDR obtained with different MBPs in a UAV mission using the open-delta formation with (a) $\boldsymbol{\lambda = 7}$ and (b) $\boldsymbol{\lambda = 9}$. The reference speed varies from $\boldsymbol{v_r = 15}$ to $\boldsymbol{v_r = 27.5}$ m/s. The results were obtained by averaging a minimum of 2000 runs to achieve statistical significance.

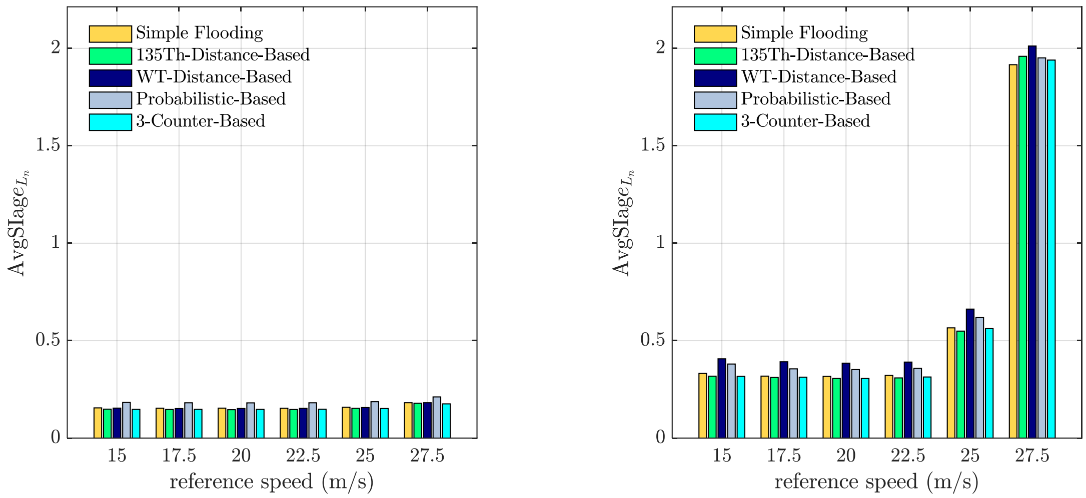

(a) (b)

Figure 18. $\mathbf{AvgSIage_{L_m}}$ obtained with different MBPs in a UAV mission using the open-delta formation with $\boldsymbol{\lambda = 7}$ for (a) $\boldsymbol{L_3}$ and (b) $\boldsymbol{L_4}$. The reference speed varies from $\boldsymbol{v_r = 15}$ to $\boldsymbol{v_r = 27.5}$ m/s. The results were obtained by averaging a minimum of 2000 runs to achieve statistical significance.

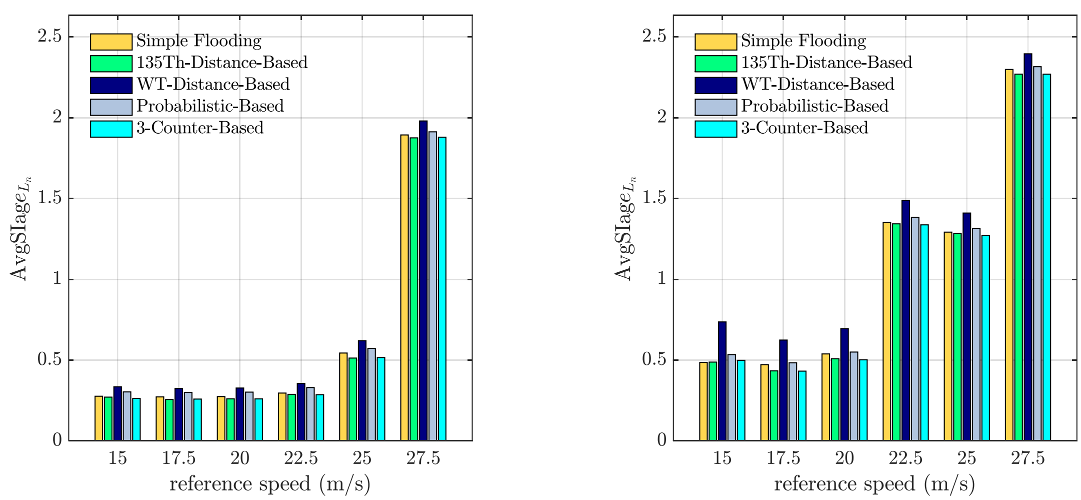

(a) (b)

Figure 19. $\mathbf{AvgSIage_{L_m}}$ obtained with different MBPs in a UAV mission using the open-delta formation with $\boldsymbol{\lambda = 9}$ for (a) $\boldsymbol{L_4}$ and (b) $\boldsymbol{L_5}$. The reference speed varies from $\boldsymbol{v_r = 15}$ to $\boldsymbol{v_r = 27.5}$ m/s. The results were obtained by averaging a minimum of 2000 runs to achieve statistical significance.

Figure 20 and Figure 21 show the P-RMSE and LU results obtained for the MBPs under evaluation for the delta formation and different reference speeds. In these figures, it can be seen that both the P-RMSE and LU increase as the reference speed increases (particularly from 25 m/s to 27.5 m/s). As in the open-delta formation, some of this behavior can be attributed to factors related to the controller and the UAV flight dynamics. Similar to the open-delta formation, there are no lost UAVs in the ideal case. However, when using MBPs, the LU metric increases significantly for 25 m/s and 27.5 m/s (especially for the largest formation size). Nevertheless, note that the trajectory metrics obtained for the delta formation are better than those obtained for the open-delta formation.

By closely examining Figure 20 and Figure 21, the following observations can be made:

- Overall, the worst performance is obtained when using the WT-Distance-Based protocol (as with the open-delta formation).

- For low (15 m/s and 17.5 m/s) to medium (20 m/s and 22.5 m/s) reference speeds, the performance of all MBPs is similar, except for the WT-Distance-Based protocol.

- The P-RMSE and LU metrics are the worst for larger formation sizes, as expected.

- The 135Th-Distance-Based protocol seems to work well for $\lambda = 10$ at low and medium speeds. However, as the speed increases to 27.5 m/s, its performance worsens (see the LU metric in Figure 21).

- For $\lambda = 15$, the performance drop exhibited by 135Th-Distance-Based as the speed increases is notorious. Furthermore, its performance at 27.5 m/s is even worse than that provided by WT-Distance-Based.

- The Probabilistic-Based protocol seems to provide the best trajectory performance overall.

- The P-RMSE and LU metrics are better for the delta formation than for the open-delta formation.

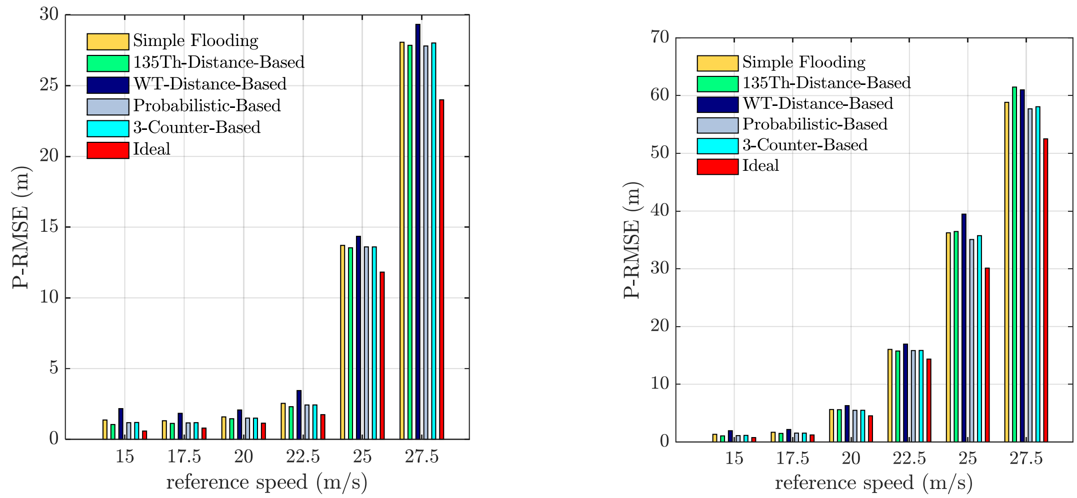

(a) (b)

Figure 20. P-RMSE obtained with different MBPs in a UAV mission using the delta formation with (a) $\boldsymbol{\lambda = 10}$ and (b) $\boldsymbol{\lambda = 15}$. The reference speed varies from $\boldsymbol{v_r = 15}$ to $\boldsymbol{v_r = 27.5}$ m/s. The results were obtained by averaging a minimum of 2000 runs to achieve statistical significance.

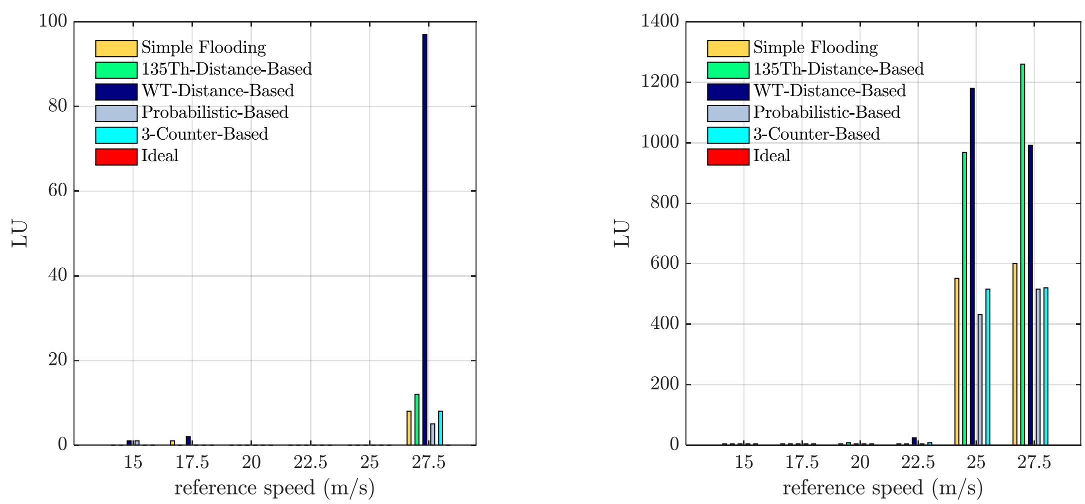

(a) (b)

Figure 21. LU (lost UAVs) metric obtained with different MBPs in a UAV mission using the delta formation with (a) $\boldsymbol{\lambda = 10}$ and (b) $\boldsymbol{\lambda = 15}$. The reference speed varies from $\boldsymbol{v_r = 15}$ to $\boldsymbol{v_r = 27.5}$ m/s. The results were obtained by averaging a minimum of 2000 runs to achieve statistical significance.

The average PDR and $\mathrm{AvgSIage}_{\mathrm{L_m}}$ for this setup are presented in Figure 22, Figure 23, and Figure 24. Only plots of $\mathrm{AvgSIage}_{\mathrm{L_m}}$ for the last two formation levels are provided in Figure 23 ($\lambda = 10$) and Figure 24 ($\lambda = 15$). The following observations can be made from these figures:

- For both formation sizes ($\lambda = 10$ and $\lambda = 15$), WT-Distance-Based exhibits the worst performance (lowest PDR and higher $\mathrm{AvgSIage}_{\mathrm{L_m}}$).

- For low (15 m/s and 17.5 m/s) to medium (20 m/s and 22.5 m/s) reference speeds, the 135Th-Distance-Based and the Probabilistic-Based MBPs exhibit the best PDR and $\mathrm{AvgSIage}_{\mathrm{L_m}}$ metrics.

- For high reference speeds (25 m/s and 27.5 m/s), the network performance of 135Th-Distance-Based worsens. The performance decrease is particularly sharp for the larger $\lambda = 15$.

- In contrast, for high reference speeds (25 m/s and 27.5 m/s) and $\lambda = 15$, the Probabilistic-Based MBP exhibits the best network performance.

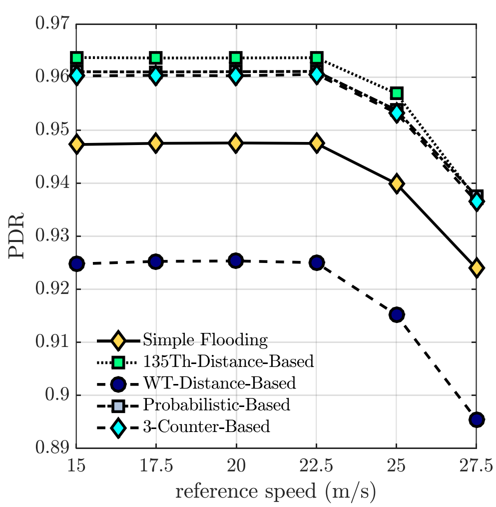

(a)

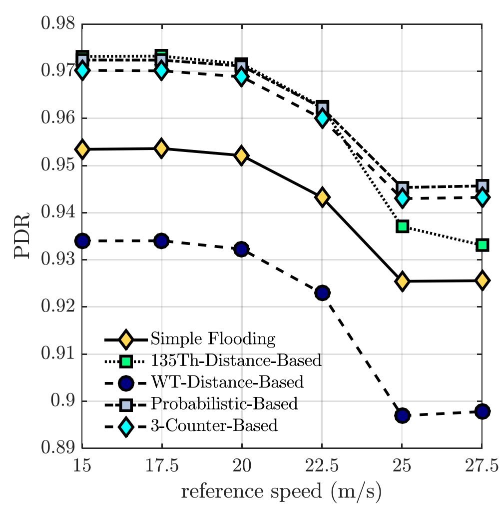

(b)

Figure 22. PDR obtained with different MBPs in a UAV mission using the delta formation with (a) $\boldsymbol{\lambda = 10}$ and (b) $\boldsymbol{\lambda = 15}$. The reference speed varies from $\boldsymbol{v_r = 15}$ to $\boldsymbol{v_r = 27.5}$ m/s. The results were obtained by averaging a minimum of 2000 runs to achieve statistical significance.

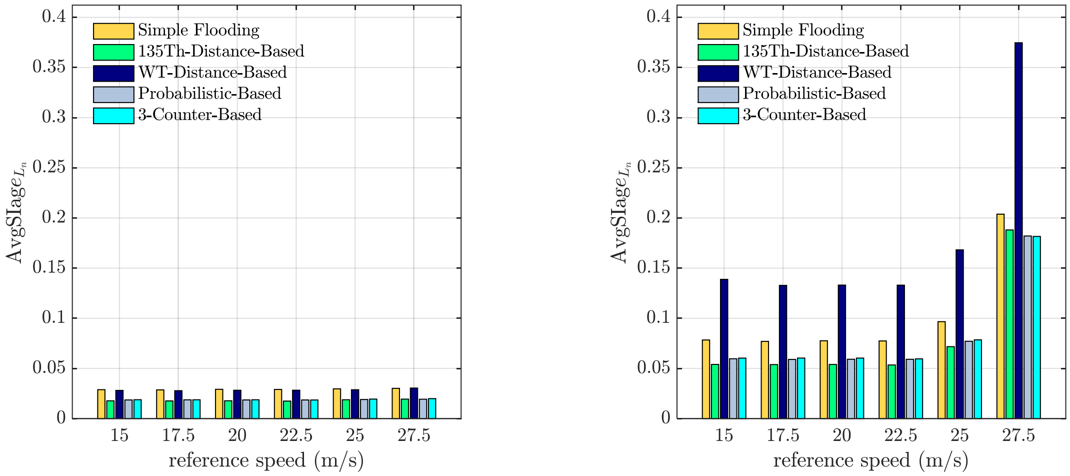

(a)

(b)

Figure 23. $\mathbf{AvgSIage_{L_m}}$ obtained with different MBPs in a UAV mission using the delta formation with $\boldsymbol{\lambda = 10}$ for (a) $\boldsymbol{L_3}$ and (b) $\boldsymbol{L_4}$. The reference speed varies from $\boldsymbol{v_r = 15}$ to $\boldsymbol{v_r = 27.5}$ m/s. The results were obtained by averaging a minimum of 2000 runs to achieve statistical significance.

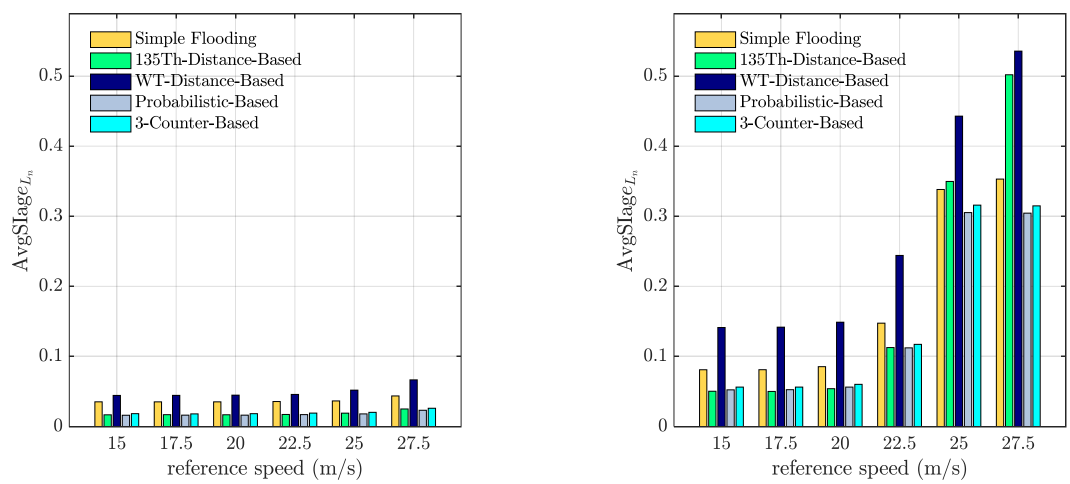

(a)

(b)

Figure 24. $\mathbf{AvgSIage_{L_m}}$ obtained with different MBPs in a UAV mission using the delta formation with $\boldsymbol{\lambda = 15}$ for (a) $\boldsymbol{L_4}$ and (b) $\boldsymbol{L_5}$. The reference speed varies from $\boldsymbol{v_r = 15}$ to $\boldsymbol{v_r = 27.5}$ m/s. The results were obtained by averaging a minimum of 2000 runs to achieve statistical significance.

By analyzing the results presented in Figure 20 to Figure 24, it can be observed that, as with the open-delta formation, in general, there is a good correspondence between the trajectory performance metrics and the network performance metrics. However, there are significant differences in the performance offered by different MBPs when the UAVs fly in delta formation compared to the performance observed for the open-delta formation. In particular, the Probabilistic-Based protocol seems to provide the best trajectory performance overall for the delta formation, which is not the case for the open-delta formation. In this sense, note that, compared to the open-delta formation, the delta formation is a denser network where each node has at least two neighbors at the beginning of the flight mission. This is an important observation since MBPs are usually designed to work over dense scenarios, such as those found in VANETs deployments. In particular, it is commonly assumed that denser networks are more challenging for MBPs. Thus, at first sight, the obtained results seem to be counterintuitive. However, it should be noted that, when compared with common ad-hoc scenarios, delta and open-delta formations are low-density scenarios. Therefore, in the evaluation scenario, the obtained results should be analyzed while considering connectivity issues. In this sense, UAVs flying in a delta formation will have higher connectivity compared to UAVs flying in an open-delta formation. This means that a UAV flying in a delta formation has more nodes within reach from which it can receive or relay packets, which in low-density scenarios can lead to improving the PDR but also to more collisions compared to the open-delta formation.

Considering that more collisions can occur in delta formations than in open-delta formations, it is worthwhile to calculate a “collision ratio” (CR) as a metric to compare the cost of the PDR achieved by each MBP under evaluation. In particular, in this thesis work, the CR is calculated by counting the total number of collisions that occur during a simulation trial and then dividing the result by the total number of packets that are sent by the leader UAV. Figure 25 shows the CR obtained for the different MBPs under evaluation for the delta formation. Note that WT-Distance-Based has the lowest CR followed by Probabilistic-Based. However, the WT-Distance-Based has the lowest PDR, which helps to explain why the trajectory performance offered by the Probabilistic-Based MBP is better. Furthermore, by observing Figures 22 to 24, it can be concluded that the Probabilistic-Based MBP offers a better tradeoff between the PDR, $\mathrm{AvgSIage}_{\mathrm{L_m}}$, and CR compared to the other MBPs under evaluation, particularly for high speeds and $\lambda = 15$. This, in turn, translates to better trajectory performance, as observed in Figures 20 to 21.

Although the previous analysis may help to explain why the Probabilistic-Based MBP provides the best trajectory metrics at high speeds, no conclusion can be made about why the 135Th-Distance-Based MBP shows the performance drop at high speeds (25 m/s and 27.5 m/s). In that sense, it is worth recalling that, except for Simple Flooding, all protocols under evaluation include mechanisms that cancel packet retransmissions when a certain criterion is fulfilled. Therefore, in addition to collisions, a distant node might not receive an SI packet because of a rebroadcast cancellation. However, for the proper functioning of the formation control strategy, it is necessary to periodically receive the SI that is generated by the leader UAV. Thus, it is worthwhile to calculate the percentage of packet rebroadcasts that are canceled (PRC) by each MBP under evaluation. The PRC is shown in Figure 26. Note how WT-Distance-Based cancels more packet rebroadcasts for this scenario than the other MBPs. This further explains why WT-Distance-Based exhibits the worst trajectory metrics. Nevertheless, note how the second MBP that cancels more rebroadcasts is 135Th-Distance-Based. This helps to explain why at high speeds this protocol has a significant performance drop, especially for $\lambda = 15$.

The PRC plot helps to explain the trajectory performance drop that is observed when using the 135Th-Distance-Based MBP for $\lambda = 15$. However, the trajectory performance exhibited by 135Th-Distance-Based is even worse for $v_r = 27.5$ than that obtained when using WT-Distance-Based (see Figure 21(b)). Therefore, to gain more insight into this behavior, an in-deep analysis of the evolution of the metrics through the trajectory is provided in the next section.

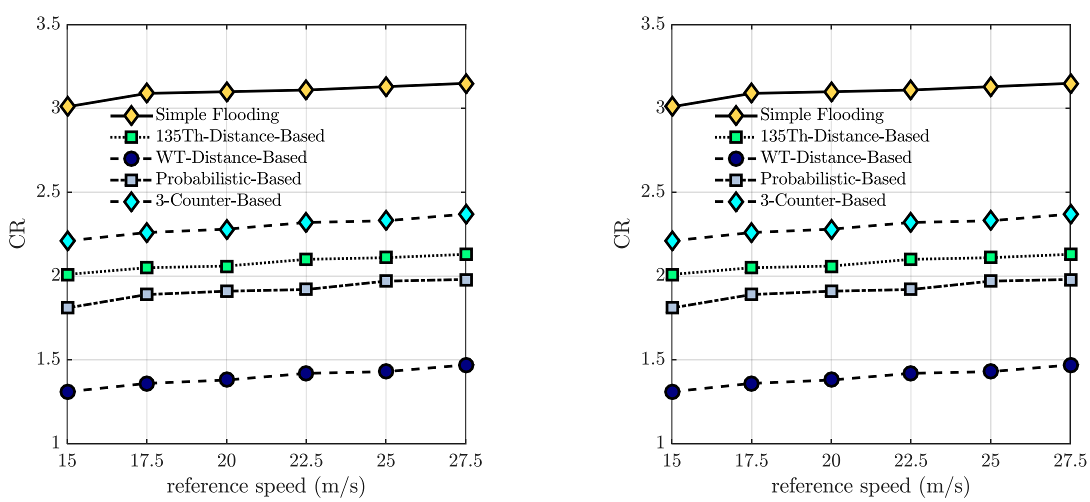

(a) (b)

Figure 25. Collision ratio (CR) obtained with different MBPs in a UAV mission using the delta formation with (a) $\boldsymbol{\lambda} = \mathbf{10}$ and (b) $\boldsymbol{\lambda} = \mathbf{15}$. The reference speed varies from $\boldsymbol{v_r} = \mathbf{15}$ to $\boldsymbol{v_r} = \mathbf{27.5}$ m/s. The results were obtained by averaging a minimum of 2000 runs to achieve statistical significance. The CR is calculated by counting the total number of collisions that occurred during the simulation and dividing that by the total number of source packets that are sent by the leader UAV.

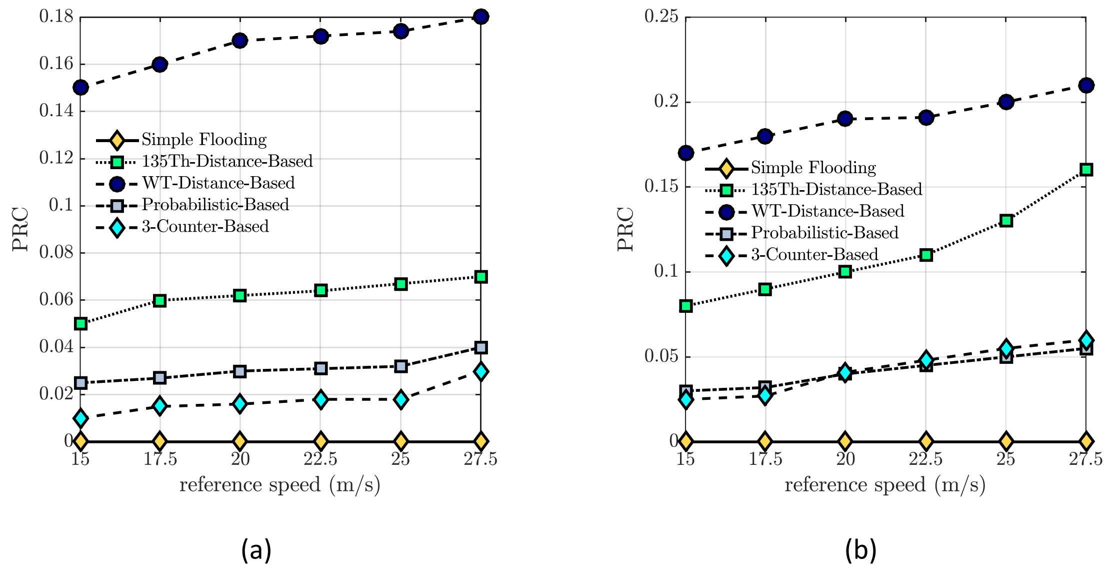

Figure 26. Percentage of packet rebroadcasts that are canceled (PRC) obtained with different MBPs in a UAV mission using the delta formation with (a) $\boldsymbol{\lambda = 10}$ and (b) $\boldsymbol{\lambda = 15}$. The reference speed varies from $\boldsymbol{v_r = 15}$ to $\boldsymbol{v_r = 27.5}$ m/s. The results were obtained by averaging.

4.4 Results by segments

In this section, an analysis considering the time evolution of the evaluation metrics is presented. Specifically, the sweep trajectory considered in the previous sections was divided into seven segments, as shown in Figure 27.

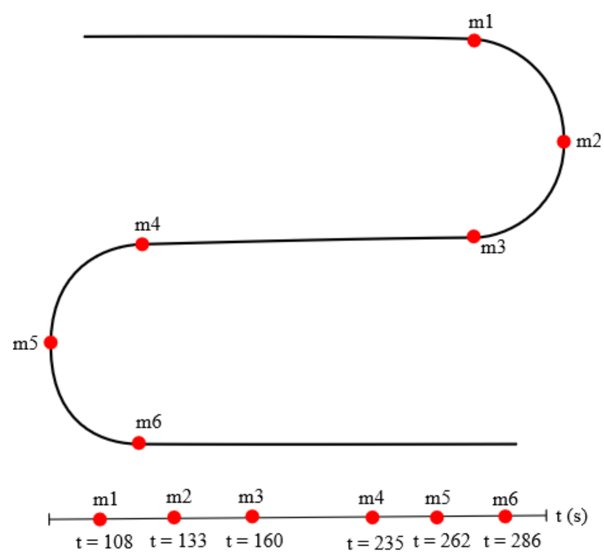

Figure 27. Reference trajectory considering its segments.

This analysis aims to track the evolution of the network metrics as the UAV formation follows the reference trajectory. To this end, the network metrics were calculated using a moving average of 10 sample periods. In this way, fast fluctuations in the performance metrics are smoothed, and good insights into the evolution of the metrics can be achieved. In addition to the network metrics used in the previous section, the burst average length (BAL) of the losses (see Section 3.3.2) is considered in the analysis.

Figure 28 shows the moving average P-RMSE obtained for the different MBPs under evaluation for the delta formation with $\lambda = 10$ and $v_r = 27.5$ m/s. For this figure, only the UAVs from the third level or higher were considered for the P-RMSE calculation. The P-RMSE is presented considering the segments shown in Figure 27. It can be seen in Figure 28 that, in general, the moving average P-RMSE of all MBPs increases as the UAVs make the turn (segments $m_1 - m_2 - m_3$ and $m_4 - m_5 - m_6$) and decreases when UAVs exit from it.

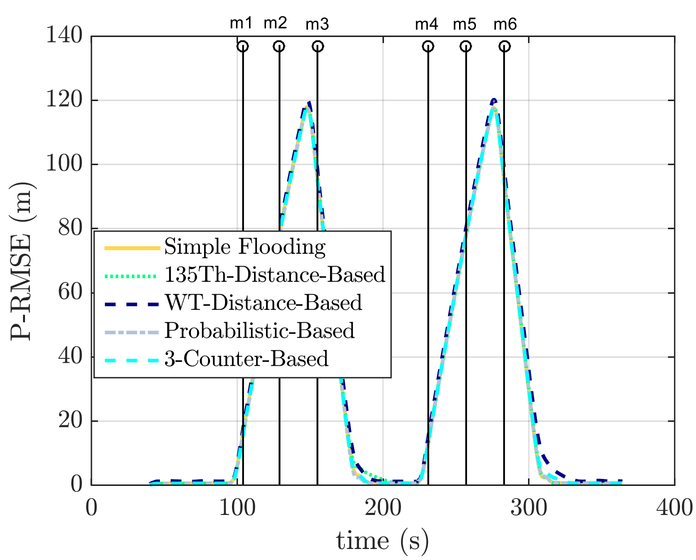

Figure 28. Moving average P-RMSE obtained when SI messages are disseminated with the different MBPs considered. For this figure, UAVs fly in delta formation with a reference speed=27.5 m/s and λ=10. The results at each sampling period were obtained using the average of a minimum of 2000 runs to achieve statistical significance. Only the UAVs from the third level or higher were considered for this figure.

Note that the P-RMSE behavior observed in Figure 28 agrees with the results of Figure 20(a) in the sense that the WT-Distance-Based MPB provides a slightly worse P-RMSE performance than the other MBPs. However, note that the behavior observed in the moving average P-RMSE does not fully explain the LU metric results shown in Figure 21(a) where the performance of WT-Distance-Based is significantly worse than the rest. The reason for this is because once a UAV is definitively lost, it is no longer considered for the P-RMSE calculation.

Furthermore, considering the wireless propagation phenomena, it is reasonable to infer that UAVs that are closer to the leader consistently have better probabilities of successful packet reception. Thus, considering these nodes in the metric calculation in scenarios with a low number of UAVs might bias the average. Therefore, the following analysis is focused on UAVs flying at the edges of the last formation level, which are more prone to experience challenging network conditions, e.g., disconnections, and fewer neighbors.

To further analyze the LU metric behavior observed in Figure 21(a) for $\lambda = 10$ and $v_r = 27.5$ m/s, the moving average PDR for the UAVs flying at the formation edges is shown in Figure 29. In particular, Figure 29(a) shows the moving average PDR of the UAV that is located in the south-west edge of the formation (referred to the rotated coordinate system $X_r O_r Y_r$ shown in Figure 7) and labeled UAV7. Similarly, Figure 29(b) shows the moving average PDR of the UAV that is located in the south-east edge of the formation and labeled UAV10.

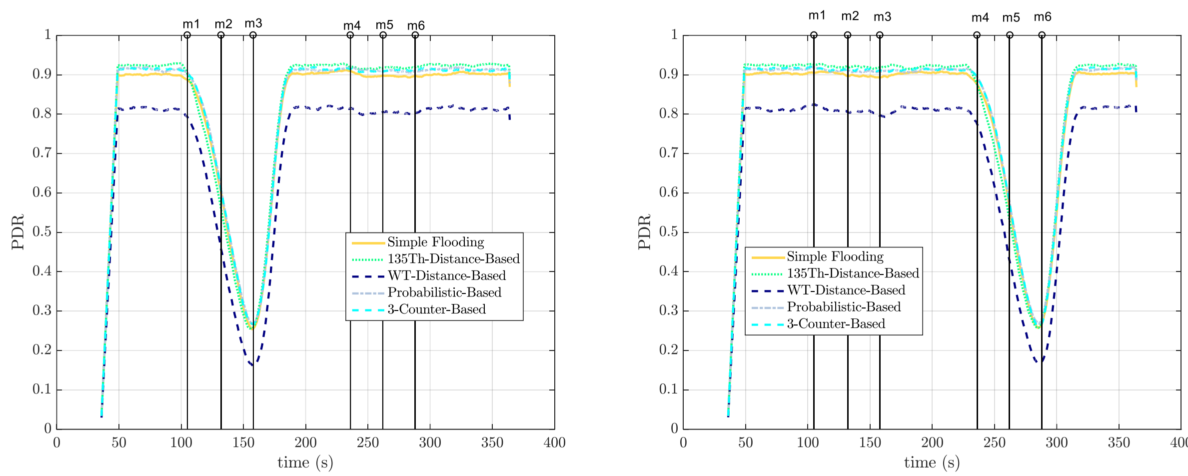

(a) (b)

Figure 29. Moving average PDR obtained when SI messages are disseminated with the different MBPs considered. For this figure, UAVs fly in delta formation with a reference speed=27.5 m/s and λ=10. Only the UAVs that are located at the (a) south-west (UAV7) and (b) south-east (UAV10) edges of the formation were considered for the calculations. The results at each sampling period were obtained using the average of a minimum of 2000 runs to achieve statistical significance.

Note in Figure 29 how the PDR significantly decays for UAV7 when it makes the first turn ($m_1 - m_2 - m_3$), while for UAV10 the PDR decays when it makes the second turn ($m_4 - m_5 - m_6$). Thus, the PDRs of UAV7 and UAV10 decay when they make a turn and are located at the outside of the curve while following the reference trajectory of Figure 27. Following the analysis, Figure 30 and Figure 31 show the moving average $\mathrm{AvgSIage}$ and BAL for UAV7 and UAV10. As with the PDR, both metrics significantly worsen when the corresponding UAV makes a turn and is located at the outside of a curve in the trajectory.

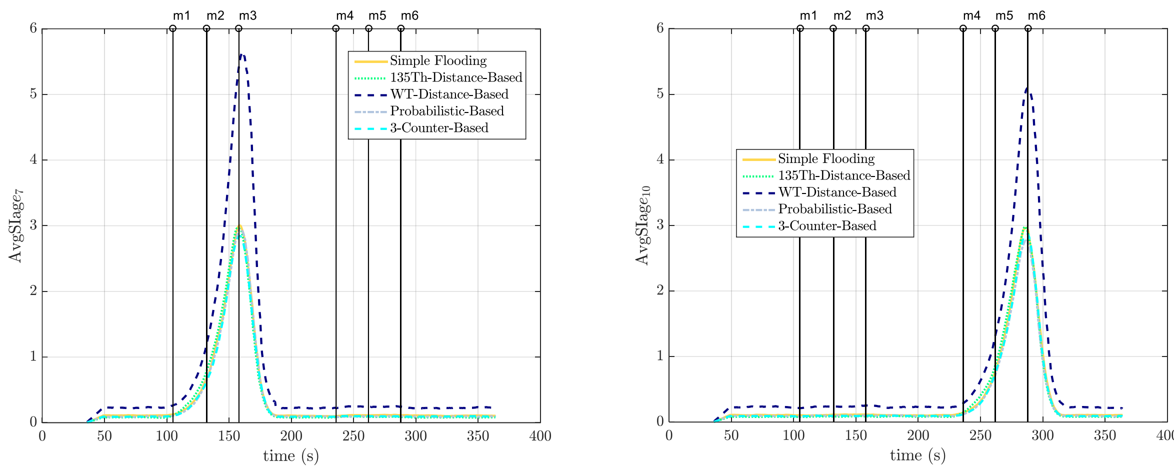

(a) (b)

Figure 30. Moving average $\mathbf{AvgSIage}$ obtained when SI messages are disseminated with the different MBPs considered. For this figure, UAVs fly in delta formation with a reference speed=27.5 m/s and λ=10. Only the UAVs that are located at the (a) south-west (UAV7) and (b) south-east (UAV10) edges of the formation were considered for the calculations. The results at each sampling period were obtained using the average of a minimum of 2000 runs to achieve statistical significance.

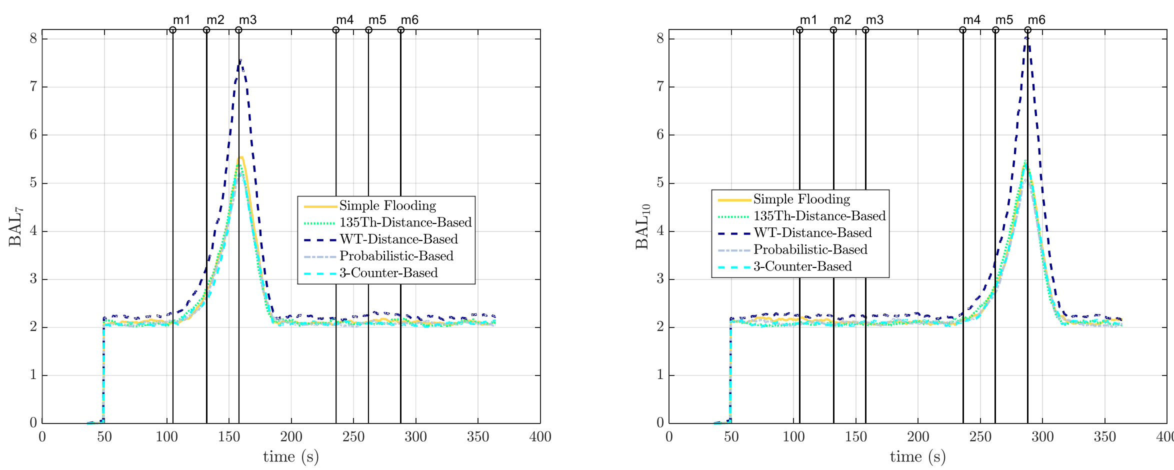

(a) (b)

Figure 31. Moving average burst average length (BAL) obtained when SI messages are disseminated with the different MBPs considered. For this figure, only burst lengths higher than 1 were considered; and UAVs fly in delta formation with a reference speed=27.5 m/s and λ=10. Only the UAVs that are located at the (a) south-west (UAV7) and (b) south-east (UAV10) edges of the formation were considered for the calculations. The results at each sampling period were obtained using the average of a minimum of 2000 runs to achieve statistical significance.

By closely analyzing the moving average PDR, AvgSIage and BAL results provided in Figure 29 to Figure 31, respectively, the following observations can be made regarding the network performance offered to the UAVs that are located at the formation edges (UAV7 and UAV10):

- The performance of all MBPs is worse at turns.

- The WT-Distance-Based protocol consistently provides the worst network performance. In addition, it is the MBP that is most affected by network conditions at turns.

- AvgSIage metric indicates that while following a straight line path, on average, the controller uses recent SI at every sampling time. However, as the formation enters the curve, the AvgSIage increases, which can be caused by significant delays or packet drops. This is particularly acute for the WT-Distance-based protocol since at one point the SI that is used by the controller can be older than 5 sampling periods on average. In contrast, for the other MBPs, the AvgSIage is below 3 sampling periods. This helps to explain why when using WT-Distance-based, more UAVs are lost.

- The BAL metric indicates that when using the WT-Distance-based protocol, the BAL is larger than for the others MBPs.

- By comprehensively analyzing the PDR, AvgSIage and BAL metrics shown in Figure 29 to Figure 31, respectively, it can be inferred that, in addition to physical link disconnections, the multi-hop broadcast approach of WT-Distance-based induces significant SI dissemination delays and packet losses such that the controller effectiveness at keeping UAV7 and UAV10 within the formation is lost in the curves.

Continuing with the analysis of the results by segments, Figure 32 shows the moving average P-RMSE obtained for the different MBPs under evaluation for a delta formation with $\lambda = 15$ and $v_r = 27.5$ m/s. For this figure, only the UAVs from the third level or higher where considered for the P-RMSE calculation. The P-RMSE is presented considering the segments shown in Figure 27. As in Figure 28, it can be seen in Figure 32 that the P-RMSE increases as the formation makes a turn and decreases when the formation exits from it. Different from the case with $\lambda = 10$, for $\lambda = 15$, the P-RMSE provided by the 135Th-Distance-Based protocol at the turns is slightly worse than that obtained when using the other MBPs.

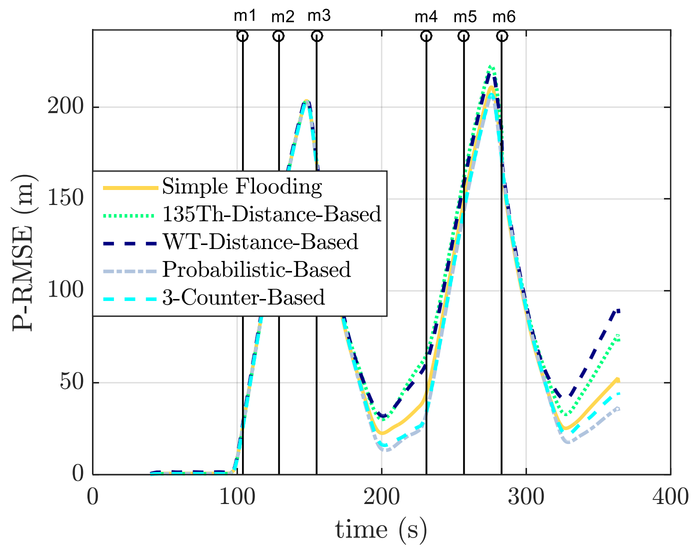

Figure 32. Moving average P-RMSE obtained when SI messages are disseminated with the different MBPs considered. For this figure, UAVs fly in delta formation with a reference speed=27.5 m/s and λ=15. The results at each sampling period were obtained using the average of a minimum of 2000 runs to achieve statistical significance.

Continuing with the analysis performed for $\lambda = 15$ and $v_r = 27.5$ m/s, Figure 33 to Figure 35 show the moving average PDR, AvgSIage, and BAL for UAVs flying at the formation edges for a delta formation with $\lambda = 15$ and $v_r = 27.5$ m/s. For these figures, the network metrics were calculated with a moving average of 10 sample periods. Similar to the previous case, the UAV that is located at the south-west edge of the formation is labeled as UAV11, and the UAV that is flying at the south-east edge of the formation is labeled as UAV15.

Note in Figure 33 to Figure 35 that, for all MBPs under evaluation, the network performance for UAV11 and UAV15 worsens as the formation makes a turn ($m_1 - m_2 - m_3$ or $m_4 - m_5 - m_6$). However, different from the delta formation with $\lambda = 10$, for the case under analysis, the worst performance at the turns is provided by the 135Th-Distance-Based protocol instead of the WT-Distance-Based MBP. This explains the P-RMSE and LU metrics results shown in Figure 21(b) and Figure 22(b), respectively, where the 135Th-Distance-Based MBP provides the larger P-RMSE and LU for $\lambda = 15$ and $v_r = 27.5$ m/s.

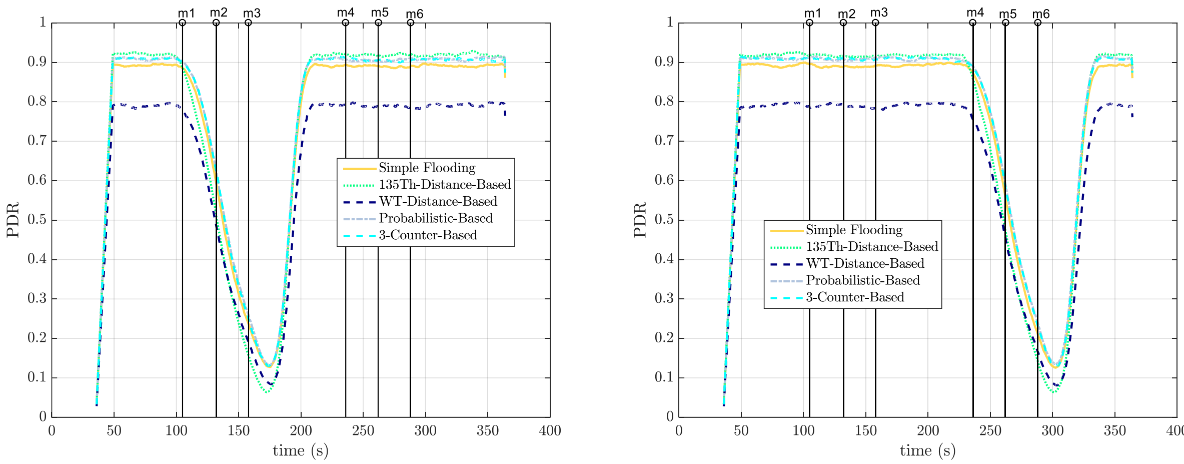

(a) (b)

Figure 33. Moving average PDR obtained when SI messages are disseminated with the different MBPs considered. For this figure, UAVs fly in delta formation with a reference speed=27.5 m/s and λ=15. Only the UAVs that are located at the (a) south-west (UAV11) and (b) south-east (UAV15) edges of the formation were considered for the calculations. The results at each sampling period were obtained using the average of a minimum of 2000 runs to achieve statistical significance.

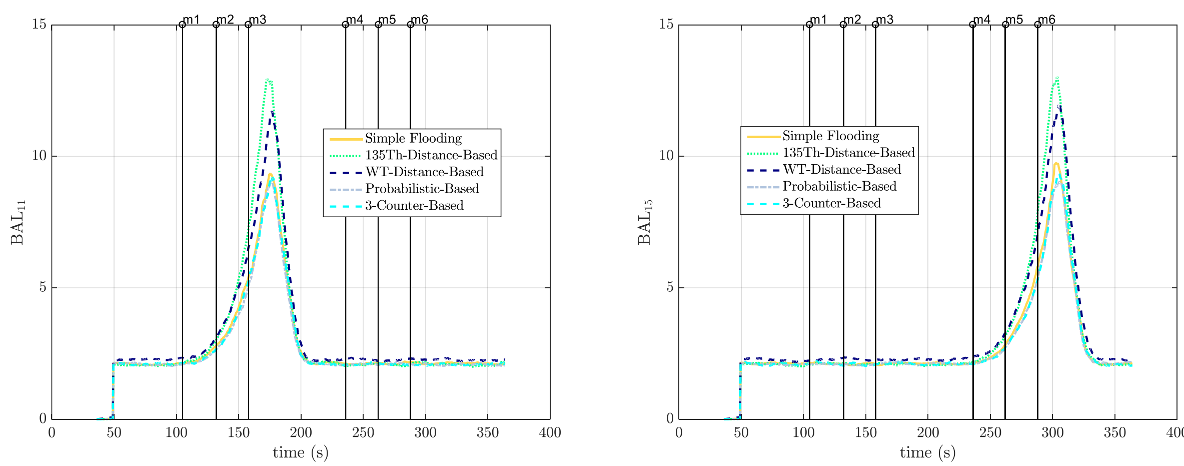

(a) (b)

Figure 34. Moving average **AvgSIage** obtained when SI messages are disseminated with the different MBPs considered. For this figure, UAVs fly in delta formation with a reference speed=27.5 m/s and λ=15. Only the UAVs that are located at the (a) south-west (UAV11) and (b) south-east (UAV15) edges of the formation were considered for the calculations. The results at each sampling period were obtained using the average of a minimum of 2000 runs to achieve statistical significance.

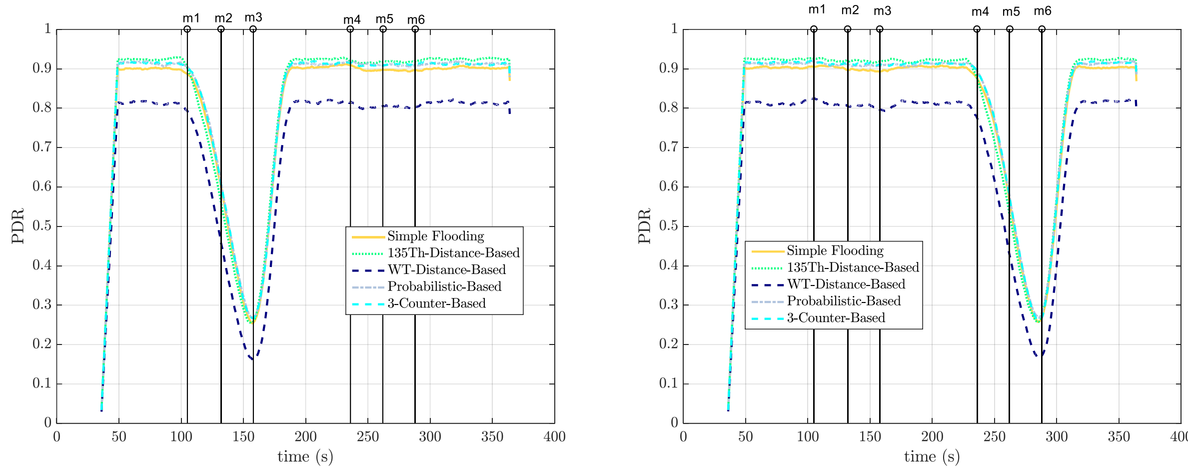

(a) (b)

Figure 35. Moving average burst average length (BAL) obtained when SI messages are disseminated with the different MBPs considered. For this figure, only burst lengths higher than 1 were considered; and UAVs fly in delta formation with a reference speed=27.5 m/s and λ=15. Only the UAVs that are located at the (a) south-west (UAV11) and (b) south-east (UAV15) edges of the formation were considered for the calculations. The results at each sampling period were obtained using the average of a minimum of 2000 runs to achieve statistical significance.

In summary, for the UAVs that are located at the south-west and south-east edges of a delta formation, the network performance provided by the different MBPs is acceptable while flying on straight lines. However, Figure 28 to Figure 35 show that the performance significantly worsens at turns when the UAV is located at the outside of the trajectory curve. Although the performance drop is experienced by all MBPs under evaluation, it is important to note that for $\lambda = 10$, the worst network performance at curves is provided by the WT-Distance-Based protocol, while for $\lambda = 15$, the worst network performance is obtained when using the 135Th-Distance-Based MBP. This is a very important observation since it explains the changes in the trajectory performance (i.e., P-RMSE and LU) offered by both protocols when λ increases from 10 to 15 (see Figure 21 and Figure 22). Furthermore, note how the trajectory performance is mainly affected by the network performance the nodes that are located at the formation edges. Thus, the network performance metrics that are traditionally calculated by averaging over all nodes (e.g., Figure 22 to Figure 24) within an ad-hoc network deployment (e.g., MANETs and VANETs) cannot be used to fully explain the behavior observed in the trajectory metrics (Figure 21 and Figure 22). Therefore, for UAV formation control applications, the results presented in this section underline the importance of the trajectory path and time evolution analysis proposed in this thesis work to evaluate the MBPs suitability for SI dissemination.

4.5 Case study

As mentioned in the introduction, remote sensing is one of the main applications for multi-UAV systems, e.g., [14], [15], [53], [54], and [56]–[58]. In a remote sensing multi-UAV mission, each UAV captures a series of images (e.g., in the visible light, near infrared or mid-infrared bands) with a high spatial resolution while flying in formation over a predefined area. Then, the images from all UAVs must be stitched together to obtain the full image of the area of interest and post-processing is performed to extract the desired information, e.g., vegetation indexes. Thus, maintaining a flight formation is crucial in order to be able to cover the desired imaging area with a single flight multi-UAV mission. As such, to further show the relevance of the study performed in this thesis work, an example of the suitability of the MBPs to disseminate SI messages while performing a multi-UAV imaging remote sensing mission is presented next.

In imaging remote sensing missions, important parameters such as the camera footprint of each UAV or sensing area can be related to flight formation parameters such as the longitudinal and lateral distances between neighbor nodes. Figure 36 depicts this relationship where the flight formation and overlap parameters (e.g., the overlap between neighboring sensing areas) are shown. The parameters considered for this application example were extracted from existing literature, e.g., [57] and [58], and are shown in Table 5 with their corresponding value.

For each simulation run, a mission is considered to be successful if none of the UAVs in the formation leave the sweep area shown in Figure 36 during the entire mission. Note that the area itself moves following the reference point during the mission execution. Figure 37 to Figure 39 show the number of missions successfully completed with the considered MBPs as the reference speed, v_r, increases when UAVs fly in open-delta and delta formations. The formation size λ ranges from small (Figure 37) to large (Figure 39) for each formation type.

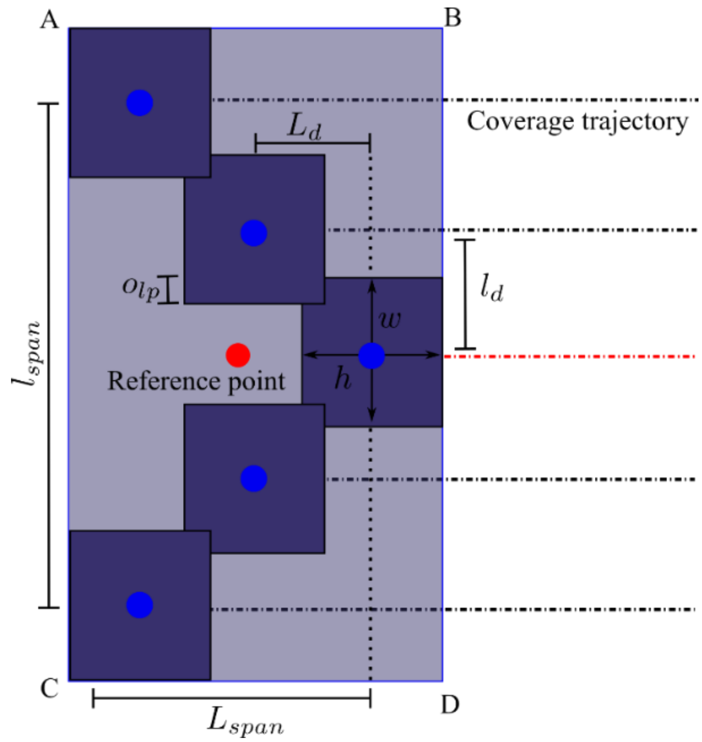

Figure 36. Example of a UAV formation for an imaging remote sensing application. l_{span} and L_{span} are the lateral and longitudinal spans of the UAV formation, respectively. l_d and L_d are the lateral and longitudinal distances of adjacent UAVs in the formation, respectively. w and h are the width and height of the camera (sensor) footprint of each UAV, respectively. The rectangle ABCD defines the area where the UAVs have to simultaneously acquire an image at predefined times.

Table 5. Mission scenario parameters.

Parameters	Value
Overlap between neighboring sensing areas, o_{lp}	10 m
Width of neighboring sensing area, w	110 m
Height of neighboring sensing area, h	110 m
Lateral distance, l_d	100 m
Longitudinal distance, L_d	100 m
Height of UAVs flying, H	120 m
Reference trajectory	Sweep trajectory

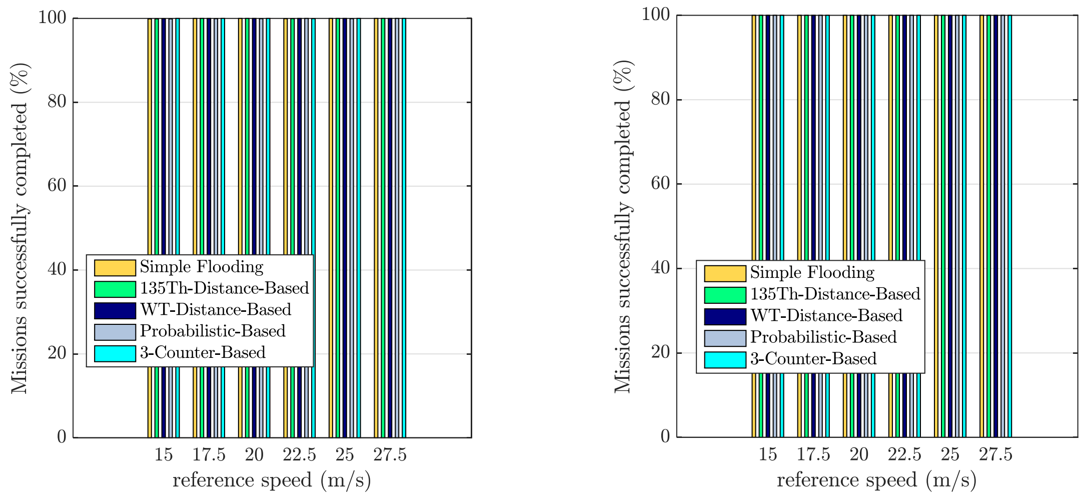

(a) (b)

Figure 37. Number of missions that were successfully completed using different MBPs for (a) open-delta (λ=5) and (b) delta (λ=6) formations when varying the reference speed, v_r. The results were obtained with a minimum of 2000 runs to achieve statistical significance.

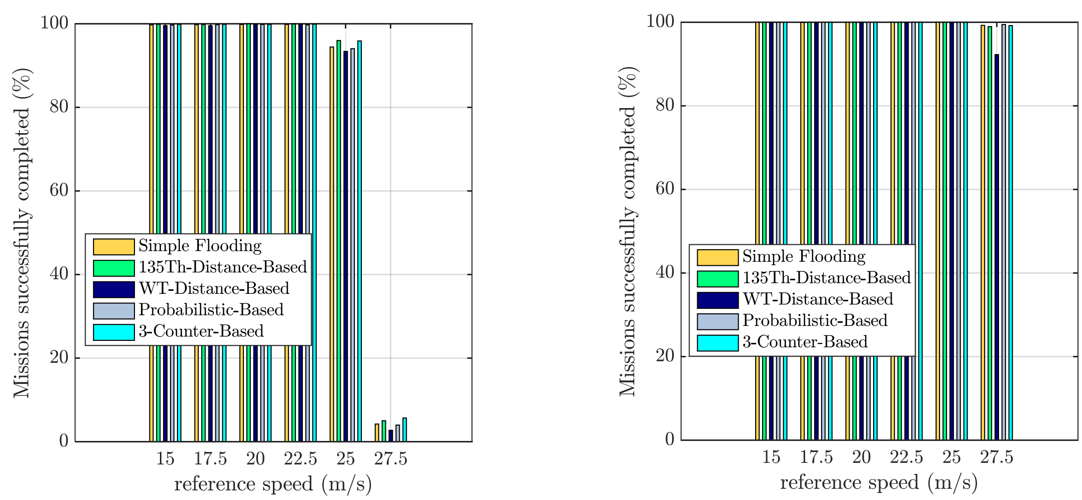

(a) (b)

Figure 38. Number of missions that were successfully completed using different MBPs for (a) open-delta (λ=7) and (b) delta (λ=10) formations when varying the reference speed, v_r. The results were obtained with a minimum of 2000 runs to achieve statistical significance.

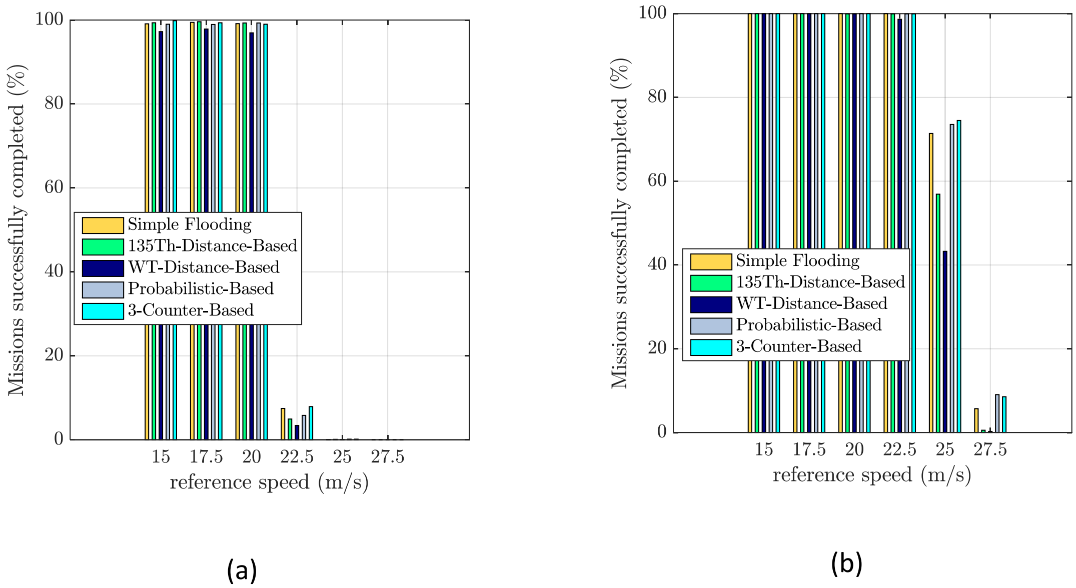

Figure 39. Number of missions that were successfully completed using different MBPs for (a) open-delta (λ=9) and (b) delta (λ=15) formations when varying the reference speed, $\boldsymbol{v_r}$. The results were obtained with a minimum of 2000 runs to achieve statistical significance.

By analyzing the results presented in Figure 37 to Figure 39, the following conclusion can be drawn:

- For missions involving a small number of UAVs (Figure 37), the selection of the MBP has little impact on the number of successful missions. Moreover, the mission can be executed at high speed ($v_r = 27.5$ m/s) without a negative impact on the mission success.

- For missions involving a medium number of UAVs (Figure 38), performance degradation starts at $v_r = 25$ m/s for the open-delta formation. In contrast, for the delta formation, a high number of successful missions can be achieved even at high speeds. Thus, for mission planning, it is important to assess the tradeoff between executing the mission with a minimum time (i.e., by using a delta formation with high speed) or with a smaller number of UAVs (i.e., by using an open-delta formation with a low to medium speed).

- For the delta formation with $\lambda = 10$ (Figure 38 (b)), although most MBPs were able to successfully complete a large number of missions for $v_r = 27.5$ m/s, the performance drop that is observed for the WT-Distance-Based protocol discourages its use for this application.

- For missions involving a large number of UAVs (Figure 39), a significant performance drop is observed at $v_r = 22.5$ m/s for the open-delta formation and at $v_r = 25$ m/s for the delta formation. Nevertheless, in this case, only the delta formation successfully completes 100% of the missions for speeds below $v_r = 25$ m/s.

- For the delta formation with $\lambda = 15$ (Figure 39 (b)), the 3-Counter-Based and Probabilistic-Based MBPs provided the best performances at high speeds. In contrast, at high speeds, the worst performance is provided by the 135Th-Distance-Based and the WT-Distance-Based protocols. This agrees with the analysis presented in the previous sections.

4.6 Conclusions

In this chapter, it was studied how the network performance offered by different MBPs that were originally proposed for MANETs and VANETs impacts the effectiveness of distributed UAV formation control to maintain flight formation during a mission execution. Some of the more relevant conclusions are presented next. Note that the results presented in this chapter were first reported in (Cabral-Pacheco et al., 2019).

The evaluation results show that even though at low speeds SI dissemination using MBPs is effective in terms of maintaining the UAV formation, as the mission reference speed increases, maintaining formation becomes harder. When comparing the results obtained when using MBPs against ideal SI dissemination, it can be observed that the P-RMSE is higher when an MBP is used. Furthermore, with the ideal SI dissemination, no UAVs are lost. In contrast, some UAVs are lost when using MBPs for SI dissemination, particularly at high speeds. Thus, in actual FANET deployments, it can be stated that the particular MBP used to disseminate SI messages plays a key role in maintaining the formation in distributed UAV formation control.

The obtained results show that factors such as packet losses or delays that inherently appear in FANETs affect the suitability of the MBPs for assisting distributed UAV controllers in maintaining a UAV formation. However, to be able to evaluate the performance of the MBPs for distributed UAV formation control applications, a more comprehensive set of metrics should be analyzed. Specifically, the performance of the MBPs was evaluated in terms of the quality of the information that the controller has at each sampling period. Thus, using the PDR is not enough since the SI age (AvgSIage) at the sampling time is also important. Therefore, the average PDR metric, which is commonly used to assess MBP performance, does not provide enough information to weigh the suitability of MBPs for SI dissemination in distributed UAV formation control applications. This is highlighted by the trajectory metrics (P-RMSE and LU) obtained for the delta formation at high speeds when using the 135Th-Distance-Based MBP, which were worse than those obtained when using Simple Flooding, even though 135Th-Distance-Based exhibits a higher average PDR.

To further analyze the performance of the MBPs, the costs of each protocol to achieve a particular PDR were evaluated using the average collision ratio (CR) and the average packet rebroadcasts canceled (PRC) metrics. The use of these average metrics is proposed in this thesis work to perform an initial assessment of the suitability of the MBPs for SI dissemination. In this sense, for the delta formation and high speeds, it can be observed that although a high PRC adversely affects the trajectory performance (e.g., WT-Distance-Based), the best trajectory performance was not obtained when the PRC was equal to zero, as in the case of Simple Flooding. In fact, for this scenario, the best performance was provided by the Probabilistic-Based and 3-Counter-Based MBPs, which exhibited relatively low PRCs and high PDRs. Therefore, it can be stated that there is a need to propose new MBPs that are specifically designed for SI dissemination and consider these issues.

Using average network metrics (which is commonly done for MANETs and VANETs) is a good starting point for the evaluation of MBPs. However, when they are used to evaluate the performance of the MBPs for SI dissemination in distributed UAV formation control applications, average network metrics do not fully explain the results observed for the trajectory metrics. Thus, in this work, the use of moving average network metrics is proposed to gain more insight into the performance of the MBPs for this kind of application. By using moving average metrics, it was found that the performance of most MBPs significantly worsens when the formation makes a turn. This is particularly acute for UAVs that are located at edges of the formation, which receive SI messages through multiple hops. Thus, by performing moving average analysis, the key zones of the flight formation where the relevance of the information quality (e.g., AvgSIage) is higher can be detected. This further highlights the need to design new MBP strategies that are focused on SI dissemination for distributed UAV formation control.

Finally, note that except for Simple Flooding, all protocols under evaluation include mechanisms that cancel packet retransmissions when a certain criterion is fulfilled. Therefore, in addition to collisions and propagation phenomena, a distant node might not receive an SI packet because of a rebroadcast cancellation. Thus, the results and analysis that are provided in this thesis work show that more than simply selecting any MBP to disseminate SI messages in FANETs, it is necessary to design a protocol that can adapt to the conditions of the target scenario.

Chapter 5. Curvature-based MBP proposal for UAV formation control applications

5.1 Introduction

This section introduces a new curvature-based multi-hop broadcast protocol (CMBP) for UAV formation control applications. The development of the CMBP considered the issues observed in the previous chapter, where traditional MBPs were used for SI dissemination for UAV formation control applications. Recall that from the controller perspective, MBPs can be seen as a black box that causes random delays and packet losses for the disseminated SI message, as depicted in Figure 40.

The results provided in Chapter 4 of this thesis work show that MBPs proposed in (Lee et al., 2014), (Tseng et al., 2002), and (Wisitpongphan et al., 2007) for MANETs and VANETs, cannot properly deal with the constraints arising in SI dissemination for distributed UAV formation control applications (e.g., higher reference speeds and adverse trajectories). Therefore, a new MBP design is proposed next, aiming to tackle some of the problems found in these kinds of scenarios.

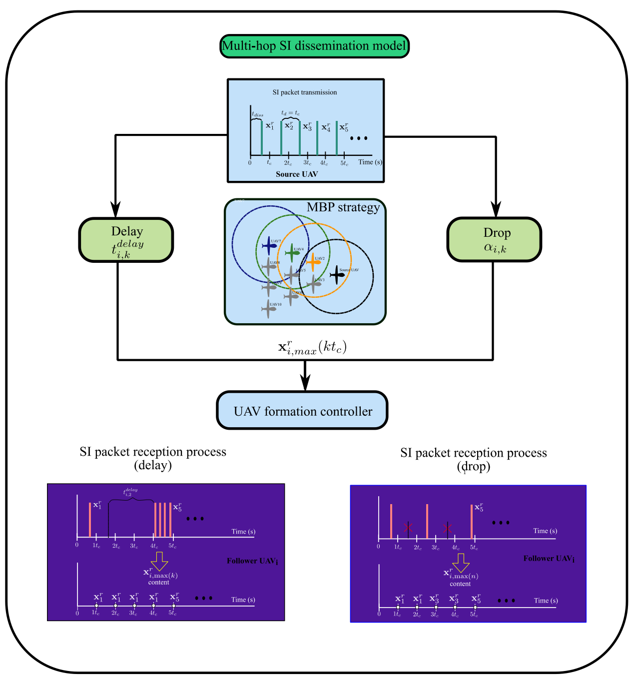

Figure 40. Multi-hop SI dissemination in UAV formation scenarios.

5.2 Curvature-based MBP design

The curvature-based multi-hop broadcast protocol (CMBP) was designed considering the conclusions presented in Section 4.6, with the aim of outperforming the MBPs evaluated in Chapter 4. The design of this CMBP is based on the insights described in Chapter 4. This protocol seeks to improve trajectory metrics such as P-RMSE and LU (described in Section 3.3.1), particularly at higher reference speeds, adverse trajectory paths, and larger formation sizes. The CMBP is based on a method for finding critical zones within the trajectory (i.e., turns) in which MBPs tends to decrease its performance (see Section 4.4).

The CMBP protocol design is divided into two stages: reception and transmission. Both stages are responsible for handling the reception and transmission of two different kinds of packets named SI packets and beacon packets. Remember from Section 2.2.2 that the SI packets contain information such as the position, speed, and heading of the reference trajectory. The beacon packets are a new class of packets that are used by CMBP. The beacon packets are intended to be transmitted by a UAV when it enters a critical zone within the course. These packets are a kind of alert message to other UAVs within the formation. This is exemplified in Figure 41, where in Figure 41(a), it can be observed that none of the UAVs is in a critical zone (e.g. a turn), and thus there is no need to send beacon packets. However, in Figure 41(b), it can be observed that UAV10 is about to be left behind by the other UAVs. This usually happens because, at turns, UAVs located at the edge of the formation in the outside of the curve (UAV3, UAV6, and UAV10) start to progressively increase its speed in order to keep in formation. Furthermore, as these UAVs are located far away from the source UAV, they are more prone to get lost if SI packets are not received timely (i.e., every sampling period). Thus, as UAV10 enters a critical zone as shown in Figure 41(c), the CMBP protocol requires to start transmitting beacon packets at specific intervals. If the beacon packet is received by another UAV, (e.g. UAV9 in Figure 41(d)), then it will rebroadcast the latest SI packet it has on buffer. In this way the probability of UAV10 breaking formation is reduced at turns.

Note that the CMBP design also uses the generic architecture (see Figure 9) of an MBP. However, the CMBP use alternative criteria to make a relay decision. Particularly, CMBP considers two stages which are explained next.

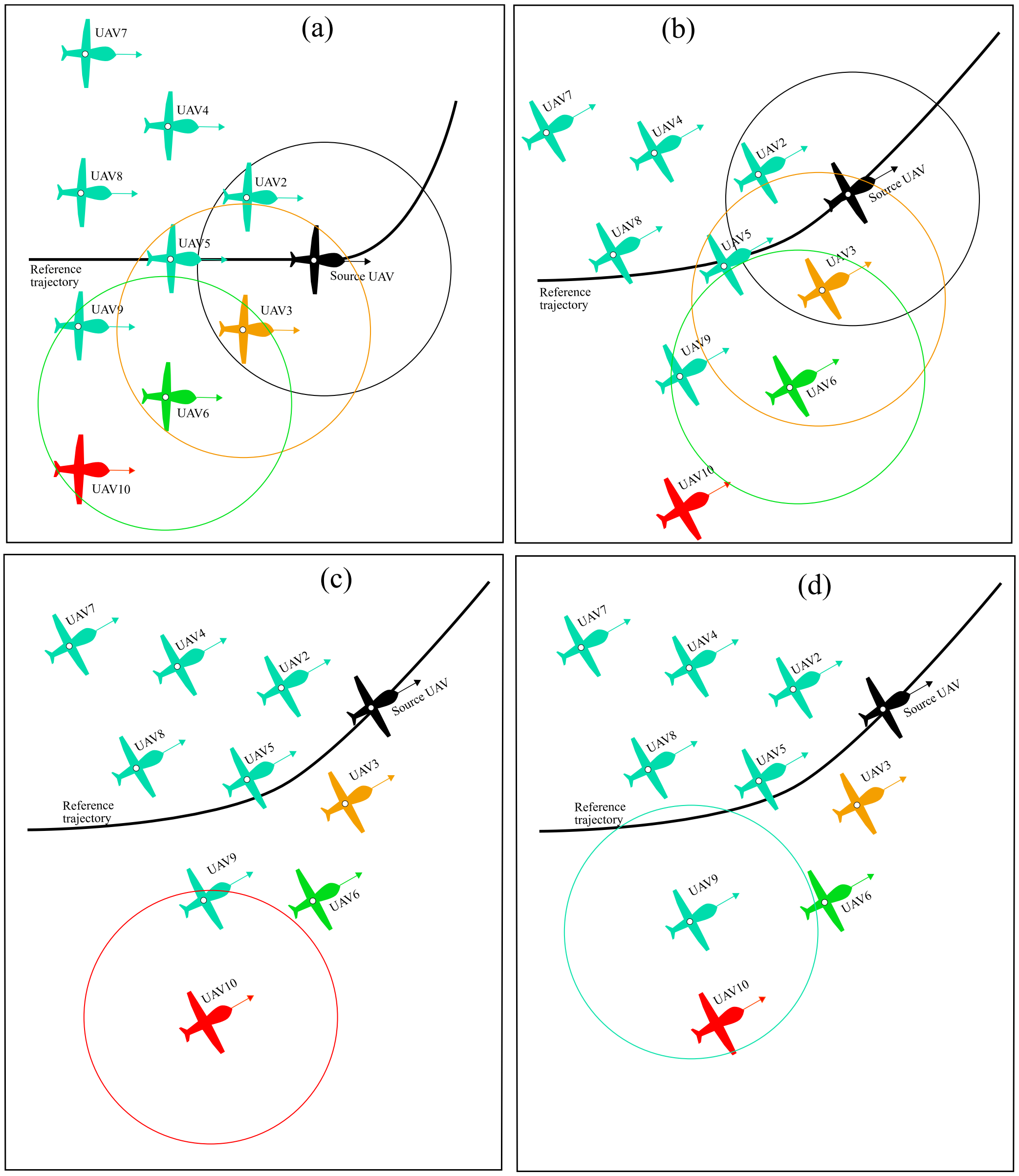

Figure 41. Beacon packet mechanism at critical zones such as turns.

5.2.1 Reception stage

This stage is responsible for handling the reception of both SI and beacon packets in each follower UAV. The procedure of this stage is shown as a pseudo-code in Figure 42. From this figure, one can observe that during the mission execution every follower UAV waits for the reception of both SI and beacon packets. From Figure 42(a), it is observed that every time a new SI packet arrives on a follower UAV, a *Counter* variable is initialized. This variable was introduced to limit the number of packets that are rebroadcasted.

Afterward, the follower UAV needs to wait a time, *WT,* before rebroadcasting the SI packet. From the evaluation of MBPs presented in Chapter 4, it was concluded that it is important to wait a time before the UAV rebroadcasts a packet. This is needed to reduce packet collisions which can induce delays in the transmission of packets or unnecessary rebroadcasts. Using the insights derived from Chapter 4, the *WT* is calculated as follows:

$$WT = -\frac{curvWT}{10}(v_r - v_{max}) + curvWT + d_{sinc}, \tag{19}$$

where $curvWT$ is the default waiting time for CMBP; v_r and v_{max}, are the reference and maximum speeds considered; and d_{sinc} is a random time used to avoid collisions between packets. For the CMBP, $curvWT = 5$ ms, $v_{max} = 27.5$ m/s, and $d_{sinc} \sim 1\text{ms} * \text{intrand}(3)$[3]. Note that v_r is contained within the SI packet. Equation (28) is designed such that WT is lower when using a higher reference speed and vice versa. This is because when using a higher reference speed, it is required to rebroadcast as soon as possible.

SMBP: Reception stage

(a) SI packets	(b) Beacon packets
Input: SI pkt, Counter	**Input:** Bcon pkt, rcvBcon
while arrives(SI pkt) **do**	**while** arrives(Bcon pkt) **do**
if new(SI pkt) **do**	rcvBcon ← True
Counter ← 0	**end while**
WT ← wait4Rebroadcast(SI pkt) (1)	
if Curvature **do**	
BT ← wait4Bcon(SI pkt) (2)	
goto (1)	
else do	
discard(SI pkt)	
end while	

Figure 42. CMBP pseudo-code of the reception stage.

[3] intrand(N) delivers a random integer number between 0 and N.

Afterward, based on a curvature method detection, each follower UAV decides whether to schedule or not a beacon packet. The curvature method detection allows the UAVs to detect critical zones within the reference trajectory, e.g., turns. In Chapter 4, it was pointed out the impact that turns have on the MBPs performance. For example, it was shown that the trajectory and network metrics performance of the MBPs drastically degrade at turns. One method to calculate the curvature, K, in the trajectory is by utilizing the following equation:

$$K = \frac{|x'y'' - y'x''|}{\left(x'^2 + y'^2\right)^{\frac{3}{2}}}, \tag{20}$$

where x', y', x'', and y'' are the speed in x-axis, speed in y-axis, acceleration in x-axis, and acceleration in y-axis, respectively. These variables can easily be calculated in a UAV by the onboard processing unit. Note from equation (20) that $\mathrm{K} = [0, \infty]$. For instance, $\mathrm{K} = 0$ means that the trajectory followed by a UAV during the calculation time of K is a straight line. Otherwise, note that $\mathrm{K} \geq 1$ means the trajectory followed by a UAV during the calculation time of K is circular or with a significant curve.

Although the aforementioned method could allow the UAVs to detect critical segments within the course, it cannot be straightforwardly used for the scenario addressed in this thesis work. For instance, by using this method, it is difficult to set a threshold for K to detect a turn since the range of K is large. Additionally, based on the results presented in Chapter 4, it can be inferred that detecting an adequate starting point within a turn segment is crucial to avoid losing UAVs at turns. Thus, to detect an adequate starting point for turns, a lower threshold for K might be needed. However, a lower threshold for K could lead to an unnecessary increase in the number of beacon packets (false positive) transmitted. For instance, at one point a UAV might detect a turn and start transmitting beacon packets. However, that turn radius might not lead to losing UAVs and therefore the beacon packets transmissions will become unnecessary protocol overhead. Otherwise, note that setting a higher threshold could hinder necessary beacon packet transmissions (false negatives), and the chances of losing UAVs will increase. Therefore, in this work, a complementary method to detect turn segments and decrease the chances of false positives and false negatives in the transmission of beacon packets is proposed.

Based on the results obtained in Chapter 4, it was found that at turns the UAVs that impact the most on the trajectory metrics performance are those located at the edge, which take the turn by the outside. In fact, it was observed that the speed of these UAVs after entering the turn can reach their maximum. Thus, CMBP proposes that at the moment when UAVs are about the reach their maximum speed in a curve, they start transmitting beacon packets to request SI packets from any neighbor. Particularly, CMBP proposes to use the next equation:

$$Turn_i[k] = \begin{cases} 1, & |v_i[k] - v_{max}| \leq v_{turn} \\ 0, & |v_i[k] - v_{max}| > v_{turn} \end{cases} \tag{21}$$

where $v_i[k]$, and v_{max}, $v_{turn}$are the speed for the i-th UAV at the sampling period, kt_c; maximum speed; and delta speed at the turn; respectively. Note from equation (21) that the $Turn_i$ variable at kt_c is set to 1 when the i-th UAV speed is about to reach or has reached the maximum speed. The small speed delta, $v_{turn} = 1$ m/s, used in equation (21) was heuristically chosen to reduce false positives in the transmission of beacon packets. Additionally, based on observations, it was determined that this value is adequate to trigger the transmission of beacon packets before a UAV is lost while following a curved trajectory. In this case, the i-th UAV at kt_c can assume is at a turn segment within the course; otherwise, it assumes that the actual point within the course is not critical (i.e., a straight line). The final decision, $\mathrm{DT_i}$ (AND operation) about the detection of a turn segment by the i-th UAV is carried out using the next equation:

$$DT_i[k] = Turn_i[k] \; AND \; K_i^*[k], \tag{22}$$

where $DT_i = \{0, 1\}$, and $\mathrm{K_i^*} = \{0, 1\}$, is calculated using the following equation:

$$K_i^* = \begin{cases} 0, & K > k_{threshold} \\ 1, & K \leq k_{threshold} \end{cases}, \tag{23}$$

where $k_{threshold}$ is a threshold to detect a turn. Note from equation (23) that $K_i^* = 0$ means that the i-th UAV is following trajectory segment similar to a straight line, and $K_i^* = 1$ means that the i-th UAV is following a critical trajectory segment, possibly a turn.

It is important to note that by using the equation (22) instead of only using equation (23) for detecting a turn segment, we provide a method to detect critical turns without unnecessarily increasing the overhead introduced by CMBP in the dissemination process.

Once the curvature method has determined that the UAV is at a critical zone like a turn, then the UAV needs to wait a beacon time (*BT*) before broadcasting a beacon packet. The *BT* is calculated as follows:

$$BT = beaconTime + d_{sinc}, \tag{24}$$

where $beaconTime$ and d_{sinc} are the interval to transmit consecutive beacon packets and a random time used for avoiding collisions between beacon and SI packets (just as in equation (19)). For the CMBP, the $beaconTime$ was set equal to 100 ms. Note when using the CMBP protocol, none of the UAVs cancel SI packet rebroadcasts when receiving duplicate SI packets for higher reference speeds. This is because as found in Chapter 4, it is better for the UAV formation control performance not to cancel SI packet rebroadcasts.

Regarding the reception of the beacon packets (Figure 42(b)), each follower UAV only needs to enable a flag variable, rcvBcon after receiving a beacon packet. Then this UAV is ready to rebroadcast SI packets to help potential disconnected UAVs to receive SI packets.

5.2.2 Transmission stage

The pseudo-code of the transmission stage of the CMBP is shown in Figure 43. In Figure 43(a), one can observe that after the WT ends, each follower UAV verifies whether or not it received a beacon packet. If the UAV received a beacon packet and its Counter is less than C, then the UAV schedules an SI packet for rebroadcast it after a waiting beacon time (WBT). The WBT is equal to BT as described in the reception stage. Moreover, if the previous condition (Counter is less than C) is satisfied, the Counter is increased by one. With this procedure, we pursue to avoid flooding the network with excessive SI packets and keep the broadcast storm problem controlled. In contrast, if Counter is bigger than C, the flag variable rcvBcon is disabled to avoid rebroadcasting future SI packets. Note that each scheduled SI packet is rebroadcasted at the final of the transmission stage procedure.

Regarding the beacon packets (Figure 43(b)), after the BT time has ended, each UAV broadcasts the beacon packet.

SMBP: Transmission stage	
(a) SI packets	(b) Beacon packets

Input: SI pkt, rcvBcon, Counter, C
while endsWT(SI pkt) || endsWBT(SI pkt) **do**
  if rcvBcon=True **&&** Counter≤C **do**
    WBT ← wait4Rebroadcast(SI pkt)
    Counter ← Counter + 1
  else if Counter>C **do**
      rcvBcon ← False
  rebroadcast(SI pkt)
end while
	Input: Bcon pkt
	while endsBT(Bcon pkt) **do**
	  broadcast(Bcon pkt)
	end while

Figure 43. CMBP pseudo-code of the transmission stage.

5.3 CMBP evaluation setup

In this section, CMBP is evaluated using the evaluation framework described Chapter 3. The particular parameters used for the CMBP are provided in Table 6. These parameters were heuristically determined to improve the trajectory metrics performance of the CMBP protocol.

Table 6. CMBP setup used for its evaluation.

Parameter	Value
C	5
$\boldsymbol{curvWT}$	5 ms
$\boldsymbol{v_{max}}$	40 m/s
$\boldsymbol{v_{turn}}$	1 m/s
$\boldsymbol{k_{threshold}}$	2
$\boldsymbol{beaconTime}$	100 ms

In order to compare the performance of CMBP with the performance offered by the MBPs evaluated in Chapter 4, CMBP was evaluated using the same simulation testbed and trajectory used in Chapter 4. Therefore, the metrics described in Section 3.3 are calculated at the end of each simulation trial.

Additionally, as in Chapter 4, the results of a minimum of 2000 trials are averaged to achieve statistical significance. Furthermore, as in Chapter 4, all metrics that are presented in the following section were obtained by considering that $t_d = t_c = 0.5$ s and a packet size of 512 bytes.

5.4 Overall results

This section presents the performance evaluation of the CMBP considering the open-delta and delta formations, two formation sizes, and different reference speeds. The metrics for the evaluation are the P-RMSE, LU, PDR, and $\mathrm{AvgSIage}_{\mathrm{L_m}}$ that were introduced in Chapter 4. Additionally, for the sake of comparison, the performance evaluation results of the MBPs evaluated in Chapter 4 are presented.

Figure 44 and Figure 45 show the P-RMSE and LU results obtained for the CMBP under evaluation for the open-delta formation and different reference speeds. By closely examining Figure 44 and Figure 45, the following observations can be made:

- For high reference speeds, the P-RMSE and LU metrics offered by the CMBP are clearly better than the other MBPs. In fact, note in Figure 45(b) that for high reference speeds (22.5 to 27.5 m/s), the LU metric offered by the CMBP is significantly lower than the other MBPs.

- Overall, for the low to high reference speeds, the P-RMSE and LU metrics offered by the CMBP are better than the others MBPs.

- The P-RMSE and LU metrics offered by the CMBP are worse for the largest formation size. This is expected because as the formation size increases, the number of hops needed to reach the UAVs that are located at the edge increases as well.

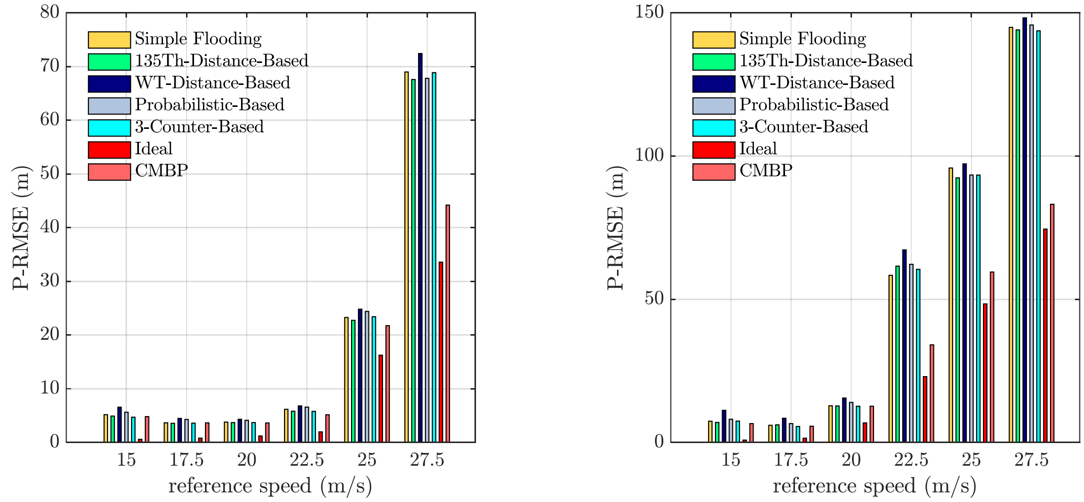

(a) (b)

Figure 44. P-RMSE obtained with the CMBP and other MBPs in a UAV mission using the open-delta formation with (a) $\boldsymbol{\lambda = 7}$ and (b) $\boldsymbol{\lambda = 9}$. The reference speed varies from $\boldsymbol{v_r = 15}$ to $\boldsymbol{v_r = 27.5}$ m/s. The results were obtained by averaging a minimum of 2000 runs to achieve statistical significance.

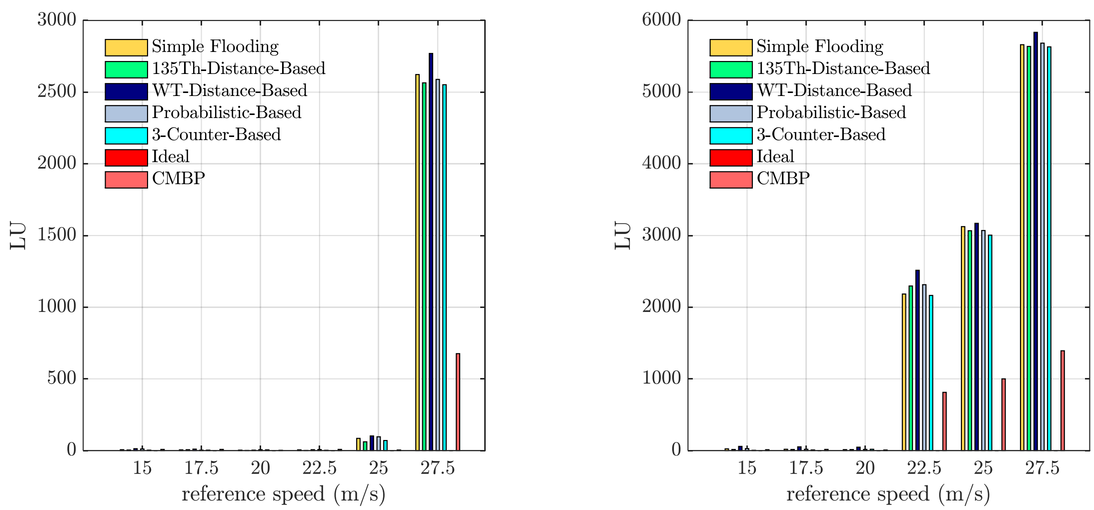

(a) (b)

Figure 45. LU obtained with the CMBP and other MBPs in a UAV mission using the open-delta formation with (a) $\boldsymbol{\lambda = 7}$ and (b) $\boldsymbol{\lambda = 9}$. The reference speed varies from $\boldsymbol{v_r = 15}$ to $\boldsymbol{v_r = 27.5}$ m/s. The results were obtained by averaging a minimum of 2000 runs to achieve statistical significance.

The average PDR and $\mathrm{AvgSIage_{L_m}}$ for this setup are presented in Figure 46, Figure 47, and Figure 48. Only plots of $\mathrm{AvgSIage_{L_m}}$ for the last two formation levels are provided in Figure 47 ($\lambda = 7$) and Figure 48 ($\lambda = 9$). The following observations can be made from these figures:

- Overall, the CMBP provides the best PDR and $\mathrm{AvgSIage_{L_m}}$ metrics among the MBPs.

- The PDR and $\mathrm{AvgSIage_{L_m}}$ are worse for $\lambda = 9$ (the largest formation size).

- As pointed out in Chapter 4, it seems that when the PDR is below 0.7 and the $\mathrm{AvgSIage_{L_m}}$ is above 1, the LU metric increases significantly for all MBPs. However for the CMBP, the PDR is always above 0.7, and the $\mathrm{AvgSIage_{L_m}}$ is always below 1.

By analyzing the results presented in Figure 44 to Figure 48, it can be observed that there is a good correspondence between the trajectory performance metrics and network performance metrics exhibited by the CMBP. For example, the results in terms of the network metrics explain why the trajectory metrics offered by the CMBP do not decrease their performance significantly for higher reference speeds. Note that the CMBP procedure, which uses beacon packets as a message alerts to request SI packets when a UAV is at a critical section within the reference trajectory, helps to significantly improve the trajectory performance metrics of the CMBP. Thus, the results allow to infer that the best option for open-delta formations is to use the CMBP protocol.

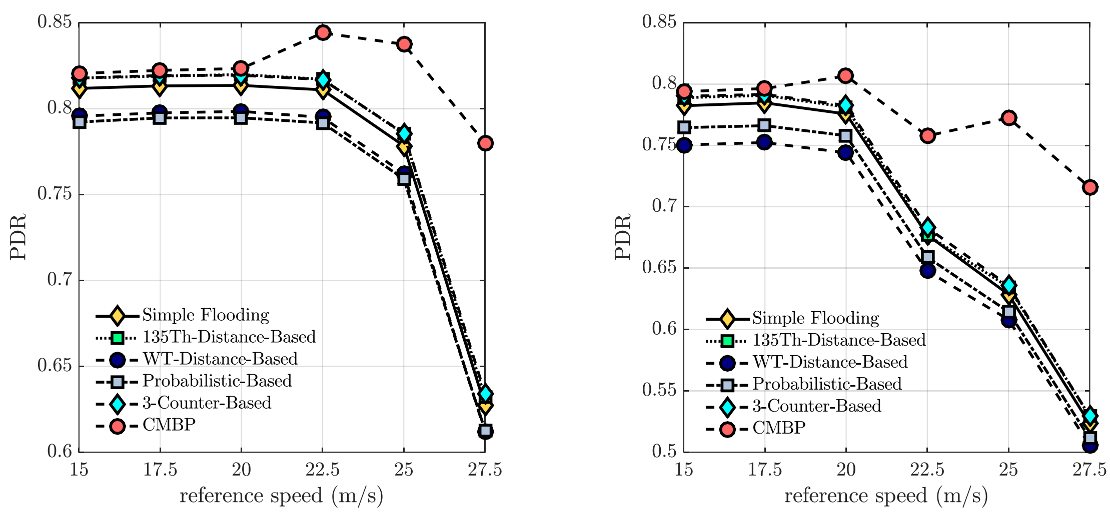

(a) (b)

Figure 46. PDR obtained with the CMBP and other MBPs in a UAV mission using the open-delta formation with (a) $\boldsymbol{\lambda = 7}$ and (b) $\boldsymbol{\lambda = 9}$. The reference speed varies from $\boldsymbol{v_r = 15}$ to $\boldsymbol{v_r = 27.5}$ m/s. The results were obtained by averaging a minimum of 2000 runs to achieve statistical significance.

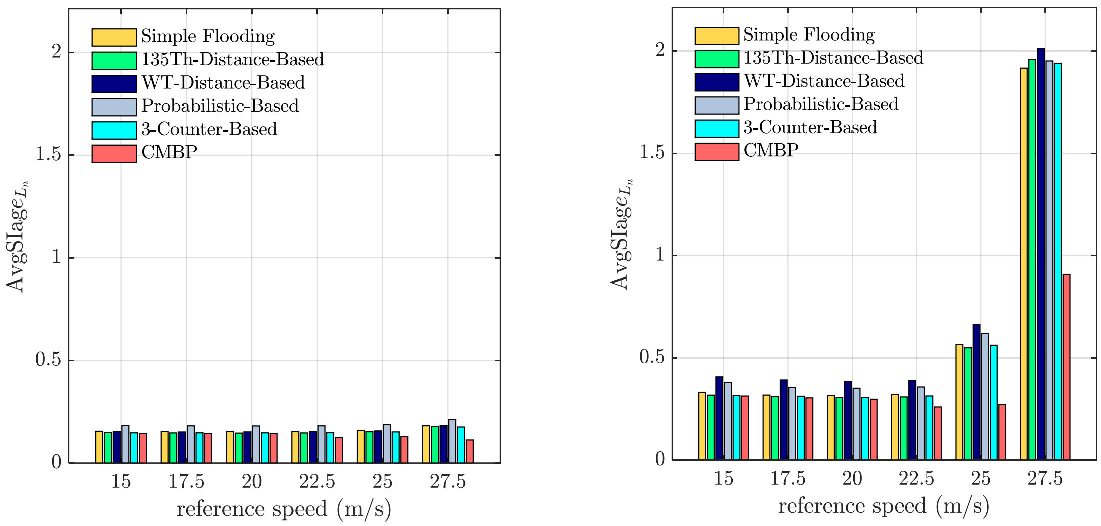

(a) (b)

Figure 47. $\mathbf{AvgSIage_{L_m}}$ obtained with the CMBP and other MBPs in a UAV mission using the open-delta formation with $\boldsymbol{\lambda = 7}$ for (a) $\boldsymbol{L_3}$ and (b) $\boldsymbol{L_4}$. The reference speed varies from $\boldsymbol{v_r = 15}$ to $\boldsymbol{v_r = 27.5}$ m/s. The results were obtained by averaging a minimum of 2000 runs to achieve statistical significance.

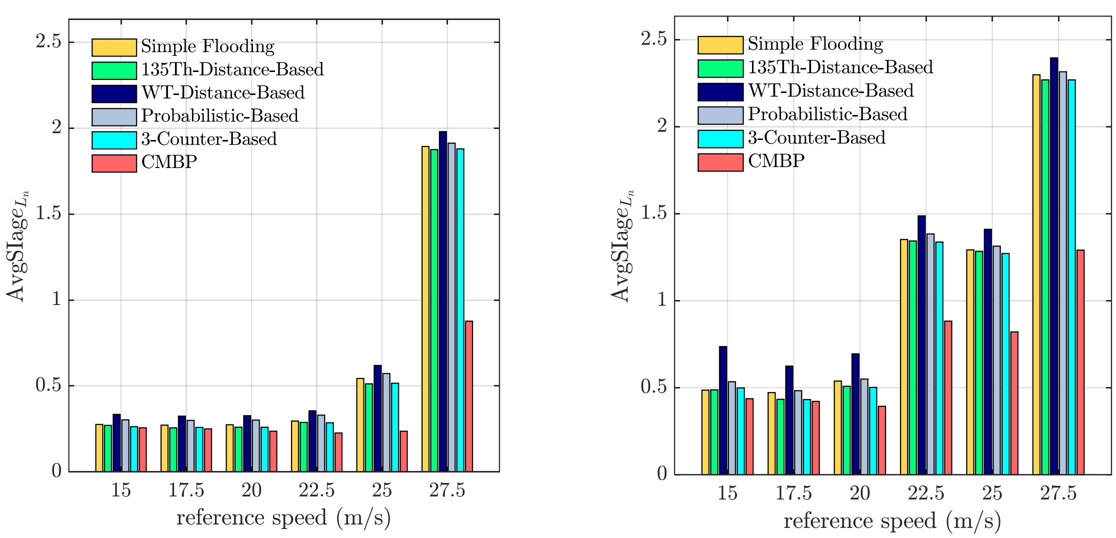

(a) (b)

Figure 48. $\mathbf{AvgSIage_{L_m}}$ obtained with the CMBP and other MBPs in a UAV mission using the open-delta formation with $\boldsymbol{\lambda = 9}$ for (a) $\boldsymbol{L_4}$ and (b) $\boldsymbol{L_5}$. The reference speed varies from $\boldsymbol{v_r = 15}$ to $\boldsymbol{v_r = 27.5}$ m/s. The results were obtained by averaging a minimum of 2000 runs to achieve statistical significance.

Figure 49 and Figure 50 show the P-RMSE and LU results obtained for the MBPs under evaluation for the delta formation and different reference speeds. In these figures, it can be seen that both the P-RMSE and LU increase as the reference speed increases (particularly from 25 m/s to 27.5 m/s).

By closely examining Figure 49 and Figure 50, the following observations can be made:

- The P-RMSE and LU metrics offered by the CMBP are better for the delta formation than for the open-delta formation, as expected.
- The CMBP protocol provides the best trajectory performance overall.
- In fact, in terms of the LU metric, the CMBP exhibits the same performance as the ideal protocol (i.e., all SI packets arrive on time to every UAV in the flight formation).

The average PDR and $\mathrm{AvgSIage}_{\mathrm{L_m}}$ for this setup are presented in Figure 51, Figure 52, and Figure 53. Only plots of $\mathrm{AvgSIage}_{\mathrm{L_m}}$ for the last two formation levels are provided in Figure 52 ($\lambda = 10$) and Figure 53 ($\lambda = 15$). The following observations can be made from these figures:

- Overall, the CMBP exhibits the best network performance metrics.
- The PDR and $\mathrm{AvgSIage}_{\mathrm{L_m}}$ metrics offered by the CMBP seem to remain the same for all reference speeds (from lower to higher). Note that the PDR is almost 1, and $\mathrm{AvgSIage}_{\mathrm{L_m}}$ closer to zero for the CMBP.
- Note that the $\mathrm{AvgSIage}_{\mathrm{L_m}}$ offered by the CMBP for higher reference speeds (25 and 27.5 m/s) and larger $\lambda = 15$, is significantly better than the other MBPs.

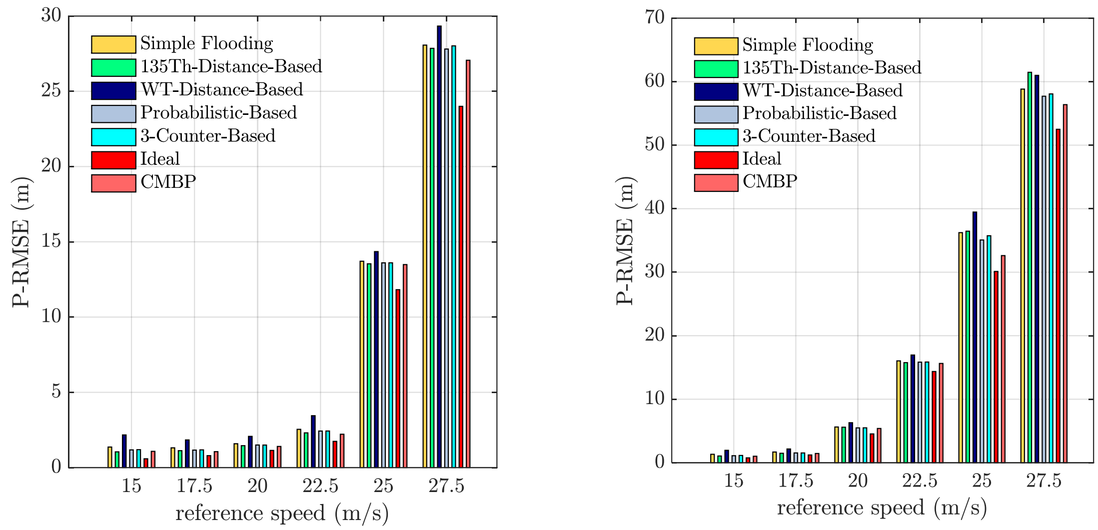

(a) (b)

Figure 49. P-RMSE obtained with the CMBP and other MBPs in a UAV mission using the delta formation with (a) $\boldsymbol{\lambda} = \mathbf{10}$ and (b) $\boldsymbol{\lambda} = \mathbf{15}$. The reference speed varies from $\boldsymbol{v_r} = \mathbf{15}$ to $\boldsymbol{v_r} = \mathbf{27.5}$ m/s. The results were obtained by averaging a minimum of 2000 runs to achieve statistical significance.

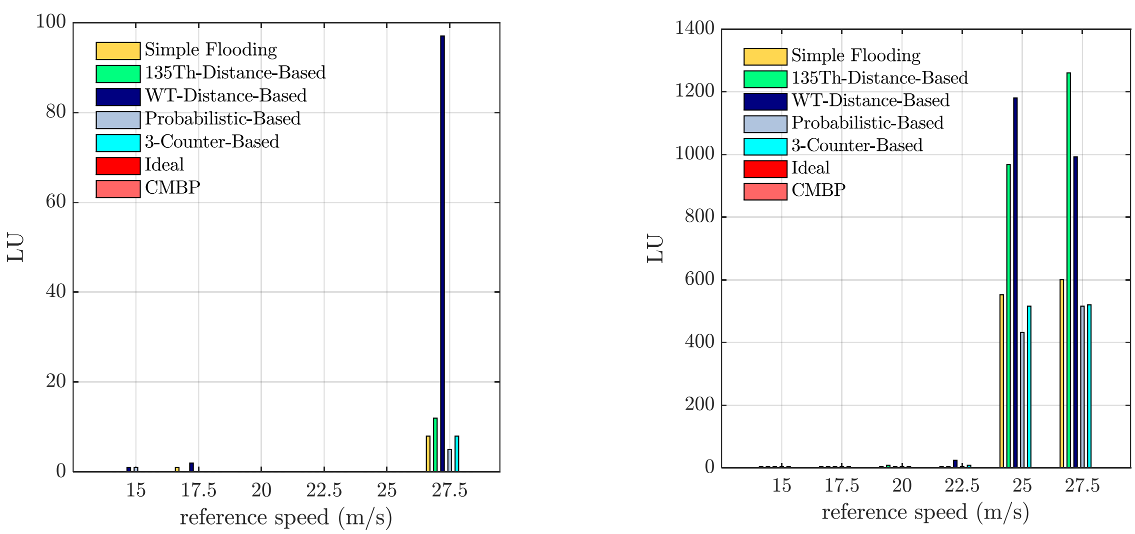

(a) (b)

Figure 50. LU obtained with the CMBP and other MBPs in a UAV mission using the delta formation with (a) $\boldsymbol{\lambda} = \mathbf{10}$ and (b) $\boldsymbol{\lambda} = \mathbf{15}$. The reference speed varies from $\boldsymbol{v_r} = \mathbf{15}$ to $\boldsymbol{v_r} = \mathbf{27.5}$ m/s. The results were obtained by averaging a minimum of 2000 runs to achieve statistical significance.

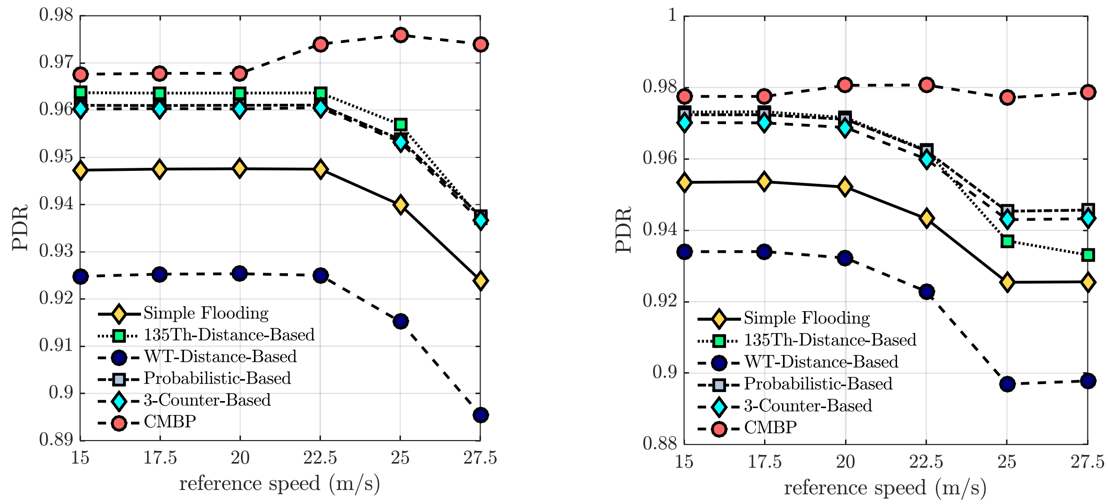

(a) (b)

Figure 51. PDR obtained with the CMBP and other MBPs in a UAV mission using the delta formation with (a) $\boldsymbol{\lambda = 10}$ and (b) $\boldsymbol{\lambda = 15}$. The reference speed varies from $\boldsymbol{v_r = 15}$ to $\boldsymbol{v_r = 27.5}$ m/s. The results were obtained by averaging a minimum of 2000 runs to achieve statistical significance.

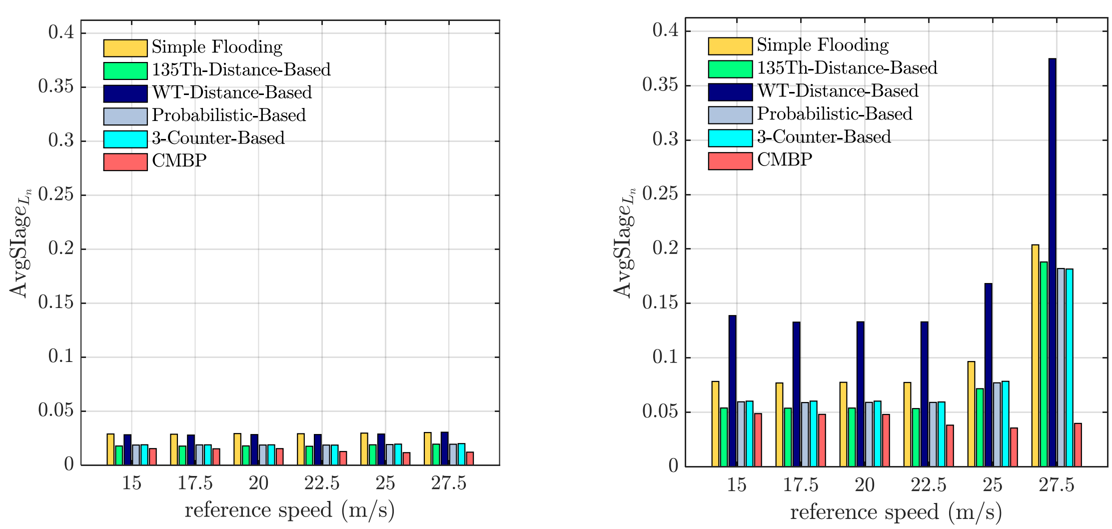

(a) (b)

Figure 52. $\mathbf{AvgSIage_{L_m}}$ obtained with the CMBP and other MBPs in a UAV mission using the delta formation with $\boldsymbol{\lambda = 10}$ for (a) $\boldsymbol{L_3}$ and (b) $\boldsymbol{L_4}$. The reference speed varies from $\boldsymbol{v_r = 15}$ to $\boldsymbol{v_r = 27.5}$ m/s. The results were obtained by averaging a minimum of 2000 runs to achieve statistical significance.

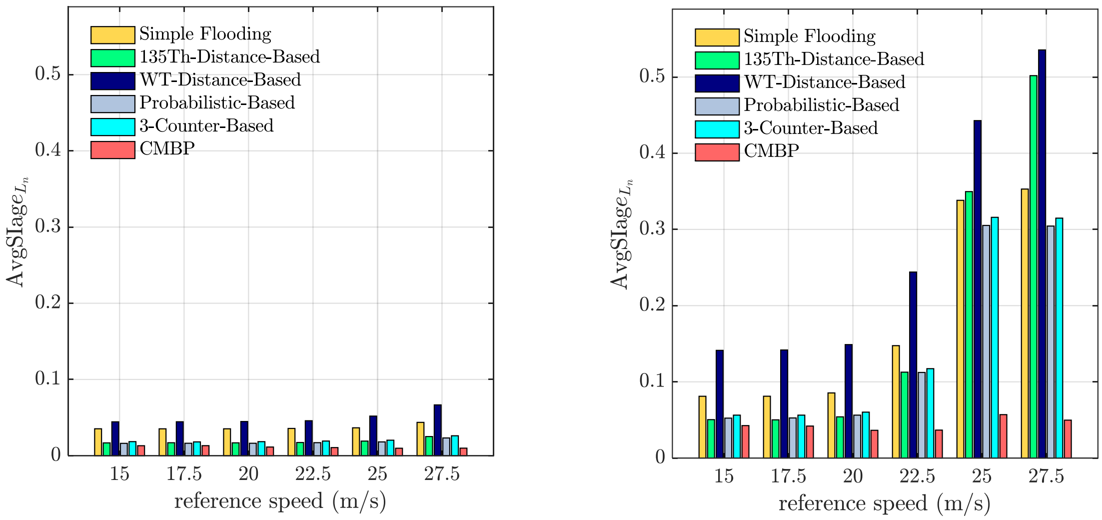

(a)

(b)

Figure 53. $\mathbf{AvgSIage_{L_m}}$ obtained with the CMBP and other MBPs in a UAV mission using the delta formation with $\boldsymbol{\lambda = 15}$ for (a) $\boldsymbol{L_4}$ and (b) $\boldsymbol{L_5}$. The reference speed varies from $\boldsymbol{v_r = 15}$ to $\boldsymbol{v_r = 27.5}$ m/s. The results were obtained by averaging a minimum of 2000 runs to achieve statistical significance.

By analyzing the results presented in Figure 49 and Figure 53, it can be observed that, as with the open-delta formation, the trajectory and network performance metrics offered by the CMBP are better than the other MBPs. Note that, compared to the open-delta formation, the delta formation is a denser network with higher connectivity. This is the reason why the CMBP performance is better when using a delta formation than when using the open-delta formation. Therefore, it can be stated that the CMBP outperforms traditional MBP when they are used for disseminating SI packets in UAV formation control scenarios. To gain more insight into this performance, an in-deep analysis of the evolution of the metrics through the trajectory is provided in the next section.

5.5 Segment results

In this section, an analysis considering the time evolution of the evaluation metrics is presented. Specifically, the sweep trajectory considered in Chapter 4, as shown in Figure 27. To this end, the network metrics were calculated using a moving average of 10 sample periods, similar to the results presented in

Section 4.4. In addition to the network metrics used in the previous section, the burst average length (BAL) of the losses (see subsection 3.3.2) is considered in the analysis.

Figure 54 shows the moving average P-RMSE obtained for the CMBP and other MBPs under evaluation for the delta formation with $\lambda = 10$ and $v_r = 27.5$ m/s. For this figure, only the UAVs from the third level or higher were considered for the P-RMSE calculation. It can be seen in Figure 54 that, in general, the moving average P-RMSE of the MBPs evaluated in Chapter 4 increases as the UAVs make the turn (segments $m_1 - m_2 - m_3$ and $m_4 - m_5 - m_6$) and decreases when UAVs exit from it. This behavior also occurs for the CMBP protocol. However, note that at turns, the P-RMSE exhibited by the CMBP is significantly lower than the other MBPs. The result observed in Figure 54 agrees with the results of Figure 49 and Figure 50 in the sense that the CMBP provides a better P-RMSE and LU performance than the other MBPs. From Figure 49, one can observe that in terms of the P-RMSE metric, the difference between the CMBP and the other MBPs is slightly small. This is because once a UAV is definitively lost, it is no longer considered for the P-RMSE calculation. Nevertheless, when the moving average P-RMSE is calculated as shown in Figure 54, the difference between the CMBP and the other MBPs is remarkably notorious.

To further analyze the performance offered by the CMBP, the moving average PDR for the UAVs flying at the formation edges is shown in Figure 55. In particular, Figure 55(a) shows the moving average PDR of the UAV that is located in the south-west edge of the formation (referred to the rotated coordinate system $X_r O_r Y_r$ shown in Figure 7) and labeled UAV7. Similarly, Figure 55(b) shows the moving average PDR of the UAV that is located in the south-east edge of the formation and labeled UAV10. As it was discussed in Chapter 4, considering the wireless propagation phenomena, UAVs that are closer to the leader consistently have better probabilities of successful packet reception. Thus, considering these nodes in the metric calculation in scenarios with a low number of UAVs might bias the average. Therefore, the subsequent analysis is focused on UAVs flying at the edges of the last formation level, which are more prone to experience challenging network conditions, e.g., disconnections, and fewer neighbors.

In Figure 55, note how the PDR significantly decays for UAV7 when it makes the first turn ($m_1 - m_2 - m_3$), while for UAV10 the PDR decays when it makes the second turn ($m_4 - m_5 - m_6$). Thus, the PDRs of UAV7 and UAV10 decay when they make a turn and are located at the outside of the curve while following the reference trajectory of Figure 27. Nevertheless, in Figure 55, it can be observed that the PDR offered by the CMBP does not decay as much as the PDR offered by the other MBPs. In fact, one can observe in Figure 55 that the PDR offered by the CMBP, actually increases when the PDR offered by the other MBPs start to decay. For example, within the segments ($m_1 - m_2$) and ($m_4 - m_5$) in Figure 55, it is clearly shown how the PDR increases with CMBP protocol. After this segments, the PDR performance offered by the CMBP starts to decay (i.e., segments ($m_2 - m_3$) and ($m_5 - m_6$)), however, the decay is slightly small compared with the other MBPs. As a matter of fact, the lowest PDR exhibited by the CMBP is equal to the higher PDR exhibited by the WT-Distance-Based protocol (PDR=0.8). Additionally, note in Figure 55 that in straight line segments (i.e., before m_1 and after m_6), the PDR exhibited by the CMBP is similar (slightly better) to the PDR exhibited by the other MBPs

Following the analysis, Figure 56 and Figure 57 show the moving average $\mathrm{AvgSIage}$ and BAL for UAV7 and UAV10. As with the PDR, both metrics significantly worsen when the corresponding UAV makes a turn and is located at the outside of a curve in the trajectory. Nevertheless, observe in these figures how the performance offered by the CMBP is significantly better than the other MBPs.

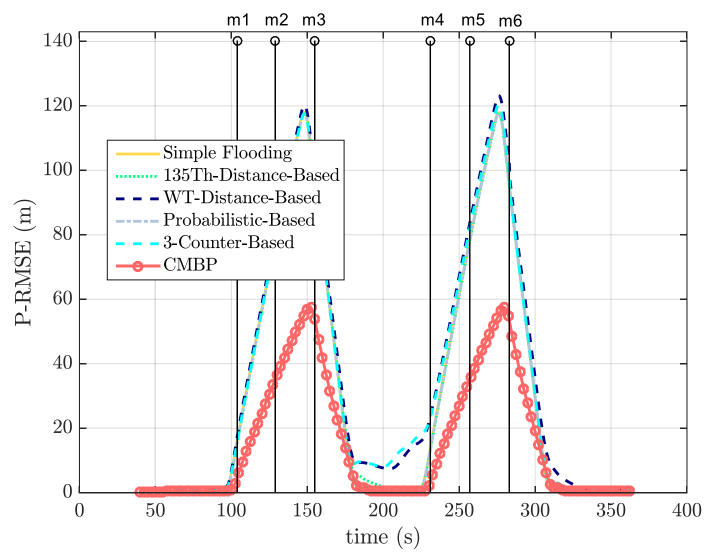

Figure 54. Moving average P-RMSE obtained when SI messages are disseminated with the CMBP and other MBPs considered in Chapter 4. For this figure, UAVs fly in delta formation with a reference speed=275 m/s and λ=10. The results at each sampling period were obtained using the average of a minimum of 2000 runs to achieve statistical significance. Only the UAVs from the third level or higher were considered for this figure.

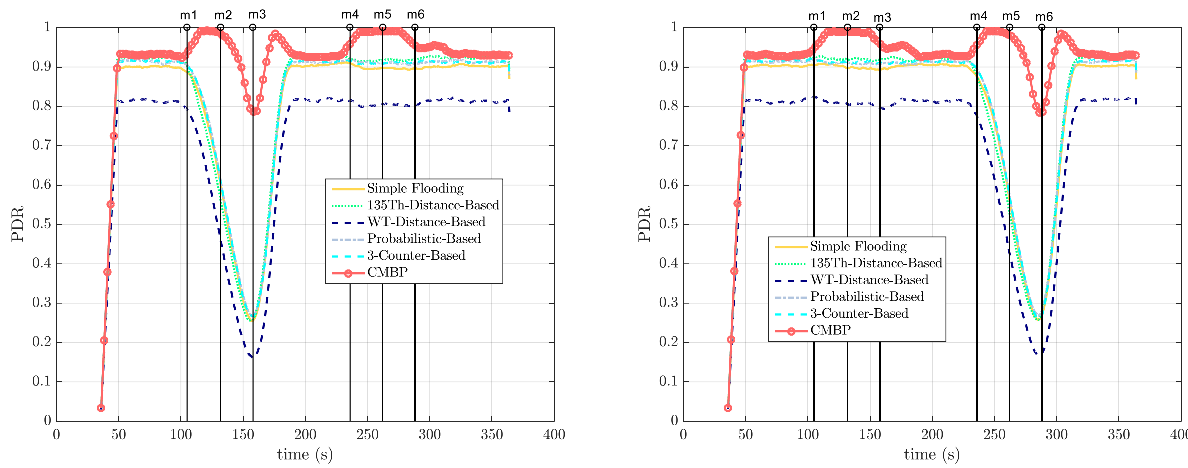

(a) (b)

Figure 55. Moving average PDR obtained when SI messages are disseminated with the CMBP and other MBPs considered in Chapter 4. For this figure, UAVs fly in delta formation with a reference speed=27.5 m/s and λ=10. Only the UAVs that are located at the (a) south-west (UAV7) and (b) south-east (UAV10) edges of the formation were considered for the calculations. The results at each sampling period were obtained using the average of a minimum of 2000 runs to achieve statistical significance.

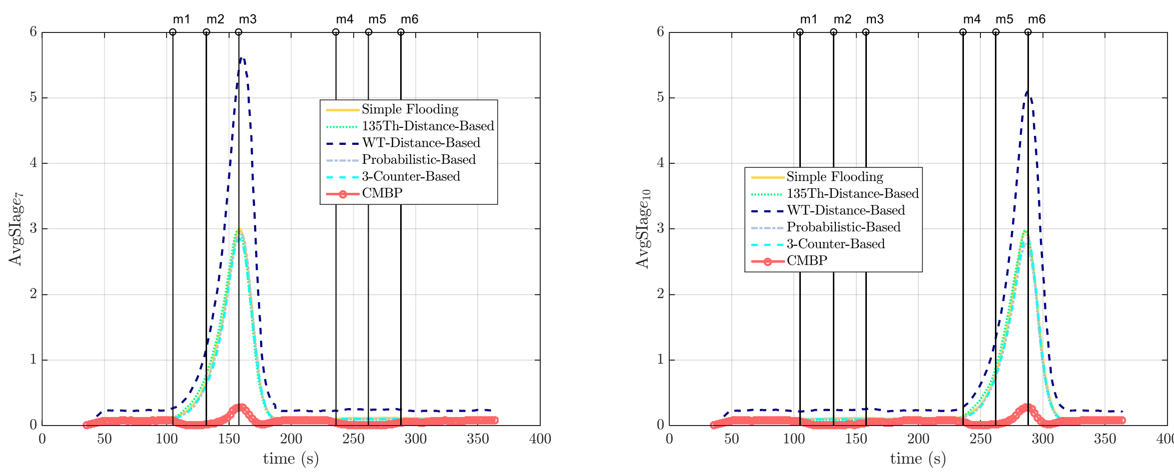

(a) (b)

Figure 56. Moving average $\mathbf{AvgSIage_{L_m}}$ obtained when SI messages are disseminated with the CMBP and other MBPs considered in Chapter 4. For this figure, UAVs fly in delta formation with a reference speed=27.5 m/s and λ=10. Only the UAVs that are located at the (a) south-west (UAV7) and (b) south-east (UAV10) edges of the formation were considered for the calculations. The results at each sampling period were obtained using the average of a minimum of 2000 runs to achieve statistical significance.

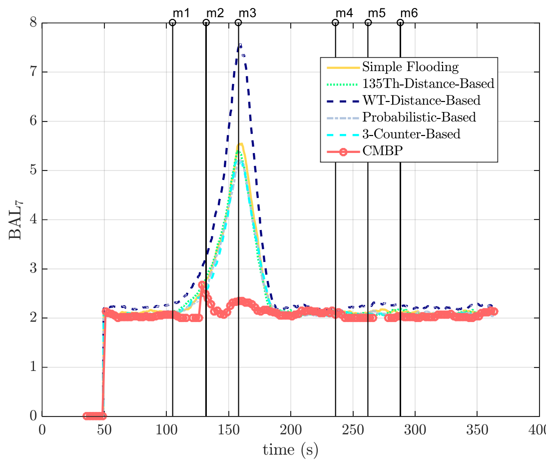

(a)

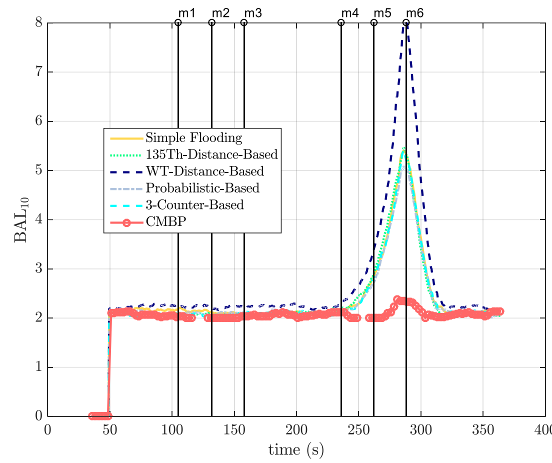

(b)

Figure 57. Moving average BAL obtained when SI messages are disseminated with the CMBP and other MBPs considered in Chapter 4. For this figure, UAVs fly in delta formation with a reference speed=27.5 m/s and λ=10. Only the UAVs that are located at the (a) south-west (UAV7) and (b) south-east (UAV10) edges of the formation were considered for the calculations. The results at each sampling period were obtained using the average of a minimum of 2000 runs to achieve statistical significance.

By closely analyzing the moving average PDR, $\mathrm{AvgSIage}$ and BAL results provided in Figure 55 to Figure 57, respectively, the following observations can be made regarding the CMBP network performance offered to the UAVs that are located at the formation edges (UAV7 and UAV10):

- The performance of the CMBP worsens at turns.

- The CMBP protocol consistently provides the best network performance. In addition, it is the MBP that is least affected by network conditions at turns.

- As $\mathrm{AvgSIage}$ metric is an indicator of the freshness of SI at every sampling time (i.e., how fresh SI is when used by the controller). Thus, it can be seen in Figure 56, as the formation enters the curve, the $\mathrm{AvgSIage}$ offered by the CMBP remains low. In contrast, the $\mathrm{AvgSIage}$ offered by the other MBPs increases (caused by significant delays or packet drops). Note from Figure 56 that the $\mathrm{AvgSIage}$ performance offered by the CMBP starts to increase (i.e., segments $(m_2 - m_3)$ and $(m_5 - m_6)$), however, the increase is slightly small compared with the other MBPs. Actually, the highest AvgSIage exhibited by the CMBP is about 1 sampling period. This helps to explain why when using CMBP protocol, there were not UAVs lost.

- The BAL metric performance offered by the CMBP is lower than for the other MBPs. In fact, observe in Figure 57 that the BAL offered by the CMBP within the segments ($m_1 - m_2$) and ($m_4 - m_5$) is null. In this segments, BAL values larger than 1 were not obtained when using the CMBP protocol. This also helps to explain why, when using CMBP protocol, there were not UAVs lost.

- By comprehensively analyzing the PDR, AvgSIage, and BAL metrics shown in Figure 55 to Figure 57, respectively, it can be inferred that the multi-hop broadcast approach of the CMBP significantly improves the performance of the more relevant network metrics to keep the UAV formation in exchange of transmitting more packets. For instance, offering lower SI dissemination delays and packet losses lead to improve the controller effectiveness at keeping UAV7 and UAV10 within the formation even though more packets are transmitted (higher overhead).

Continuing with the analysis of the results by segments, Figure 58 shows the moving average P-RMSE obtained for the CMBP and the MBPs under evaluation for a delta formation with $\lambda = 15$ and $v_r = 27.5$ m/s. For this figure, only the UAVs from the third level or higher were considered for the P-RMSE calculation. As in Figure 54, it can be seen in Figure 58 that the P-RMSE increases as the formation makes a turn and decreases when the formation exits from it. Similar to the case with $\lambda = 10$, for $\lambda = 15$, the P-RMSE provided by the CMBP protocol at the turns is significantly better than that obtained when using the other MBPs.

Continuing with the analysis performed for $\lambda = 15$ and $v_r = 27.5$ m/s, Figure 59 to Figure 61 show the moving average PDR, AvgSIage, and BAL for UAVs flying at the formation edges for a delta formation with $\lambda = 15$ and $v_r = 27.5$ m/s. For these figures, the network metrics were calculated with a moving average of 10 sample periods. Similar to the previous case, the UAV that is located at the south-west edge of the formation is labeled as UAV11, and the UAV that is flying at the south-east edge of the formation is labeled as UAV15.

Note in Figure 59 to Figure 61 that, for all MBPs under evaluation, the network performance for UAV11 and UAV15 worsens as the formation makes a turn ($m_1 - m_2 - m_3$ or $m_4 - m_5 - m_6$). Similar to the delta formation with $\lambda = 10$, for the case under analysis, the best performance at the turns is provided by the CMBP protocol. This explains and complement the P-RMSE and LU metrics results shown in Figure 49 and Figure 50, respectively, where the CMBP provides the best P-RMSE and LU metrics for $\lambda = 15$ and $v_r = 27.5$ m/s.

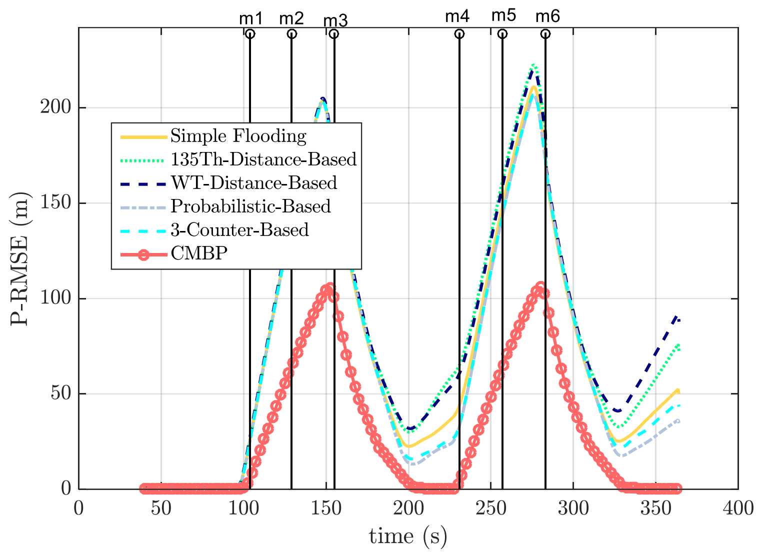

Figure 58. Moving average P-RMSE obtained when SI messages are disseminated with the CMBP and other MBPs considered in Chapter 4. For this figure, UAVs fly in delta formation with a reference speed=27.5 m/s and λ=15. The results at each sampling period were obtained using the average of a minimum of 2000 runs to achieve statistical significance. Only the UAVs from the third level or higher were considered for this figure.

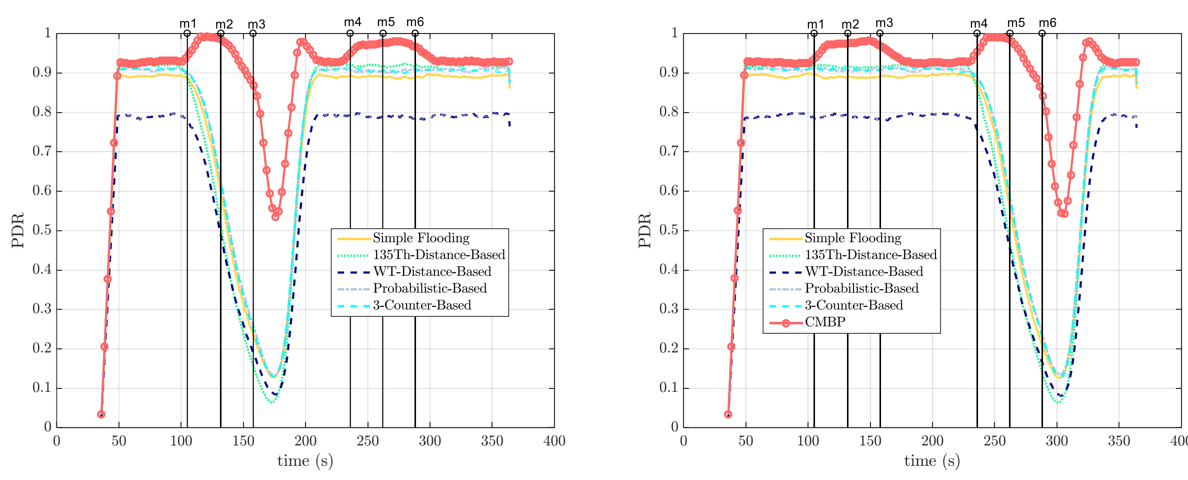

(a) (b)

Figure 59. Moving average PDR obtained when SI messages are disseminated with the CMBP and other MBPs considered in Chapter 4. For this figure, UAVs fly in delta formation with a reference speed=27.5 m/s and λ=15. Only the UAVs that are located at the (a) south-west (UAV11) and (b) south-east (UAV15) edges of the formation were considered for the calculations. The results at each sampling period were obtained using the average of a minimum of 2000 runs to achieve statistical significance.

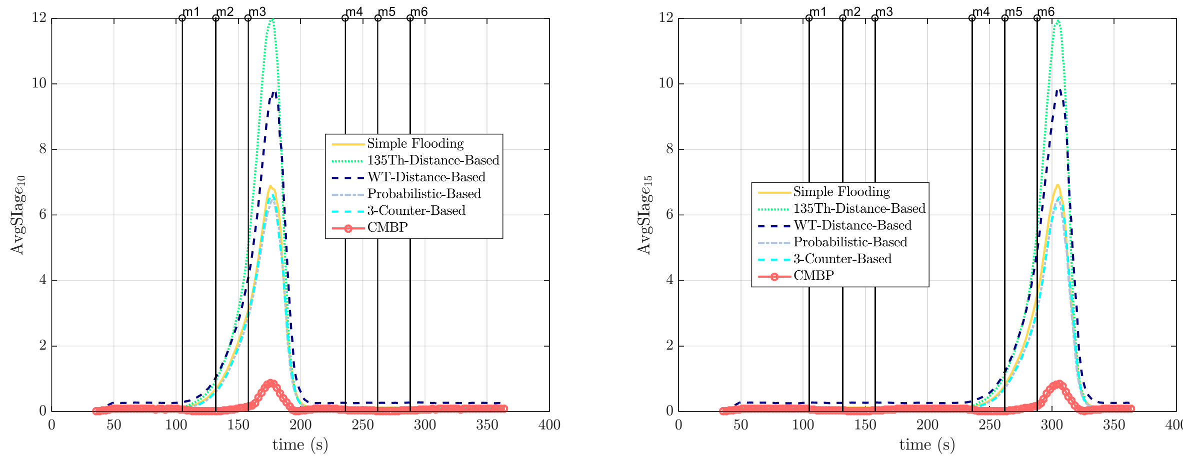

(a) (b)

Figure 60. Moving average $\mathbf{AvgSIage_{L_m}}$ obtained when SI messages are disseminated with the CMBP and other MBPs considered in Chapter 4. For this figure, UAVs fly in delta formation with a reference speed=27.5 m/s and λ=15. Only the UAVs that are located at the (a) south-west (UAV11) and (b) south-east (UAV15) edges of the formation were considered for the calculations. The results at each sampling period were obtained using the average of a minimum of 2000 runs to achieve statistical significance.

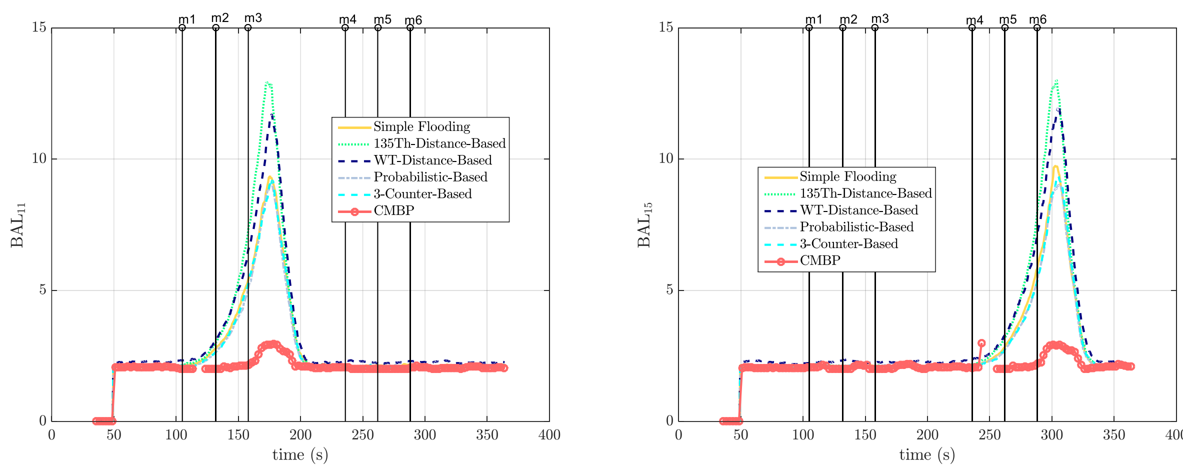

(a) (b)

Figure 61. Moving average BAL obtained when SI messages are disseminated with the CMBP and other MBPs considered in Chapter 4. For this figure, UAVs fly in delta formation with a reference speed=27.5 m/s and λ=15. Only the UAVs that are located at the (a) south-west (UAV11) and (b) south-east (UAV15) edges of the formation were considered for the calculations. The results at each sampling period were obtained using the average of a minimum of 2000 runs to achieve statistical significance.

In summary, from the analysis by segments carried out, one can observe that for the UAVs that are located at the south-west and south-east edges of a delta formation, the network performance provided by the CMBP protocol is significantly better than the other MBPs. From Chapter 4, it can be observed that traditional MBPs only provide acceptable performance in terms of network and trajectory metrics while UAVs fly on straight lines. However, the performance of these MBPs significantly worsens at turns. Although the CMBP performance also drops at turns, it is important to note that the drop is not prohibitive in terms of the trajectory metrics performance. For example, the trajectory metrics performance offered by the CMBP does not decay to the extent of losing UAVs. In fact, note from Figure 50 that the performance offered by the CMBP is equal to the ideal protocol (zero UAVs lost). Therefore, in this section, it was shown how the network performance offered by the CMBP clearly explains the trajectory metrics performance offered by the CMBP in Section 5.4. Additionally, it was shown that the curvature method detection along with the transmission of beacon packets used by the CMBP significantly improves the performance (in terms of trajectory and network metrics) offered by this protocol. This situation can be observed, in Figure 59, where at the beginning of the turns (segments ($m_2 - m_3$) and ($m_5 - m_6$)), the PDR offered by the CMBP increases. The improvement of the network metrics (e.g., PDR, $\mathrm{AvgSIage}$, and BAL) at the beginning of the turns is crucial for keeping the trajectory metrics on acceptable levels. Otherwise, the trajectory metrics worsen, as happens with the other MBPs at the beginning of the turns which drastically decrease their performance.

This improvement in network and trajectory metrics by the CMBP also is shown in the case study scenario presented in Section 4.5. The results obtained with the CMBP protocol in this scenario are presented in the next section.

5.6 Case study

As mentioned in the Section 4.5, remote sensing is one of the main applications for multi-UAV systems, e.g., [14], [15], [53], [54], and [56]–[58]. Generally, maintaining a flight formation is crucial in order to be able to cover the desired imaging area with a single flight multi-UAV mission. Thus, next an example of the suitability of the CMBP to disseminate SI messages while performing a multi-UAV imaging remote sensing mission is presented. The setup for this example is similar to that presented in Section 4.5 (see Figure 36 and Table 5).

Figure 62 to Figure 64 show the number of missions successfully completed with the considered MBPs as the reference speed, v_r, increases when UAVs fly in open-delta and delta formations. The formation size λ ranges from small (Figure 62) to large (Figure 64) for each formation type.

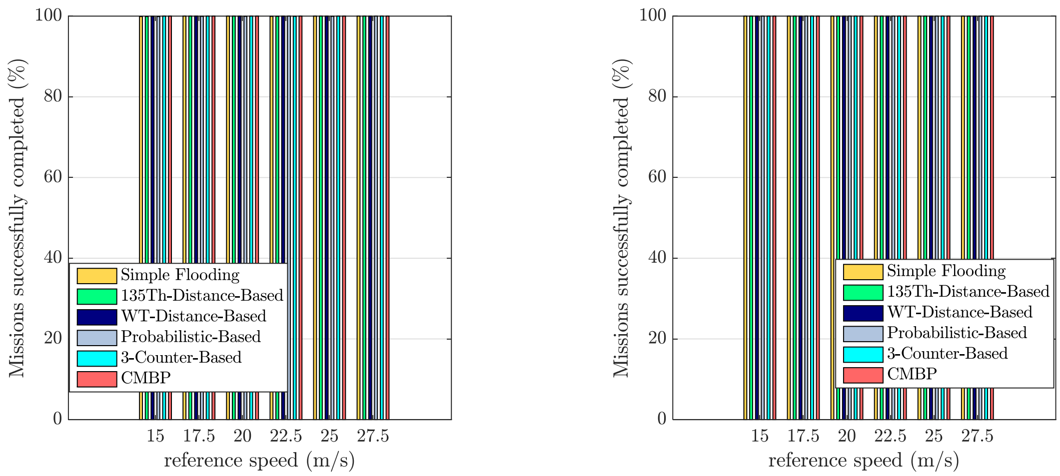

(a) (b)

Figure 62. Number of missions that were successfully completed using the CMBP and other MBPs for (a) open-delta (λ=5) and (b) delta (λ=6) formations when varying the reference speed, v_r. The results were obtained with a minimum of 2000 runs to achieve statistical significance.

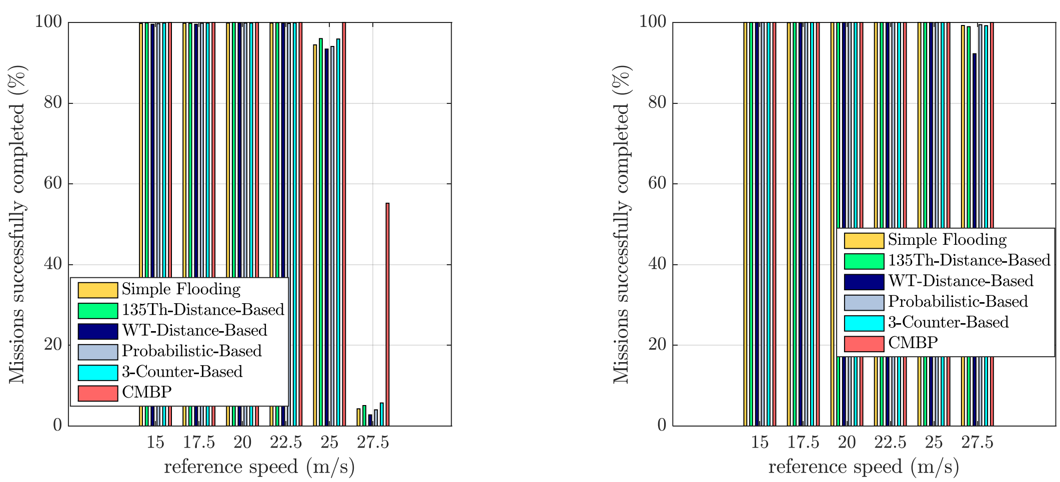

(a) (b)

Figure 63. Number of missions that were successfully completed using the CMBP and other MBPs for (a) open-delta (λ=7) and (b) delta (λ=10) formations when varying the reference speed, v_r. The results were obtained with a minimum of 2000 runs to achieve statistical significance.

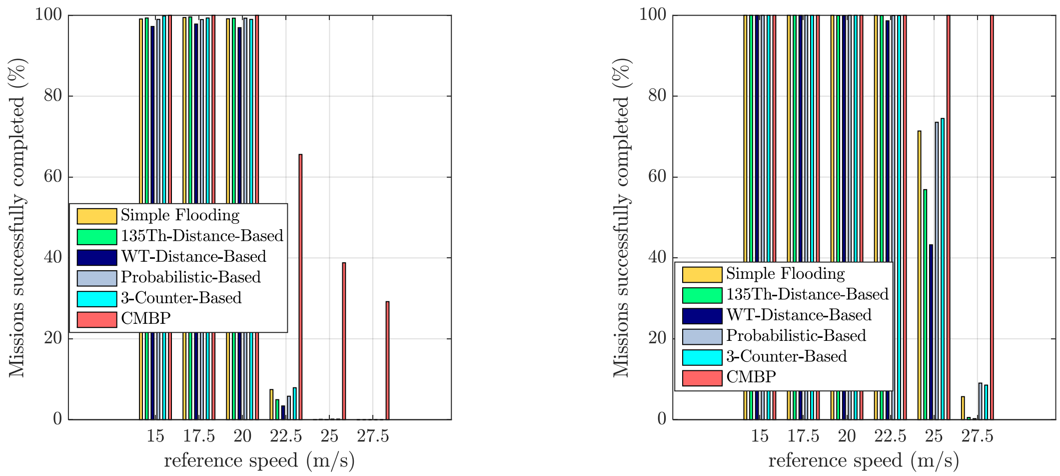

(a) (b)

Figure 64. Number of missions that were successfully completed using the CMBP and other MBPs for (a) open-delta (λ=9) and (b) delta (λ=15) formations when varying the reference speed, $\boldsymbol{v_r}$. The results were obtained with a minimum of 2000 runs to achieve statistical significance.

By analyzing the results presented in Figure 62 to Figure 64, the following conclusion can be drawn:

- For missions involving a small number of UAVs (Figure 62), the selection of the MBP has little impact on the number of successful missions (as shown in Section 4.5). In fact, all the MBPs offered the same performance, including the CMBP.

- For missions involving a medium number of UAVs (Figure 63Figure 38), performance degradation starts at $v_r = 25$ m/s for the open-delta formation for the MBPs evaluated in Chapter 4. However, when using the CMBP protocol, the degradation starts at $v_r = 27.5$ m/s. From Figure 63(a), one can observe that the performance offered by the CMBP at $v_r = 27.5$ m/s is significantly better than the other MBPs. In contrast, for the delta formation, a high number of successful missions can be achieved even at high speeds for all MBPs, including the CMBP protocol, which offered the best performance.

- For missions involving a large number of UAVs (Figure 64), a significant performance drop is observed at $v_r = 22.5$ m/s for the open-delta formation and at $v_r = 25$ m/s for the delta formation for the MBPs evaluated in Chapter 4. Nevertheless, when using the CMBP protocol, there is a significant improvement for both the open-delta and delta formations compared with the other MBPs. In fact, for the delta formation, the CMBP protocol completes 100% of the missions for all reference speeds.

- For the delta formation with $\lambda = 15$ (Figure 64Figure 39(b)), the CMBP protocol provides the best results (100% of the completed missions for all reference speeds.). This agrees with the analysis presented in the previous sections where the LU offered by this protocol was zero for all the reference speeds.

Thus, for mission planning, the results presented in this section are important because it was shown that one protocol can successfully complete all the mission scenarios considered. For example, when using the delta formation, even the most adverse mission scenario (larger formation size and higher reference speeds) can be successfully completed using the CMBP protocol. Thus, it was shown from the perspective of the communication protocols that it is possible executing the mission with a minimum time without compromising its performance.

5.7 Summary and discussion

In Section 5.2 an MBP protocol (in terms of trajectory metrics; see subsection 3.3.1) for distributed UAV formation control applications was proposed. This protocol uses a curvature-based method to offer a good performance in terms of P-RMSE and LU metrics. Evaluation results show that the CMBP protocol effectively disseminates SI packets in distributed UAV formation control scenarios, allowing them to maintain UAV formation from the communication perspective.

Using the evaluation framework proposed in Chapter 3. in Section 5.4 overall performance results obtained with the CMBP were reported. In addition, for the sake of comparison, the overall results obtained by the CMBP were contrasted with those obtained with the MBPs evaluated in Chapter 4. From this comparison, it can be concluded that, in terms of trajectory and network performance, the CMBP outperforms the other MBPs for all the scenarios analyzed. It was shown that for the case of the delta formation, the performance offered by the CMBP protocol in terms of trajectory metrics performance is similar to that offered by an ideal protocol (i.e., which provides insignificant delays and zero packet losses).

In Section 5.5, a more in-depth analysis was carried out to obtain insights about the results found in Section 5.3. In addition, the moving average metrics results offered by the CMBP were reported. These results have shown the capability of the CMBP to counter the trajectory or channel impairments within distributed UAV formation control scenarios (from lower (15 m/s) to higher (27.5 m/s) reference speeds; from low-connected (open-delta) to higher-connected (delta) scenarios; and, from lower to larger formation sizes). Results of this evaluation were satisfactory. It was found a great similarity between the moving average results obtained by the CMBP and its overall results reported in Section 5.3. Nevertheless, with the moving average results, it can be clearly observed how the network metrics performance of the CMBP at the beginning of turns was improved (due to curvature-based approach along the transmission of beacon packets). This desired improvement is a key factor in eventually keeping a good performance in terms of trajectory metrics as shown in the reported results.

In Section 5.6, a case study similar to that presented in Section 4.5 was conducted. From this case study, it was shown the effectiveness of the CMBP protocol to provide satisfactory SI dissemination among a UAV formation to guarantee the execution of a remote sensing mission. The results reported in this section shown that the use of the CMBP for these kinds of missions is a better option than the other MBPs evaluated in Chapter 4. For example, it was shown that the CMBP offers a 100% of mission completion when using the delta formation even for higher reference speeds. This result is important because by using the CMBP, UAV formation control missions can be completed faster without compromising them.

In Sections 5.2 to Section 5.6, it was shown the importance of detecting critical zones within the reference trajectory, and the use of beacon packets to counter the trajectory impairments in the CMBP protocol performance. It is important to note that this protocol was designed to specifically improve the trajectory metrics performance (i.e., P-RMSE and LU metrics) as shown in the results reported in Section 5.4 to 5.6. However, regarding the overall performance taking into account trajectory and network metrics, there is still room to improve. For example, efficiency of the CMBP protocol in terms of retransmissions can still be improved. Thus, a future goal would be to achieve the same results reported in Chapter 5. with significantly less number of rebroadcasts during the mission execution.

Chapter 6. Contribution, conclusions and areas of future research

6.1 Contributions

The main contribution of this thesis work is a study (which to best of our knowledge has not been addressed before) about the impact that multi-hop broadcast protocols (MBPs) have on the dissemination of state information (SI) for maintaining UAV formation control. To this end, an evaluation framework methodology was proposed using a network modeler (OMNeT++, 2012) and a toolkit for automatic control (Houska et al., 2013). Within the evaluation framework methodology, a set of metrics that were classified as trajectory and network metrics for evaluating MBPs in UAV formation control applications were proposed. By using these metrics, a new method to evaluate the effectiveness of MBPs on UAV formation control scenarios has been proposed. This evaluation framework methodology also introduces the use of moving average metrics (i.e., taking into account the evolution of this metrics as UAVs flight over the reference trajectory) instead of overall average metrics (commonly calculated in MANET and VANET scenarios) to gain more insight about the performance of the MBPs.

Based on the conducted study using the evaluation framework, a curvature-based multi-hop broadcast protocol (MBPs) was proposed. This protocol proved to offer better performance in terms of trajectory metrics than common MBPs used in MANETs and VANETs. Additionally, it was shown that the CMBP protocol was able to offer acceptable results in UAV formation control scenarios, even in challenging scenarios (higher reference speeds).

6.2 Conclusions

In this thesis, common multi-hop broadcast protocols (MBPs) used in MANETs and VANETs were evaluated for the dissemination of SI packets in distributed UAV formation control applications. The presented results show that the performance of these protocols in terms of network metrics has a significant impact in maintaining UAV formation (this was evaluated using trajectory metrics proposed in Chapter 3.). This result is important since, from the UAV formation control perspective, the impact that dissemination protocols have on UAV formation controllers performance is commonly obviated. In fact, when comparing the results offered by the MBPs against an ideal SI dissemination protocol, it was observed that in terms of the P-RMSE and LU metrics, the MBPs performance is significantly worst. This difference in the performance of the MBPs is even more remarkable in adverse scenarios, e.g., at higher reference speeds. Therefore, the suitable selection of a dissemination protocol in UAV formation control scenarios is crucial for the successful execution of a particular mission that involves a distributed UAV formation control as shown in Chapter 4.

Evaluation results show that even though at low speeds SI dissemination using MBPs is effective in terms of maintaining the UAV formation, as the mission reference speed increases, maintaining formation becomes harder. This adverse performance is also true when using a larger formation size because the number of hops increases and thus the delays and packet losses increase as well. Moreover, it was shown that trajectory factors such as turns impact significantly the performance of the MBPs. In this sense, a more comprehensive set of metrics was proposed to clearly observe the trajectory factors effects.

In this thesis, it was shown that using average network metrics (which is commonly done for MANETs and VANETs) is a good starting point for the evaluation of MBPs. However, when they are used to evaluate the performance of the MBPs for SI dissemination in distributed UAV formation control applications, average network metrics do not fully explain the results observed for the trajectory metrics. Thus, in this work, the use of moving average network metrics was proposed to gain more insight into the performance of the MBPs for this kind of application. By using moving average metrics, it was found that the performance of most MBPs significantly worsens when the formation makes a turn. This is particularly acute for UAVs that are located at edges of the formation, which receive SI messages through multiple hops. Thus, by performing moving average analysis, the key zones of the flight formation where the relevance of the information quality is higher can be detected. Thus, the results and analysis that was provided in this work show that more than simply selecting any MBP to disseminate SI messages in FANETs, it is necessary to design a protocol that can counter the conditions of adverse conditions such as those found at turns.

Finally, in this thesis, a multi-hop broadcast protocol (CMBP) specifically designed for dissemination SI packets over a UAV formation missions has been proposed. This protocol was designed using the insights obtained in Chapter 4. Specifically, the curvature-based detection and beacon packet transmission procedures of the CMBP protocol to counter turns effects has been evaluated using the evaluation framework proposed. It has been shown that the CMBP procedures help to keep UAV formation control, thus showing its feasibility in UAV formation control applications when it is required that SI is disseminated to feed UAV formation controllers. In fact, it was shown that the CMBP protocol outperforms the other MBPs for all of the scenarios considered in this thesis work.

6.3 Areas of future research

Some interesting areas of future research identified are:

- Perform MBPs evaluations using the proposed evaluation framework methodology considering different UAV formation control strategies and controllers.
- Perform MBP evaluations for adverse conditions considering wind disturbances.
- Integrate into the evaluation framework, a 3D-based mobility model of the UAVs for resembling a more accurate evaluation scenario.
- Improve the CMBP protocol for adapting to the target scenario conditions and react accordingly. This protocol does not only need to improve the trajectory metrics as the CMBP but disseminate SI packets efficiently, keeping low the number of the rebroadcast. This is for preserving as much of possible the autonomy of the UAV formation control missions.
- Perform an energy analysis of the MBPs when they are used in UAV formation control applications.
- Perform an experimental evaluation of the MBPs in a realistic UAV formation control scenario considering true equipment.

List of references

Abdessameud, A., Polushin, I. G., Tayebi, A. 2015. Motion coordination of thrust-propelled underactuated vehicles with intermittent and delayed communications. Systems & Control Letters, 79, 15–22. Recovered May 2019 from: http://dx.doi.org/10.1016/j.sysconle.2015.02.006

Anderson, B., Fidan, B., Yu, C., Walle, D. van der. 2008. UAV formation control: theory and application. recent advances in learning and control, LNCIS 371, 15–33.

Andre, T., Hummel, K. A., Schoellig, A. P., Yanmaz, E., Asadpour, M., Bettstetter, C., Grippa, P., Hellwagner, H., Sand, S., Zhang, S. 2014. Application-driven design of aerial communication networks. IEEE Communications Magazine, 52(5), 129–137.

Avellar, G. S. C., Pereira, G. A. S., Pimenta, L. C. A., Iscold, P. 2015. Multi-UAV routing for area coverage and remote sensing with minimum time. Sensors (Switzerland), 15(11), 27783–27803.

Badarneh, O. S., Kadoch, M. 2009. Multicast routing protocols in mobile ad hoc networks: a comparative survey and taxonomy. EURASIP Journal on Wireless Communications and Networking, 2009, 26. Recovered Apr 2017 from http://www.hindawi.com/journals/wcn/2009/764047/

Balampanis, F., Maza, I., Ollero, A. 2017. Coastal areas division and coverage with multiple UAVs for remote sensing. Sensors, 17(4), 808.

Bekmezci, I., Sahingoz, O. K., Temel, Ş. 2013. Flying Ad-Hoc Networks (FANETs): a survey. Ad Hoc Networks, 11, 1254–1270.

Bekmezci, I., Sen, I., Erkalkan, E. 2015. Flying Ad Hoc Networks (FANET) test bed implementation. En Recent Advances in Space Technologies (RAST), 2015 7th International Conference On, 2015, IEEE, pp. 665–668. IEEE. pp. 665–668.

Ben-Asher, Y., Feldman, S., Gurfil, P., Feldman, M. 2008. Distributed decision and control for cooperative UAVs using ad hoc communication. IEEE Transactions on Control Systems Technology, 16(3), 511–516.

Bujari, A., Calafate, C. T., Cano, J.-C., Manzoni, P., Palazzi, C. E., Ronzani, D. 2017. Flying ad-hoc network application scenarios and mobility models. International Journal of Distributed Sensor Networks, 13(10), 1550147717738192. Recovered Jul 2018 from http://journals.sagepub.com/doi/10.1177/1550147717738192

Cabral-Pacheco, E. G., Villarreal-Reyes, S., Galaviz-Mosqueda, A., Villarreal-Reyes, S., Rivera-Rodriguez, R., Perez-Ramos, A. E. 2019. Performance analysis of multi-hop broadcast protocols for distributed UAV formation control applications. IEEE Access, 7, 113548–113577. doi:10.1109/ACCESS.2019.2935307

Cai, G., Dias, J., Seneviratne, L. 2014. A survey of small-scale unmanned aerial vehicles : Recent Advances and Future Development Trends. Unmanned Systems, 2(02), 175–199.

Cao, Y., Yu, W., Ren, W., Chen, G. 2013. An overview of recent progress in the study of distributed multi-agent coordination. IEEE Transactions on Industrial Informatics, 9(1), 427–438. doi:10.1109/TII.2012.2219061

Chao, H., Baumann, M., Jensen, A. 2008. Band-reconfigurable Multi-UAV-based cooperative remote sensing for real-time water management and distributed irrigation control. En IFAC Proceedings Volumes, 2008, IFAC, 41(2), pp. 11744–11749. IFAC. pp. 11744–11749.

Chao, Z., Zhou, S.-L., Ming, L., Zhang, W.-G. 2012. UAV formation flight based on nonlinear model predictive control. Mathematical Problems in Engineering, 2012. Recovered Ago 2016 from http://dx.doi.org/10.1155/2012/261367

Chen, J., Sun, D., Yang, J., Chen, H. 2010. Leader-follower formation control of multiple non-holonomic mobile robots incorporating a receding-horizon scheme. The International Journal of Robotics Research, 29(6), 727–747.

Chevet, T., Vlad, C., Stoica, C., Youmin, M. 2019. Decentralized MPC for UAVs formation deployment and reconfiguration with multiple outgoing agents. Journal of Intelligent & Robotic Systems, 1–16.

Do, K. D., Pan, J. 2007. Nonlinear formation control of unicycle-type mobile robots. Robotics and Autonomous Systems, 55(3), 191–204.

Dobrokhodov, V. 2015. Kinematics and dynamics of fixed-wing UAVs. In Handbook of Unmanned Aerial Vehicles. pp. 243–277.

Erdelj, M., Król, M., Natalizio, E. 2017. Wireless sensor networks and multi-UAV systems for natural disaster management. Computer Networks, 124, 72–86.

George, J., Sujit, P. B., Sousa, J. B. 2011. Search strategies for multiple UAV search and destroy missions. Intelligence & Robotic Systems, 61(1), 355–367.

Goddemeier, N., Wietfeld, C. 2015. Investigation of air-to-air channel characteristics and a uav specific extension to the rice model. En IEEE Globecom Workshops, 2015, pp. 1–5. pp. 1–5.

Gu, Y. G. Y., Seanor, B., Campa, G., Napolitano, M. R., Rowe, L., Gururajan, S., Wan, S. W. S. 2006. Design and flight testing evaluation of formation control laws. IEEE Transactions on Control Systems Technology, 14(6), 1105–1112. doi:10.1109/TCST.2006.880203

Gupta, L., Jain, R., Vaszkun, G. 2016. Survey of important issues in UAV communication networks. IEEE Communications Surveys and Tutorials, 18(2), 1123–1152. doi:10.1109/COMST.2015.2495297

Hassanalian, M., Abdelkefi, A. 2017. Classifications, applications, and design challenges of drones: A review. Progress in Aerospace Sciences, 91, 99–131.

Hayat, S., Yanmaz, E., Muzaffar, R. 2016. Survey on unmanned aerial vehicle networks for civil applications: a communications viewpoint. IEEE Communications Surveys and Tutorials, Vol. 18. doi:10.1109/COMST.2016.2560343

Hazel, B., Aoude, G. 2015. In commercial drones, the race is on. In Oliver Wyman. Recovered Ago 2016 from https://www.oliverwyman.com/our-expertise/insights/2015/apr/in-commercial-drones--the-race-is-on.html

Houska, B., Ferreau, H. J., Vukov, M., Quirynen, R. 2013. ACADO toolkit users manual. Recovered Jul 2016 from http://www.acadotoolkit.org

IEEE Standar for information technology—local and metropolitan area networks—specific requirements-part 11: wireless LAN Mediuam Access Control (MAC) and Physical Layer (PHY) specifications amendment 6: wireless accesss in vehicular environments. 2010. IEEE Std 80211p-2010 Amend. IEEE Std 80211- 2007 Amend. IEEE Std 80211k-2008 IEEE Std 80211r-2008 IEEE Std 80211y-2008 IEEE Std 80211n-2009 IEEE Std 80211w-2009. pp. 1–51.

Ille, M., Namerikawa, T. 2017. Collision avoidance between multi-UAV-systems considering formation control using MPC. En 2017 IEEE International Conference on Advanced Intelligent Mechatronics (AIM), 2017, pp. 651–656. pp. 651–656.

Jayakumar, G., Gopinath, G. 2007. Ad hoc wireless networks routing protocols - a review. Journal of Computer Science, 3(8), 574–582.

Ju, C., Son, H. 2018. Multiple UAV systems for agricultural applications: control, implementation, and evaluation. Electronics, 7(9), 162.

Ke, Y., Wang, J., Wang, J. 2018. Nonlinear formation control of small fixed-wing uavs with velocity and heading rate constraints. En 2018 IEEE International Conference on Mechatronics and Automation, ICMA, 2018, IEEE, pp. 1275–1280. IEEE. pp. 1275–1280.

Ko, Y. B., Vaidya, N. H. 2002. Flooding-based geocasting protocols for mobile ad hoc networks. Mobile Networks and Applications, 7(6), 471–480.

Korkalainen, M., Sallinen, M., Kärkkäinen, N., Tukeva, P. 2009. Survey of wireless sensor networks simulation tools for demanding applications. 2009 Fifth International Conference on Networking and Services, 102–106. Recovered May 2017 from http://ieeexplore.ieee.org/lpdocs/epic03/wrapper.htm?arnumber=4976744

Kristiansen, R., Oland, E., Narayanachar, D. 2012. Operational concepts in UAV formation monitoring of industrial emissions. 3rd IEEE International Conference on Cognitive Infocommunications, CogInfoCom 2012 - Proceedings, 339–344.

Kruggl, K., Shah, M., Bhattacharya, S., Wischounig-Strucl, D., Rinner, B., Quaritsch, M. 2010. Networked UAVs as aerial sensor network for disaster management applicationsVernetzte unbemannte Fluggeräte als “fliegende Sensornetzwerke” für Anwendungen in Katastrophenfällen. E & i Elektrotechnik Und Informationstechnik, 127(3), 56–63.

Kuriki, Y., Namerikawa, T. 2015. Formation control with collision avoidance for a multi-UAV system using decentralized MPC and consensus-based control. Journal of Control, Measurement, and System Integration, 8(4), 285–294.

Lawton, J. R., Young, B. J., Beard, R. W. 2003. A decentralized approach to elementary formation maneuvers. IEEE Transactions on Robotics and Autonomous Systems, 19(6), 933–941.

Lee, D., Chang, S., Lee, S. 2014. Analysis and design on efficient message relay methods in VANET. multimedia tools and applications, 74(16), 6331–6340.

Lei, M., Zhou, S., Yang, X., Yin, G. 2012. Complex formation control of large-scale intelligent autonomous vehicles. Mathematical Problems in Engineering, 2012.

Li, Z., Mohapatra, P. 2003. HostCast: a new overlay multicasting protocol. IEEE International Conference on Communications, 1, 702–706.

Mansouri, S. S., Kanellakis, C., Georgoulas, G., Kominiak, D., Gustafsson, T., Nikolakopoulos, G. 2018. 2D visual area coverage and path planning coupled with camera footprints. En Control Engineering Practice, 2018, 75, pp. 1–16. pp. 1–16.

Maza, I., Ollero, A. 2007. Multiple UAV cooperative searching operation using polygon area decomposition and efficient coverage algorithms. En Distributed Autonomous Robotic Systems 6, 2007, pp. 221–230. doi:10.1007/978-4-431-35873-2_22

OMNeT++. 2012. INET framework for OMNeT++. Recovered Apr 2016 from https://inet.omnetpp.org/.

Oubbati, O. S., Lakas, A., Zhou, F., Güneş, M., Yagoubi, M. B. 2017. A survey on position-based routing protocols for flying ad hoc networks (FANETs). Vehicular Communications, 10, 29–56.

Panichpapiboon, S., Pattara-atikom, W. 2012. A review of information dissemination protocols for vehicular ad hoc networks. Communications Surveys Tutorials, IEEE, 14(3), 784–798.

Park, C., Cho, N., Lee, K., Kim, Y. 2015. Formation flight of multiple UAVs via onboard sensor information sharing. Sensors, 15(7), 17397–17419. Recovered May 2016 from http://www.scopus.com/inward/record.url?eid=2-s2.0-84940190412&partnerID=tZOtx3y1

Pires, R. D. M., Arnosti, S. Z., Sandro, A., Pinto, R., Branco, K. R. L. J. C. 2016. Experimenting broadcast storm mitigation techniques in FANETs. En 2016 49th Hawaii International Conference on System Sciences (HICSS), 2016, IEEE. IEEE.

pwc. 2017. PwC Sees US$9.46 billion drone solutions market for power, utilities industries. Recovered Ago 2019 from https://www.pwc.com/gx/en/news-room/press-releases/2017/pwc-sees-us-9_46-billion-drone-solutions-market-for-power-utilities-industries.html

Rappaport, T. S. 2002. Wireless communications PRINCIPLES AND PRACTICE (2nd. ed). Prentice Hall PTR.

Rehmani, M. H., Viana, A. C., Khalife, H., Fdida, S. 2012. Improving data dissemination in multi-hop cognitive radio ad-hoc networks. Ad Hoc Networks, 89, 117–130.

Ren, W., Atkins, E. M. 2005. Nonlinear trajectory tracking for fixed wing UAVs via backstepping and parameter adaptation. Proceedings of the AIAA Guidance, Navigation, and Control Conference and Exhibit, (November), 1–11. from papers2://publication/uuid/77E52D5B-9703-4A5E-80A6-853E74E1A0DC

Rosário, D., Zhao, Z., Braun, T., Cerqueira, E., Santos, A., Alyafawi, I. 2014. Opportunistic routing for multi-flow video dissemination over flying ad-hoc networks. En World of Wireless, Mobile and Multimedia Networks (WoWMoM), 2014 IEEE 15th International Symposium on A, 2014, IEEE, pp. 1–6. IEEE. pp. 1–6.

Sahingoz, O. K. 2014. Networking models in flying ad-hoc networks (FANETs): concepts and challenges. journal of intelligent and robotic systems: Theory and Applications, 74, 513–527.

Schwartz, R. S., Rafael, R. R., Meratnia, N., Heijenk, G., Scholten, H. 2011. A directional data dissemination protocol for vehicular environments. Computer Communications, 34(17), 2057–2071. from http://dx.doi.org/10.1016/j.comcom.2011.03.007

Shakhatreh, H., Sawalmeh, A., Al-Fuqaha, A., Dou, Z., Almaita, E., Khalil, I., Othman, N. S., Khreishah, A., Guizani, M. 2019. Unmanned aerial vehicles: a survey on civil applications and key research challenges. IEEE Access, 7, 48572–48634. Recovered Oct 2019 from http://arxiv.org/abs/1805.00881

Sharma, V., Chen, H. C., Kumar, R. 2017. Driver behaviour detection and vehicle rating using multi-UAV coordinated vehicular networks. Journal of Computer and System Sciences, 86, 3–32.

Sharma, V., Kumar, R., Rathore, N. 2015. Topological broadcasting using parameter sensitivity-based logical proximity graphs in coordinated ground-flying ad hoc networks. Journal of Wireless Mobile Networks, Ubiquitous Computing, and Dependable Applications (JoWUA), 6(3), 54–72.

Shraim, H., Awada, A., Youness, R. 2018. A survey on quadrotors: configurations, modeling and identification, control, collision avoidance, fault diagnosis and tolerant control. IEEE Aerospace and Electronic Systems Magazine, 33(7), 14–33.

Simunek, M., Fontán, F. P., Pechac, P. 2013. The UAV low elevation propagation channel in urban areas: statistical analysis and time-series generator. IEEE Transactions on Antennas and Propagation, 61(7), 3850–3858.

Tseng, Y. C., Ni, S.-Y., Chen, Y.-S., Sheu, J.-P. 2002. The broadcast storm problem in a mobile ad hoc network. Wireless Networks, 8(2–3), 153–167.

Turpin, M., Michael, N., Kumar, V. 2012. Trajectory design and control for aggressive formation flight with quadrotors. Autonomous Robots, 33(1–2), 143–156.

Varga, A., Hornig, R. 2008. An overview of the OMNeT++ simulation environment. En Proceedings of the 1st International Conference on Simulation Tools and Techniques for Communications, Networks and Systems & Workshops, 2008, pp. 60. from http://dl.acm.org/citation.cfm?id=1416222.1416290

Vidal, I., Valera, F., Diaz, M. A., Bagnulo, M. 2014. Design and practical deployment of a network-centric remotely piloted aircraft system. IEEE Communications Magazine, 52(10), 22–29.

Wang, X., Zeng, Z., Cong, Y. 2016. Multi-agent distributed coordination control: developments and directions via graph viewpoint. Neurocomputing, 199, 204–218. from http://linkinghub.elsevier.com/retrieve/pii/S0925231216300418

Wisitpongphan, N., Tonguz, O. K., Parikh, J. S., Mudalige, P., Bai, F., Sadekar, V. 2007. Broadcast storm mitigation techniques in vehicular ad hoc networks. IEEE Wireless Communications, 14(6), 84–94.

Zeng, Y., Zhang, R., Lim, T. J. 2016. Wireless communications with unmanned aerial vehicles: opportunities and challenges. IEEE Communications Magazine, 54(5), 36–42. from http://arxiv.org/abs/1602.03602

Zhang, Y., Mehrjerdi, H. 2013. A survey on multiple unmanned vehicles formation control and coordination: normal and fault situations. En 2013 International Conference on Unmanned Aircraft Systems, ICUAS 2013, 2013, pp. 1087–1096. pp. 1087–1096.

Zou, Y., Pagilla, P. R., Ratliff, R. T. 2009. Distributed formation flight control using constraint forces. Journal of Guidance, Control, and Dynamics, 32(1), 112–120. doi:10.2514/1.36826